2

Dislocation models for interfaces

2.1 INTRODUCTION

In this chapter we shall consider the modelling of interfaces by continuously or discretely distributed arrays of dislocations. Many models use the known properties of discrete dislocations to deduce properties of an interface. In this way energies, elastic stress and strain fields, diffusion coefficients, point defect source and sink efficiencies, segregation kinetics, roughening transitions, migration, sliding, and internal friction of interfaces have been modelled. This extensive list of properties makes the dislocation model of prime importance in the field of interfaces.

The history of the model spans more than half a century and its conception dates from G. I. Taylor's pioneering work on crystal plasticity. Taylor (1934) calculated the elastic displacement and stress fields of a wall of crystal lattice edge dislocations forming what he called a 'surface of misfit', illustrated schematically in Fig. 2.1. Today we would call Taylor's surface of misfit a small-angle symmetrical tilt boundary. J. M. Burgers (1939) calculated the elastic displacement and stress fields of a small-angle symmetrical tilt boundary and also an epitaxial heterophase interface containing a single array of crystal lattice edge dislocations with Burgers vectors parallel to the interface, illustrated in Fig. 2.2. J. M. Burgers (1940) recognized that an asymmetric tilt boundary could be constructed from two sets of edge dislocations (see Fig. 2.3). Similarly, twist grain

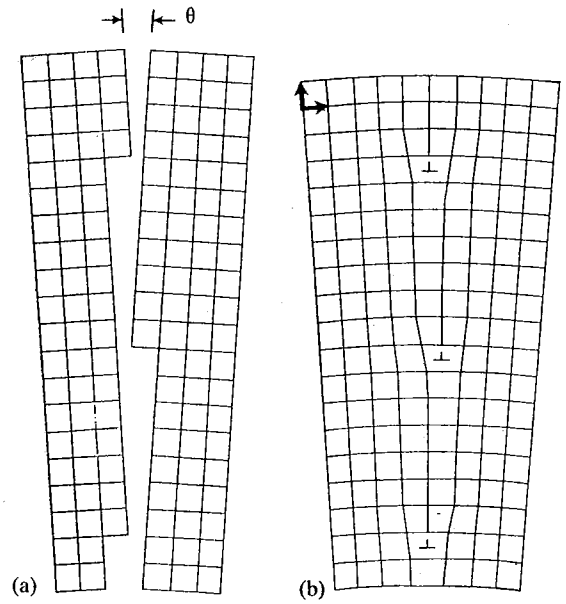

Fig. 2.1 Schematic illustration of the formation of symmetric tilt boundary of misorientation θ in (b) by bonding together two crystals in (a) with high index free surfaces. The steps on the free surfaces in (a) become edge dislocations in the boundary in (b). (From Read (1953)).

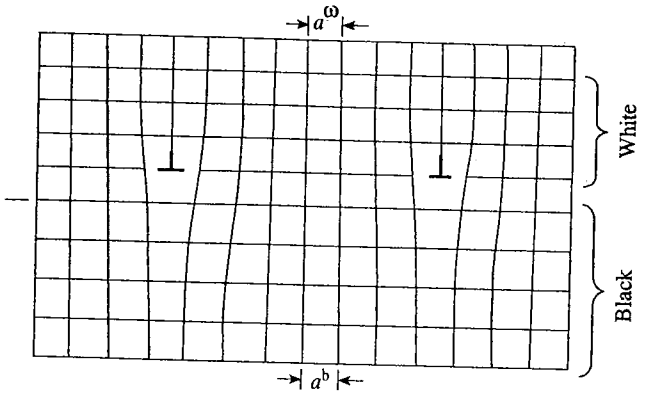

Fig. 2.2 Schematic illustration of an epitaxial interface between black and white crystals with lattice parameters a^b and a^w, where $a^b > a^w$. The difference in lattice parameters is accommodated by edge dislocations.

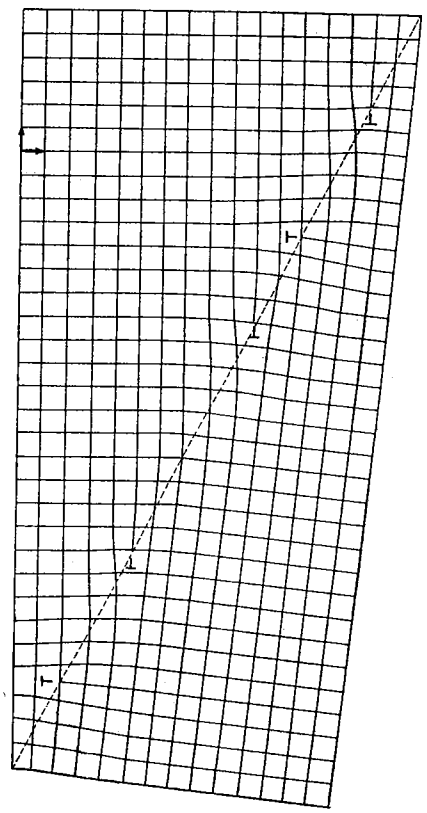

Fig. 2.3 A schematic illustration of an asymmetric tilt boundary along the dashed line. Note that there are two sets of edge dislocations. (From Read (1953)).

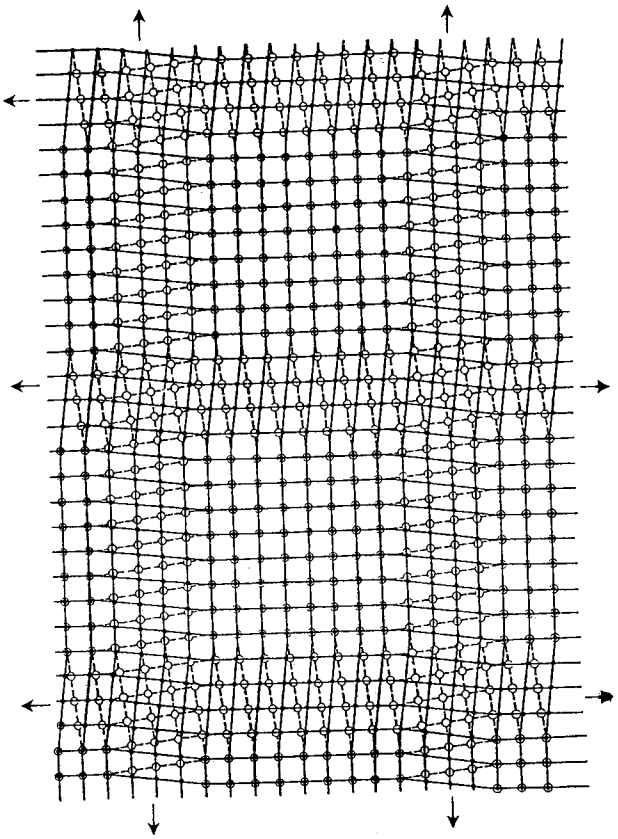

Fig. 2.4 A schematic illustration of a twist boundary seen in plan view. Sites of the two crystal lattices are represented by dots and circles. The boundary contains two sets of screw dislocations along the arrows which tend to localize the twist misorientation leaving relatively large patches of almost perfect crystal between them. (From Read (1953)).

boundaries could be constructed from grids of screw dislocations, as shown in Fig. 2.4. These early authors were primarily concerned with small-angle grain boundaries, such as sub-grain boundaries comprising the mosaic structure formed during cold work. It was not until 1947 that W. G. Burgers (the brother of J. M. Burgers) gave a description of large-angle grain boundaries in terms of dislocations. This proposal was consistent with the growing concensus that large-angle grain boundaries were not amorphous layers some 100 atoms in thickness as had been argued much earlier by Rosenhain and coworkers, e.g. Rosenhain and Humphrey (1913). However, it was recognized that the description of a large-angle boundary in terms of crystal lattice dislocations was limited in its usefulness owing to the close separation of the dislocations.

Read and Shockley (1950) considered the energy of a small-angle grain boundary composed of an array of crystal lattice dislocations. The classic Read-Shockley formula for the energy-misorientation relation, $\sigma(\theta) = \sigma_0\theta(A - \ln\theta)$, appeared in this paper. This formula predicts that $\sigma(\theta)$ increases with increasing θ and possesses a sharp cusp as $\theta \to 0$. Although this formula was derived for small-angle boundaries, $\theta \leqslant 15°$, the paper also addressed the structures and energies of large-angle grain boundaries. Read and Shockley recognized that their formula applied only when the dislocations in the boundary were

uniformly spaced. But this is possible only in special cases when the spacing of the dislocations is an integer multiple of some crystal lattice spacing. The non-uniformities in the spacings of the dislocations, which exist in more general cases, may be thought of as perturbations superimposed on an array of uniformly spaced dislocations. Read and Shockley showed that the perturbations may be thought of as another array of dislocations with smaller (weaker) Burgers vectors. Thus, there are additional weaker cusps in the energy-misorientation relation at periodic boundaries. These ideas are equivalent to modern dislocation models of large-angle grain boundaries involving DSC dislocations (see Section 1.7.2.1). We shall derive the Read–Shockley formula in Section 2.10.3.

To understand current dislocation models it is essential to distinguish two types of interface. The first has no stress field in either crystal far from the interface. The stress field associated with the interface decays exponentially over a distance comparable to a characteristic wavelength in the interface, such as the average spacing of an array of dislocations. This is the type of interface that is produced when two stress-free crystals are bonded together with no constraints applied externally to the bicrystal. The second type of interface is associated with a long-range stress field. Far from the interface the stress tensor approaches a constant non-zero value. This type of interface occurs naturally, for example in thin-film specimens containing interfaces between thin epitaxial layers and thick substrates. Once the epilayer reaches a certain critical thickness it becomes energetically favourable for the interface to relieve the long-range stress field by the introduction of an array of dislocations at the interface. This transition is discussed in Section 2.10.6.

In this chapter we shall be concerned mainly with interfaces that are free of long-range stresses. For such an interface Frank (1950) and Bilby (1955) showed that the dislocation content is determined by a purely geometrical condition. They viewed the interface as a transformation front; as it moves it transforms one crystal lattice adjoining the interface into the other. The transformation may be a rotation, as in the case of a grain boundary, or a general affine transformation. In general, the transformation would open gaps or produce overlapping material at the interface. The interface is then said to contain incompatibilities. Dislocations are required geometrically to eliminate the incompatibilities. It is only when the interface is fully compatible that it is free of stress at long range. Once a description of the relationship between the crystal lattices has been selected, the dislocation content of the interface is obtained in a straightforward way from the Frank–Bilby equation, which is derived in Section 2.3. One of the difficulties with the Frank–Bilby theory is that the relationship between the crystal lattices for a given interface may be specified in an infinite number of ways. It follows that there is an infinite number of Frank–Bilby descriptions of the dislocation content of an interface, all satisfying the condition of no long-range stresses. Problems associated with this feature of dislocation models of interfaces and the question of whether there is a 'best' description are discussed in Section 2.4.

There is an important distinction between the interfacial dislocations that were considered in Section 1.7 and the interfacial dislocations that are used in dislocation models of interfaces. The interfacial dislocations of Section 1.7 are *isolated* Volterra dislocations. Their Burgers vectors are defined without reference to any other structure. By contrast, a dislocation model of an interface involves one or more *arrays* of dislocations. The existence of an array of dislocations alters the orientational and/or deformational relationship between the adjoining crystal lattices from that of some reference structure, where the corresponding array of dislocations is absent. It is therefore more appropriate for the Burgers vectors of dislocations in an array to be defined by a Burgers circuit

construction in a reference lattice. Such a procedure enables the systematic variations of the spacings and line directions of the dislocations in the interface to be modelled as the orientational and/or deformational relationship between the adjoining crystal lattices varies. As we shall see in Section 2.2 the choice of reference lattice is not unique. Provided the closure failure of the Burgers circuit is always measured in the reference lattice the value obtained is independent of the spacing of the dislocations in the array. On the other hand the 'local' Burgers vector (Hirth and Lothe 1982), which is obtained by measuring the closure failure in the interface where the dislocations are located, varies as the dislocation spacing varies.

2.2 CLASSIFICATION OF INTERFACIAL DISLOCATIONS

In Section 1.7 we classified interfacial line defects according to bicrystal symmetry. The classification was based on the condition that the line defect separated regions of interface that were related by symmetry and hence energetically degenerate. An interfacial dislocation was created by a Volterra process involving a uniform displacement across a cut and subsequent rebonding. The Burgers vector of the dislocation was equal to the uniform displacement across the cut. An isolated perfect dislocation in a crystal lattice may be created by a similar Volterra process in which the displacement across the cut is a translation vector of the crystal lattice. Similarly, the Burgers vector of a *perfect* interfacial dislocation is a translation vector of the reference lattice. However, it was noted in Section 1.7 that the classification was not complete because other interfacial dislocations could be envisaged that did not separate energetically degenerate regions of an interface. For example, a dislocation with a Burgers vector that is not a translation vector of the reference lattice will not, in general, separate energetically degenerate regions of the interface. Such dislocations are called *partial* interfacial dislocations, by analogy with partial crystal lattice dislocations such as Frank and Shockley partial dislocations in an f.c.c. lattice (Read 1953). However, we note that the analogy with the classification of crystal lattice dislocations is not exact. Whereas partial interfacial dislocations can separate energetically degenerate interfacial domains (e.g. see Section 1.7.2), a partial crystal lattice dislocation introduces a stacking fault, which has a different energy from the rest of the crystal (Read 1953).

Over the past 30 years there has been a proliferation in the types of interfacial dislocations which have been identified. In addition, dislocations of a given type have often been called by different names, e.g. see Balluffi and Olson (1985). Thus, intrinsic (Hirth and Balluffi 1973), extrinsic (Hirth and Balluffi 1973), coherency (Olson and Cohen 1979), anticoherency (Olson and Cohen 1979), twinning (Christian 1981), transformation (Christian 1981), primary or crystal lattice interfacial dislocations (Bollmann 1970), secondary (Bollmann 1970), tertiary (Bollmann 1970), virtual (Hirth and Balluffi 1973), surface (Bilby 1955), misfit (Frank and van der Merwe 1949), perfect (Pond 1977), partial (Pond 1977), Somigliana (Bonnet *et al.* 1985), Volterra (Pond and Vlachavas 1983), and DSC dislocations (Bollmann 1970) have appeared in the literature. One reason for this proliferation is the different roles that interfacial dislocations are perceived to play in determining the stress field of an interface. Another reason is the concept of a reference structure and the different choices of reference structure that may be adopted, as discussed later in this section and in Section 2.4.

In recent years Olson and Cohen (1979) and Bonnet (1981*a*,*b*,*c*, 1982, 1985) have developed a general approach to describe the elastic fields of interfaces in terms of dislocations. A useful discussion of the method has been given by Dupeux (1987). The

basic idea is to use two arrays of dislocations with Burgers vector densities of opposite sign and different distributions. The short-range elastic field of an interface that has no long-range stress field is modelled by two cancelling arrays of dislocations. Thus the net dislocation content of such an interface is zero. One array may be regarded as an array of *stress-generator dislocations* and the other as an array of *stress-annihilator dislocations*. The elastic field of an interface that is associated with a long-range stress field is modelled by an incomplete cancellation of the two arrays, or, in the simplest case, by only one array. In such cases the net dislocation content of the interface is not zero. In our view this approach has many advantages and we shall therefore adopt it throughout this book.

To illustrate the use of stress generator and annihilator arrays consider the formation of a grain boundary that is free of long-range stresses by the following imaginary four-step process (see Fig. 2.5). We begin with a reference structure consisting of a stress-free, single crystal, Fig. 2.5(a). The crystal is gripped and bent elastically through an angle θ between the grips, Fig. 2.5(b). The long-range stress field that is set up by this elastic distortion is modelled by a continuous distribution of dislocations acting as stress generators in the distorted region. We emphasize that the bending of the crystal is elastic and that the dislocations that are continuously distributed are not 'real' dislocations, in the conventional sense, but they serve as a device to model the elastic stress field of the bent crystal. They may be compared with the use of continuous distributions of dislocations to model the elastic fields of loaded cracks (Hirth and Lothe 1982). The bent crystal is in mechanical equilibrium only because the crystal halves are being clamped in position far from the boundary plane. If the clamps were removed the bicrystal would return to Fig. 2.5(a). The long-range stress field is eliminated by introducing a second distribution of crystal lattice dislocations acting as stress annihilators, with exactly the opposite Burgers vector density, see Fig. 2.5(c). These dislocations are 'real' dislocations. It is emphasized that in this representation the stress field produced by the stress annihilator dislocations is that produced under the constraint that no bending (rotation) of the crystal is allowed during their introduction. Finally, the elastic energy of the system is minimized by localizing all dislocations in the boundary plane, as shown in Fig. 2.5(d). The details of the short-range stress field of the boundary then depend on the distribution of the Burgers vector density that is assumed for the stress annihilators.

In Fig. 2.5 one half of the bicrystal is produced from the other by the transformation **T** (see Section 1.3.2), which in this case is a rotation, where the half-crystals are rotated by equal and opposite amounts.

Prior to the introduction of the stress annihilators (Fig. 2.5(b)) the continuity of the reference lattice is maintained across the interface, although it is elastically deformed; in this state the interface is said to be in a state of forced elastic coherence or simply 'coherent'.

To illustrate the same approach for a heterophase interface, that is free of long-range stresses, we consider an analogous four step process, illustrated in Fig. 2.6. We begin with a reference structure consisting of a single crystal of the α phase, Fig. 2.6a. One half of the reference crystal lattice is elastically transformed into the β phase, by the transformation **T**, which produces a change of shape of the reference crystal as shown in Fig. 2.6(b). Again the crystal halves are clamped in position far from the interface to prevent the β half transforming back to α or the α half transforming to β. Continuity of the reference lattice is maintained across the interface by an elastic distortion of the adjoining α and β crystals, and the interface is coherent. The interface is associated with a long range stress field, which is modelled by the continuous distribution of stress

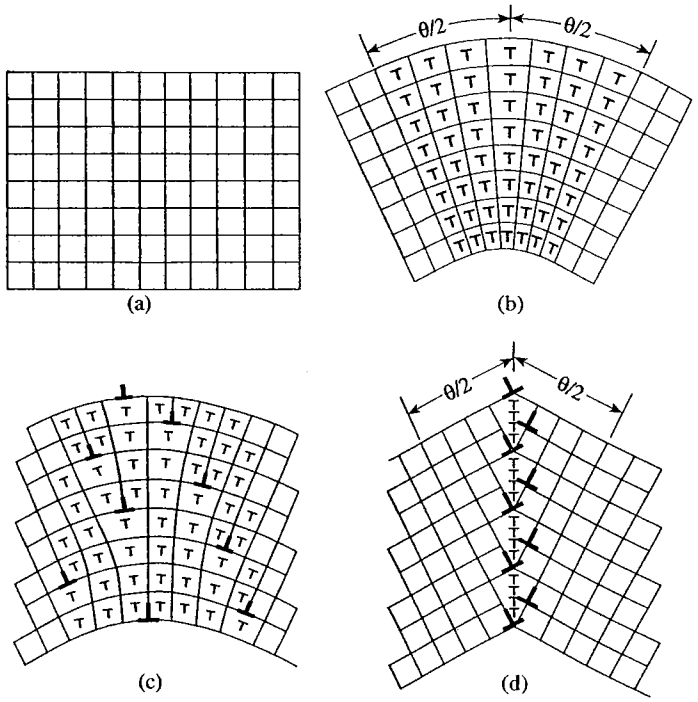

Fig. 2.5 The formation of a grain boundary that is free of long-range stresses by a four-step process. Starting from a single crystal reference lattice in (a) the crystal is gripped at the left and right sides and bent elastically to introduce the misorientation θ in (b). The long-range elastic field is modelled by a continuous distribution of stress generator dislocations. In (c) stress annihilator dislocations are introduced, whose Burgers vector density cancels that of the stress generator dislocations. There is now no long-range elastic field associated with the boundary. The elastic energy is minimized by rearranging the dislocations into the boundary plane in (d).

generators, shown in Fig. 2.6(b). The stress annihilators, which may be crystal lattice dislocations, are introduced in the third step and cancel the longe-range field, Fig. 2.6(c). In the final step the stress generators and annihilators rearrange their positions to minimize the interfacial energy, Fig. 2.6(d), which need not restrict them to lying in the chemical interface depending on the relative elastic constants of the two phases (see Section 4.4.3).

For interfaces that are free of long-range stresses the cancellation of the Burgers vector densities of the stress generator and annihilator arrays ensures that no macroscopic change in the relative orientation or structures of the adjoining crystals is effected by the two arrays. It is because of this that the method models the elastic field that would be produced by bonding together parallel surfaces of two crystals that are *already* misoriented or transformed in the desired way. We note that when the two sets of dislocations are in balance, neither set can be uniquely identified as stress generators or stress annihilators, since it is clear that the order in which the above set of operations is carried out can be altered without affecting the final state of the system.

This approach may be contrasted with the more commonly used Read–Shockley approach for grain boundaries. Dislocations in a single crystal are run into a plane, which becomes the boundary plane. No constraints are applied externally to the crystal and one crystal half rotates with respect to the other by θ about an axis $\hat{\rho}$. If the rotation were

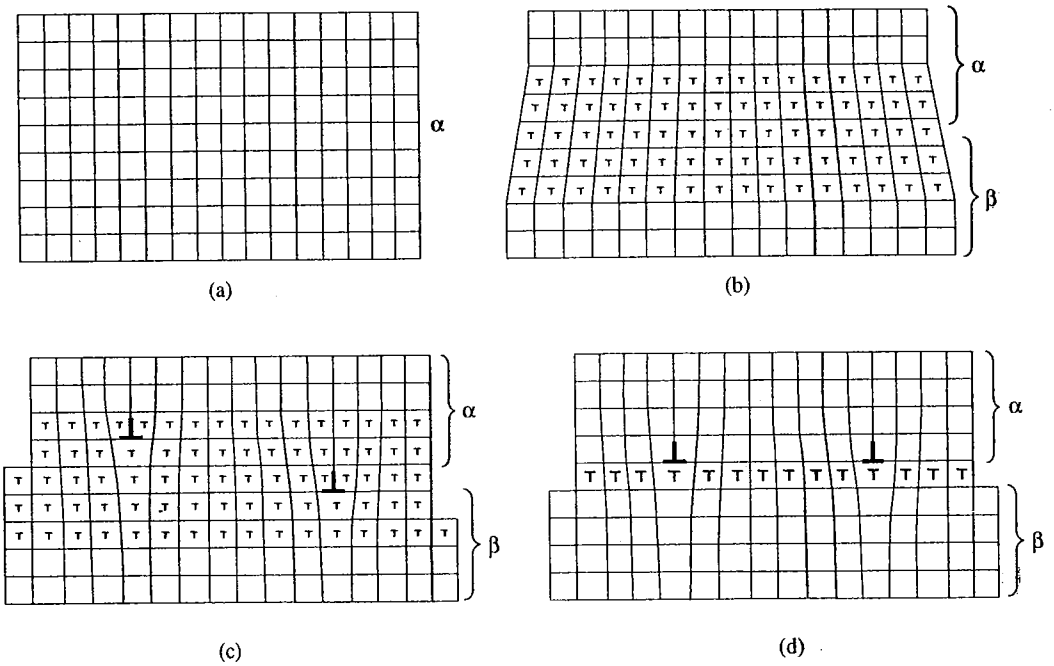

Fig. 2.6 The formation of a heterophase interface that is free of long-range stresses by a four-step process. One half of the reference single crystal lattice of the α phase in (a) is transformed elastically in (b) into the the lattice of the β phase. The long-range stress field of the resulting bicrystal is modelled by a continuous distribution of stress generator dislocations. Stress annihilator dislocations are introduced in (c) with an equal and opposite Burgers vector density to cancel that of the stress generators. The interface is now free of long-range stresses. In (d) the stress generator and annihilator dislocations rearrange so as to minimize the elastic strain energy.

suppressed by external constraints a long-range stress field would be set up and the dislocations would be an array of stress generators. But the coexistence of the rotation and the dislocations in the boundary produces a bicrystal that is free of long-range stresses. Thus, in the Read–Shockley approach the dislocation array serves two purposes: (i) its distortion field effects a change in the orientational relationship between the crystal lattices, and (ii) it introduces a Burgers vector density to relieve incompatibilities at the interface that are produced by (i). Provided the change in the relationship between the crystal lattices in (i), and the net Burgers vector density of the dislocations in (ii), are related by the Frank–Bilby equation (see Section 2.3) the interface is free of long-range stresses. The stress field in the bicrystal is the same as that obtained by bonding parallel surfaces of two crystals that are already misoriented by θ about $\hat{\boldsymbol{\rho}}$. Thus the Read–Shockley and Olson–Cohen–Bonnet approaches describe the same final state: *in the absence of long-range stresses the two approaches are equivalent.* As discussed in Section 2.10.4, great care with the boundary conditions far from the interface has to be taken with the use of elasticity theory in the Read–Shockley approach to ensure that the absence of external constraints on the bicrystal is implicit in the elastic distortion field. Otherwise, the Frank–Bilby equation is not satisfied by the distortion field and spurious long-range stresses are found. One of the advantages of the Olson–Cohen–Bonnet approach is that an interface *is guaranteed* to have no long-range stress field by using cancelling arrays of dislocations. But more significantly, it has the added advantage that it can be readily

applied to interfaces that do have long-range stress fields, because of particular circumstances in which those interfaces were produced, so that the Burgers vector densities of the stress generator and annihilator arrays do not cancel.

An example of an interface with a long-range stress field that looks like that produced by several closely spaced dislocation loops is a lenticular mechanical twin within a crystal, as illustrated in Fig. 2.7. In this case the longe-range field is caused by the coexistence of a sheared volume inside an unsheared crystal. An enlarged view of the interface near one of the dislocations is shown in Fig. 2.8(d) where it is seen that the dislocation has step character. The dislocation is a stress generator. Continuity of the reference lattice, which in this case is the untwinned crystal lattice, is maintained everywhere and therefore the stepped interface is coherent. No stress annihilators are present and therefore the stress field of the stress generators is not cancelled: the interface has a long-range stress field.

Similar, constrained, changes of shape occur when small precipitates of new phases are formed within a material. Continuity of some reference lattice is maintained across the interface for precipitate sizes below some critical value. The interface is coherent and the stress fields of these inclusions may be modelled by continuously or discretely distributed arrays of stress generators at the interface. In both the twin and the precipitate cases, however, the long-range stress fields can be eliminated by running crystal lattice dislocations into the interfaces. These then are the stress annihilators.

In the previous examples the choice of reference lattice was the lattice of a single crystal. With the help of stress-generator dislocations continuity of the reference lattice across the interface was maintained and the interface was then described as coherent. The coherency of the interface was disrupted by the introduction of stress-annihilator crystal lattice dislocations. But we may also have situations where it is useful to start with a reference structure consisting of a bicrystal. By applying a suitable transformation, **T**, to one of the crystals of such a reference bicrystal a new interface can be produced having geometrical parameters which deviate only slightly from those of the original reference interface. Provided the reference interface has a relatively low energy the deviated interface may be expected to relax to a configuration consisting of patches of the reference interface separated by appropriate interfacial dislocations. In this way the deviated interface is described as the reference interface with a superimposed array of interfacial dislocations. Such situations can also be described in terms of cancelling arrays of stress generator and stress annihilator dislocations.

Suppose that we choose a reference interface that has a quasiperiodic structure. This is conceivable because relatively low-energy quasiperiodic interfaces can exist, e.g. (100)/(110) grain boundaries in Al have been observed to be of relatively low energy (Dahmen and Westmacott 1988). Choosing a quasiperiodic reference structure is equivalent to choosing a periodic reference structure in the limit that the period tends to infinity. A possible drawback of choosing a periodic reference structure with a long period is that there may be local relaxation patterns *within* the period of the reference structure which will not be described by this choice. To account for such local relaxations it is necessary to choose the appropriate shorter period reference structure that is being preserved by the local relaxations. Similarly, there may be local relaxations at a quasiperiodic reference structure, which would be arranged quasiperiodically. Between these local relaxations there is some periodic approximant to the quasiperiodic interface. To account for them one should choose the periodic approximant that is being preserved. This is known as the 'near CSL model', where the existence of a nearby periodic interfacial structure implies the existence of a nearby CSL (and periodic DSC lattice) in one, two, or three dimensions. However, it is conceivable that there are no local relaxations at a

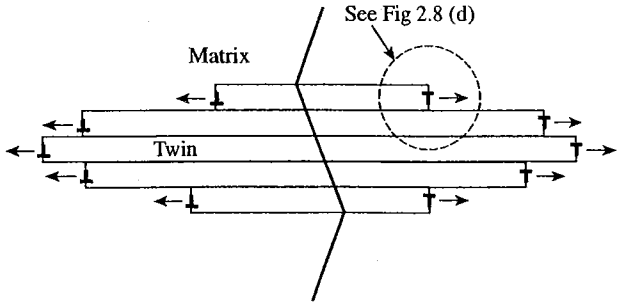

Fig. 2.7 Schematic illustration of a lenticular mechanical twin within a crystal. The twin is 5 layers thick. Each layer is bounded by a dislocation loop and an enlarged view of the step associated with each dislocation is shown in Fig. 2.8(d). The twin elongates by the lateral motion of the dislocations as indicated by the arrows.

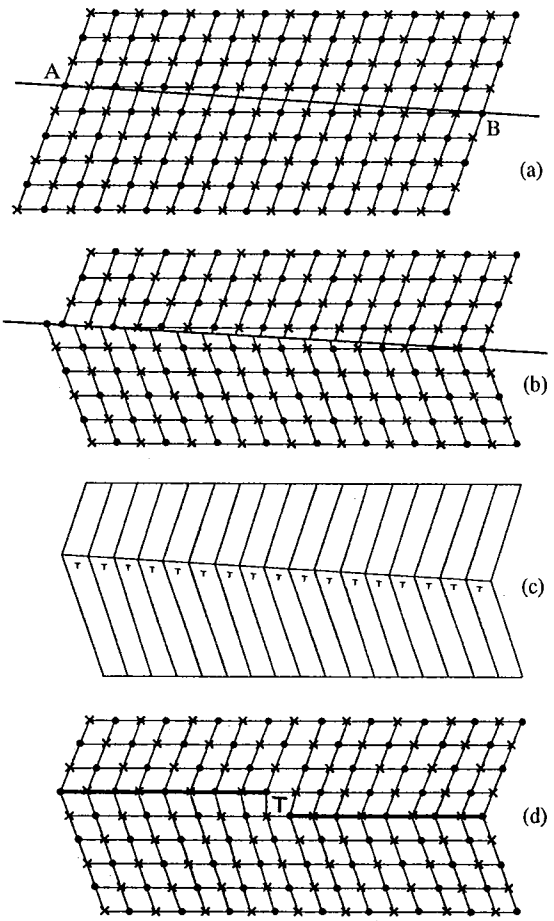

Fig. 2.8 The formation of a step in a (111) mechanical twin boundary in an f.c.c. lattice. Starting from a single f.c.c. lattice in (a), seen in projection along $[1\bar{1}0]$, where the dots and crosses refer to lattice sites on successive (220) planes, the crystal lattice is cut along AB. The lower half undergoes the mechanical twinning shear in (b), and it is seen that the two halves no longer fit together along AB. In (c) a continuous distribution of stress generator dislocations (i.e. coherency dislocations) is introduced along AB in order to make the two crystal halves commensurate. These continuously distributed dislocations localize into a $\frac{1}{6}[11\bar{2}]$ coherency dislocation associated with a step of one (111) plane height in (d).

quasiperiodic reference structure (though on physical grounds it would seem unlikely) and in that case the quasiperiodic interface itself can serve as a reference structure to describe local relaxations in deviated interfaces.

To illustrate a reference structure consisting of a bicrystal consider a short period symmetric [001] tilt boundary between two crystals misoriented to produce the $\Sigma = 5$ CSL and DSC lattice as shown in Fig. 2.9(a). The deviated boundary, obtained by a transformation, **T**, corresponding to a small tilt rotation, $\Delta\theta$, around [001], is shown schematically in Fig. 2.9(b). By analogy with Fig. 2.5 we may imagine producing the deviated boundary by first gripping the reference bicrystal and bending it elastically so that the misorientation is increased by $\Delta\theta$. The elastic stress field of the bicrystal may then be modelled by a continuous distribution of stress generators along the boundary, as shown in Fig. 2.9(b). The stress generators maintain the continuity of the DSC lattice across the interface, as opposed to the crystal lattice in Fig. 2.5(b). The reference lattice is thus the DSC lattice in the present case. The long-range stress field of the bicrystal is then eliminated by introducing a cancelling distribution of stress annihilators, as shown in Fig. 2.9(c). The Burgers vectors of the stress annihilators are DSC lattice vectors: these stress annihilators are, therefore, often called DSC dislocations. The final state, Fig. 2.9(c), being free of long-range stresses, is analogous to Fig. 2.5(d).

The procedure may be readily generalized (Bonnet and Durand 1975, Balluffi *et al.* 1982) to include the near CSL model for a quasiperiodic interface. Two crystals which meet this near CSL criterion are shown in Fig. 2.10, where the black and white crystal lattices are almost commensurate. They almost form a two-dimensional CSL with a corresponding DSC lattice that is periodic in two dimensions. Here, CSL^w and CSL^b are sublattices of the two crystal lattices which are almost identical. If $\mathbf{T}^{(1)}$ is the transformation generating the CSL^b sublattice from the CSl^w sublattice we may apply $\mathbf{T}^{(1)}$ to the white crystal lattice to generate the white′ lattice shown in Fig. 2.10(d). Then it is seen (Figs. 2.10(b,d)) that the black sublattice CSL^b and the sublattice, $CSL^{w'}$, of the white′ lattice form a CSL identical to CSL^b. A periodic DSC lattice is also formed which we label the DSC^b lattice. In a similar manner we may operate on the black lattice with the inverse of $\mathbf{T}^{(1)}$ to produce a black′ lattice which, in concert with the white crystal lattice, produces a CSL identical to CSL^w and a periodic DSC lattice which we label the DSC^w lattice (Figs 2.10(a,c)). Note that the CSL^b may be generated from the CSL^w, or the DSC^b lattice may be generated from the DSC^w lattice, by applying $\mathbf{T}^{(1)}$. We may now choose as a reference structure a specially constructed bicrystal consisting of the white crystal and the black crystal meeting along a periodic interface. The DSC^w lattice will now serve as a common framework across the interface. Using this reference structure we may produce the original quasiperiodic bicrystal by a procedure exactly analogous to those used previously. First we apply the transformation $\mathbf{T}^{(1)}$ to the black crystal elastically to return the black crystal to its original structure. During this process the continuity of the DSC^w lattice is maintained elastically and the interface is coherent. The bicrystal will be associated with a long-range stress field which may be modelled by a continuous distribution of stress generator dislocations in the interface, as shown in Fig. 2.10(e). The long-range elastic field of the interface is eliminated by introducing stress annihilators which have Burgers vectors of the DSC^w lattice (see Fig. 2.10(e)). But because the original interface is quasiperiodic the spacing of the stress annihilators will also be quasiperiodic.

Having related the quasiperiodic reference structure to a periodic reference structure we may now consider the effect of an additional misorientation, $\mathbf{T}^{(2)}$, applied to the black crystal of the quasiperiodic reference structure. Instead of applying only the

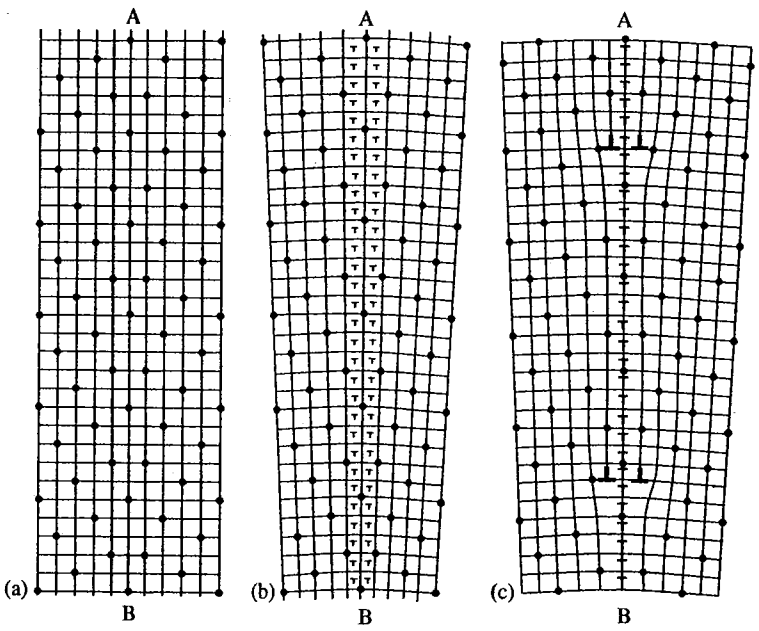

Fig. 2.9 The use of a bicrystal as a reference structure. (a) The reference structure, consisting of a bicrystal containing a $\Sigma = 5$ (210) symmetric tilt boundary along AB; the reference lattice is the $\Sigma = 5$ DSC lattice, also shown. In (b) an additional misorientation $\Delta\theta$ is introduced elastically about the [001] tilt axis. This gives rise to a continuous distribution of stress generator dislocations, which maintain coherency (continuity) of the DSC reference lattice. In (c) an array of discrete stress annihilator dislocations, with Burgers vectors of the DSC lattice, has been introduced which cancels the long-range stresses and which destroys locally the continuity of the reference lattice.

transformation $\mathbf{T}^{(1)}$ to the black crystal of the periodic reference structure, as we did before, we now apply $\mathbf{T}^{(2)}\mathbf{T}^{(1)}$ to it instead. In this way we see that deviations from a quasiperiodic reference structure may always be considered as slightly different deviations from a nearby periodic reference structure.

In all cases considered thus far we began with a reference structure and an associated reference lattice. When the reference structure was a single crystal the reference lattice was the corresponding crystal lattice. When the reference structure was a bicrystal the reference lattice was the corresponding DSC lattice which served as the common framework for the bicrystal. It is obvious that a single crystal may also be regarded as a bicrystal in which the two crystal halves are the same. Similarly a single crystal lattice may be regarded as a DSC lattice of a bicrystal in which there is no change of the crystal lattice across the interface. In this sense a single crystal reference structure and a single crystal reference lattice are special cases of a bicrystal reference structure and a DSC reference lattice. It follows that the reference structure is always a bicrystal, which may happen to be a single crystal, and that the reference lattice is always a DSC lattice, which may happen to be a single crystal lattice.

The array of stress generator dislocations maintained the continuity of the reference lattice across the interface, that is, they maintained the coherency of the interface. In the language of Olson and Cohen (1979), the stress generators are *coherency dislocations*. On the other hand, the stress annihilator dislocations destroyed the continuity of the reference lattice across the interface locally, that is, they destroyed the coherency of the

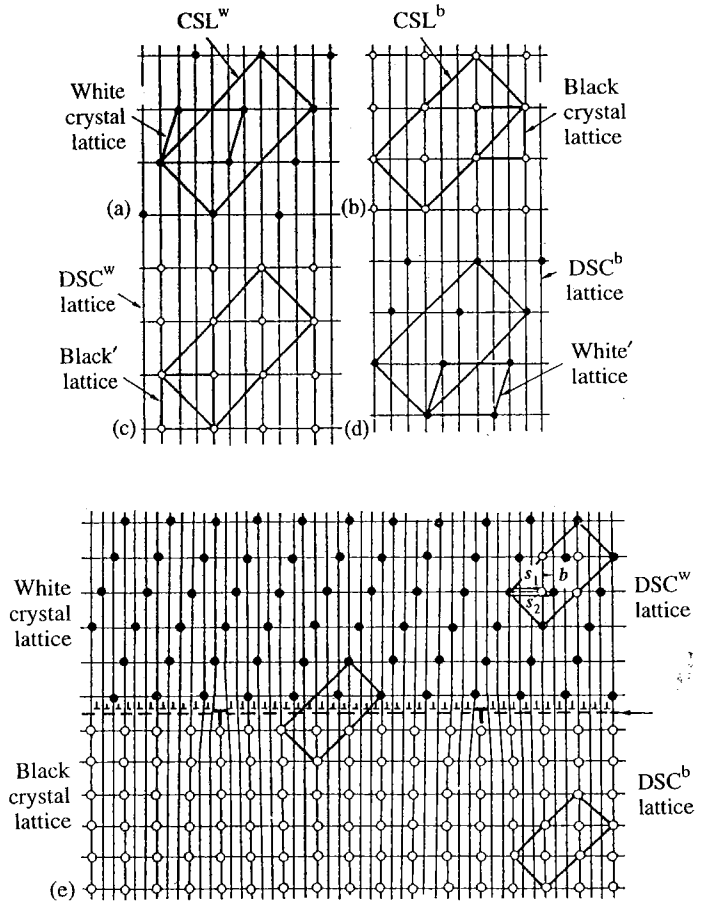

Fig. 2.10 The near CSL model for a quasiperiodic interface. The incommensurate white and black crystal lattices are shown in (a) and (b). The cells labelled CSL^w and CSL^b are nearly commensurate with each other. In (c) the black crystal lattice is deformed slightly to produce the black′ lattice, with the result that the $CSL^{b\prime}$ cell is commensurate with the CSL^w cell and a periodic DSC lattice is produced, labelled DSC^w. Alternatively, in (d), the white lattice is deformed slightly so that the $CSL^{w\prime}$ cell is commensurate with the CSL^b cell and a periodic DSC lattice is produced, labelled DSC^b. Choosing the reference structure to be a bicrystal comprising the white and black′ lattices meeting along a periodic interface, the DSC^w lattice becomes the reference lattice. Allowing the black′ lattice to return to the undeformed black lattice in (e) then introduces a continuous distribution of stress generator dislocations, maintaining the continuity of the DSC^w lattice, with an array of discrete stress annihilator dislocations with Burgers vectors of the DSC^w lattice. (From Balluffi *et al.* (1982).)

interface locally. Olson and Cohen (1979) called the stress annihilators *anticoherency dislocations*. This will serve as a useful further basis for classifying interfacial dislocations throughout the remainder of this book. It obviates the need for introducing a number of the dislocation types listed at the beginning of this section such as, for example, 'virtual' interfacial dislocations. We emphasize that the systematic use of such a method of classification depends upon the clear identification of the assumed reference lattice. Similarly a 'coherent' interface refers to the continuity of a particular reference lattice across the interface. It is noted that in all previous examples the stress generators were

coherency dislocations. However, this need not be the case as will be seen below in other situations.

The above concepts and terminology also allow us to classify interfaces as coherent, semicoherent, or incoherent. At a coherent interface the continuity of the reference lattice, whatever that is chosen to be, is maintained, and there are no anticoherency dislocations. In the limit of an incoherent interface the continuity of the reference lattice is destroyed everywhere along the interface. This limit is reached when the spacing of the anticoherency dislocations is comparable to the width of their cores. In a semicoherent interface the spacing of the anticoherency dislocations is greater than their core width so that significantly large regions of forced elastic coherence exist between successive anticoherency dislocations.

In later chapters we shall see that many of the physical properties of these different types of interfaces differ considerably. For example, in Chapter 9 we shall see that the motion of an interface possessing some degree of coherency often causes a change in the macroscopic shape of the bicrystal. This arises from the maintenance of continuity of the reference lattice across the coherent regions of the interface. On the other hand, no shape change is induced by the motion of an incoherent interface since there is no continuity of the reference lattice to be maintained.

The concepts of 'intrinsic' and 'extrinsic' dislocations in interfaces are related to the concepts of stress generators and annihilators. In the absence of external constraints we do not expect a grain boundary to be associated with a long-range stress field. This is achieved by obtaining an exact balance between the stress annihilator and stress generator Burgers vector densities. These dislocations constitute then the 'intrinsic' dislocation content of the interface. As shown below in Sections 2.3 and 2.5 the Burgers vector density of the intrinsic stress annihilator dislocations (or, alternatively, the negative of the Burgers vector density of the stress generators) of an interface may be deduced from the Frank–Bilby equation.

The concept of an extrinsic dislocation is often associated with a crystal lattice dislocation that enters a grain boundary, which is initially free of long-range stress, as discussed by Hirth and Balluffi (1973) and Dupeux (1987). The dislocation is called extrinsic because it is not part of the intrinsic boundary structure, but is an extra dislocation which entered the boundary from the bulk. More precisely, it is extrinsic because its Burgers vector is not part of the Burgers vector density of the stress annihilators required by the Frank–Bilby equation with the boundary misorientation fixed at its value before the dislocation entered. It is therefore associated with a long-range stress field. However, it becomes part of the intrinsic array once the boundary misorientation, as measured far from the boundary plane, changes slightly. The small change in misorientation is equivalent to a small change in the Burgers vector density of the stress generator array, the integral of which just cancels the change in Burgers vector density of the stress annihilators due to the added dislocation. Once this happens the extrinsic dislocation becomes an intrinsic dislocation and the long-range field associated with it is removed. The distinction between intrinsic and extrinsic dislocations may be difficult to establish experimentally, because it relies on a very accurate measurement of the misorientation far from the boundary plane (see Dupeux 1987). Experimental observations of the conversion of extrinsic dislocations to intrinsic dislocations are described in Section 12.4.

We may illustrate many of the concepts described in this section with the example of the interfaces associated with mechanical twins in f.c.c. crystals. It is well known (Christian 1981) that such twinning takes place on (111) planes with a shear of $2^{-\frac{1}{2}}$ in

a $[11\bar{2}]$ direction. Also, this is achieved by gliding interfacial dislocations, with $\boldsymbol{b} = \frac{1}{6}[11\bar{2}]$, on successive (111) planes, as shown schematically in Fig. 2.7. Each of these dislocations is associated with a boundary step of height equal to one (111) spacing as seen in Fig. 2.8(d). Consider first the nature of these dislocations. We begin by taking the reference structure to be the single crystal (Fig. 2.8(a)) and the transformation, **T**, to be the above shear. We then cut it along **AB** and transform the lower half by **T**. As seen in Fig. 2.8(b) the two crystal halves are no longer commensurate along **AB**. (In the language of deformation twinning the plane **AB** is not an invariant plane of the shear transformation.) In order to join the crystal halves together commensurately, so that the single crystal reference lattice is continuous across the interface, and the interface is coherent, it is necessary to introduce a distribution of stress generators (coherency dislocations) along **AB**, as in Fig. 2.8(c). The interface is now associated with a long-range stress field. Because the coherent interface has a particularly low energy when it lies on the (111) plane the coherency dislocations localize as shown in Fig. 2.8(d). The localized step seen in Fig. 2.8(d) is thus associated with a discrete $\frac{1}{6}[11\bar{2}]$ coherency dislocation. If a train of such dislocations were present, as in Fig. 2.7 and 2.11(a), the longe-range stress field of the interface could be cancelled by introducing crystal lattice dislocations (which would be classified as stress annihilator or anticoherency dislocations) of total Burgers vector $-\frac{1}{2}[11\bar{2}]$ for every three coherency dislocations. These could be $\frac{1}{2}[\bar{1}01]$ and $\frac{1}{2}[0\bar{1}1]$ crystal lattice dislocations, for example, as shown schematically in Fig. 2.11(a).

If these dislocations group together so that for every three coherency dislocations there are two anticoherency dislocations, line defects of the type shown in Fig. 2.11(b) will be formed. These line defects have no net Burgers vector content and, hence, are pure steps of height three (111) spacings. However, the reference lattice, i.e. the crystal lattice, is discontinuous at the pure step owing to its anticoherency dislocation content, and the interface is, therefore, semicoherent. If a large number of such steps accumulate, a giant step will be formed which would then more appropriately be regarded as a vertical segment of a symmetric tilt boundary running parallel to $(11\bar{2})$ with the intrinsic stress generator and stress annihilator content shown in Fig. 2.11(c).

Let us now consider the same boundary but with the $\Sigma = 3$ DSC lattice as the reference lattice, rather than either crystal lattice. The boundary belongs to the $\Sigma = 3$ coincidence system because it may be created by a rotation of $\cos^{-1}\frac{1}{3}$ about the $[1\bar{1}0]$ axis. Both the CSL and DSC lattice are shown in Fig. 2.12(a). The dislocation shown previously in Fig. 2.8(d) can now be introduced by a Volterra cut and displacement procedure in the DSC lattice to produce the configuration shown in Fig. 2.12(b) which is exactly the same physical object as that shown in Fig. 2.8(d). The dislocation shown in Fig. 2.12(b) has destroyed locally the continuity of the reference DSC lattice across the interface. Therefore, in the framework of the DSC lattice the dislocation is of the anticoherency type, although it is still a stress generator. Furthermore, the interface must now be regarded as semicoherent.

Consider next the configuration shown in Fig. 2.11 where stress annihilator lattice dislocations have been added in order to eliminate the long-range stresses produced by the stress generators. These dislocations will also disrupt the continuity of the reference lattice (i.e. the DSC lattice) and, hence, they must be classified as anticoherency, stress annihilator dislocations. But, if we gather these dislocations up to form a step of the type shown in Fig. 2.11(b), we obtain the step configuration shown in Fig. 2.12(c). The atomic configuration at the step in Fig. 2.12(c) is the same as that shown in Fig. 2.11(b) but it is shown in the framework of the DSC lattice as the reference lattice, rather than the

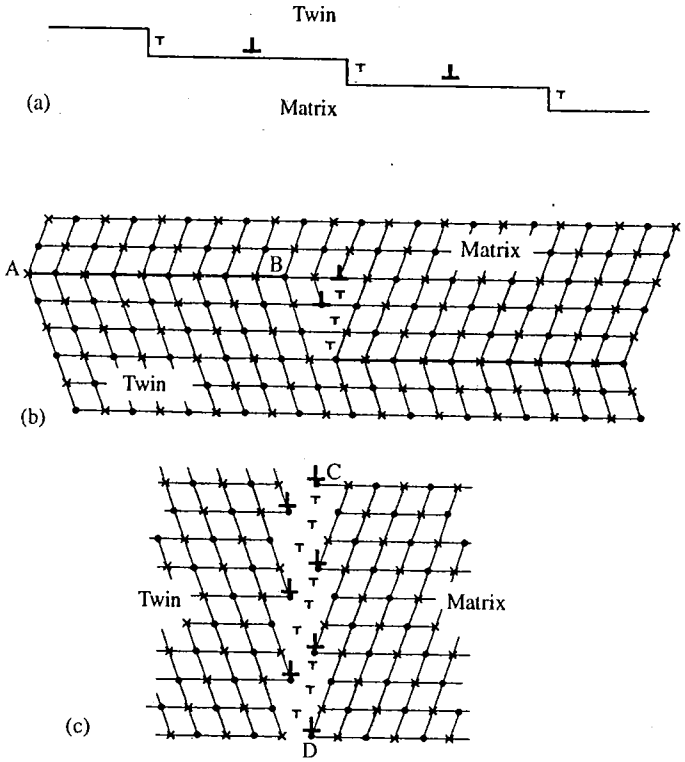

Fig. 2.11 (a) An interface between a deformation twin and matrix in an f.c.c. lattice, inclined to the (111) invariant plane, in which the stress fields of the stress generator (or coherency) dislocations associated with the steps in the interface are cancelled by crystal lattice (or anticoherency) dislocations. (b) A pure step of 3 (111) planes height in the matrix–twin interface formed by grouping together 3 coherency dislocations and two cancelling crystal lattice anticoherency dislocations. (c) A segment of the $(11\bar{2})$ symmetric tilt boundary formed by running together pure steps of the type shown in (b). With respect to the matrix (or twin) reference crystal lattice the $(11\bar{2})$ boundary is classified as incoherent.

crystal lattice as reference. Again, the total Burgers vector content of the step is zero, and furthermore the anticoherency effects of the stress generators and stress annihilators just cancel so that the continuity of the DSC lattice at the step is maintained. Therefore, with the DSC lattice as the reference lattice, both the step and the interface are coherent. Again, an accumulation of a large number of such steps would form a symmetric tilt boundary segment parallel to $(11\bar{2})$ as shown in Fig. 2.12(d). The boundary in Fig. 2.12(d) is the same physical object as that shown in Fig. 2.11(c). However, in the DSC reference lattice framework of Fig. 2.12(d) we must regard it as a coherent interface devoid of any net dislocation content. It could be generated from the reference bicrystal (Fig. 2.12(a)) by simply rotating the boundary plane from (111) to $(11\bar{2})$ by a process of shuffling atoms within the framework of the CSL without the introduction of any dislocations. Even more simply, it could be adopted as a reference structure itself, that is, a coherent bicrystal in the $\Sigma = 3$ DSC lattice with its interface parallel to $(11\bar{2})$.

Our example of a (111) twin boundary demonstrates that the same physical dislocation may be classified as either coherency or anticoherency, depending on the choice of reference lattice. It is therefore necessary to specify the choice of reference lattice when

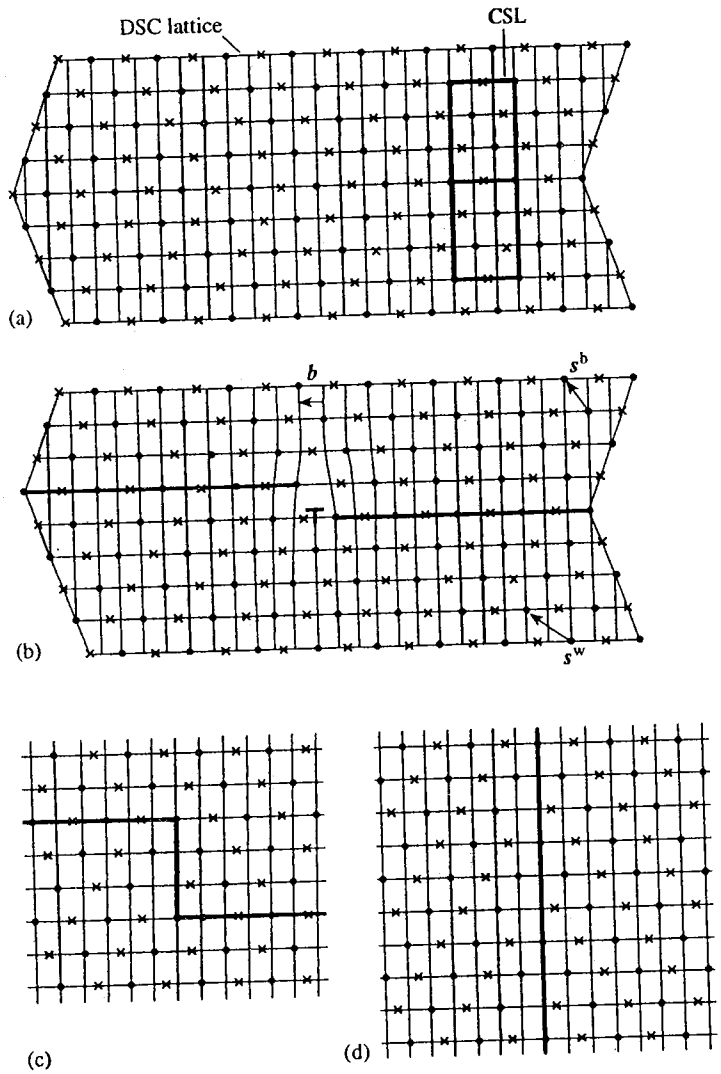

Fig. 2.12 (a) The (111) interface between matrix and twin in an f.c.c. lattice showing the $\Sigma = 3$ DSC lattice and two cells of the $\Sigma = 3$ CSL. (b) The same $\frac{1}{6}[11\bar{2}]$ stress generator dislocation as seen in Fig. 2.8(d), and the step vectors s^b and s^w. This dislocation destroys the continuity of the $\Sigma = 3$ DSC reference lattice, and it is now therefore classified as anticoherency. (c) The same pure step as seen in Fig. 2.11(b), but now in the framework of the $\Sigma = 3$ DSC reference lattice: note the continuity of the DSC lattice. (d) The same $(11\bar{2})$ boundary as shown in Fig. 2.11(c) showing the continuity of the $\Sigma = 3$ DSC lattice across the interface. With respect to the $\Sigma = 3$ DSC reference lattice the $(11\bar{2})$ boundary is coherent.

classifying dislocations as coherency or anticoherency, in the same way as it is when classifying interfaces as coherent, semicoherent, or incoherent.

2.3 THE FRANK-BILBY EQUATION

Frank (1950) and Bilby (1955) addressed the following question: given an affine transformation relating two lattices, what is the Burgers vector density that is required to make

the two lattices fit together compatibly at the interface? In general, when one lattice is acted on by the transformation, overlapping regions and/or gaps are produced at the interface, as already seen in Figs 2.5 and 2.6. In other words, the interface is not, in general, an invariant plane of the transformation. To remove the incompatibilities between the lattices, dislocations are required in the interface. We may take these to be stress annihilators for reasons that are described below. Once the incompatibilities are removed the bicrystal is free of stress far from the interface. Frank–Bilby theory provides the net Burgers vector, $\boldsymbol{B}$, of the stress annihilators crossing a vector $\boldsymbol{p}$ lying in the interface. Since the total Burgers vector content of the stress generators is just the negative of that of the stress annihilators, we may also recover $\boldsymbol{B}$ for the stress generators. The resolution of $\boldsymbol{B}$ into Burgers vectors of individual dislocations is not unique geometrically and may be without physical significance if $|\boldsymbol{B}|$ is large. In any event the interface may always be described as a 'surface dislocation', which is a single entity that is characterized by a second rank tensor. There are two methods of deriving the main result: one using a Burgers circuit construction and the other is based on the theory of continuous distributions of dislocations. Both methods are instructive in that they illustrate different aspects of the theory, and we shall develop them both. Our treatment follows Christian (1981).

Consider two lattices which meet along a flat interface, with normal $\hat{\boldsymbol{n}}$. Let the lattices on the positive and negative sides of the normal $\hat{\boldsymbol{n}}$ be coloured black and white. In general the lattices are not identical and there is a misorientation between them. The two lattices are considered to be generated from a reference lattice by affine transformations $\mathbf{S}^{\mathrm{b}}$ and $\mathbf{S}^{\mathrm{w}}$. In accordance with the discussion of Section 2.2 the two lattices may be black and white crystal lattices or $\mathrm{DSC}^{\mathrm{b}}$ and $\mathrm{DSC}^{\mathrm{w}}$ lattices (see Fig. 2.10), depending on whether we are working with a single crystal or bicrystal reference structure. The corresponding reference lattice would then be either the lattice of the white crystal or the $\mathrm{DSC}^{\mathrm{w}}$ lattice. In cases where the two lattices may be related by a pure rotation, as in the case of grain boundaries in cubic materials, the reference lattice could be the same lattice at a median orientation, i.e. a median lattice. In the language of the crystallographic theory of martensite, $\mathbf{S}^{\mathrm{b}}$ and $\mathbf{S}^{\mathrm{w}}$ are the lattice deformations. They are represented by 3×3 matrices, and for a grain boundary in a cubic material they are usually rotation matrices. When $\mathbf{S}^{\mathrm{b}}$ acts on the components of a vector of the reference lattice it transforms the components into those of a vector in the black lattice, and similarly for $\mathbf{S}^{\mathrm{w}}$. Let the reference and black and white lattices share a common origin at O, see Fig. 2.13. Here we are disregarding any relative displacement of the black and white lattices, since it does not affect the result. Let $\mathbf{OP} = \boldsymbol{p}$ be a *large* vector in the boundary, and consider a right-handed Burgers circuit $\mathrm{PA_1OA_2P}$, as shown in Fig. 2.13. The vector $\boldsymbol{p}$ must be large compared with any substructure within the interface, e.g. vicinal steps or twins emanating from the interface into the adjoining crystals. The corresponding path $\mathrm{Q_1B_1OB_2Q_2}$ in the reference lattice is obtained by applying the inverse transformations $\mathbf{S}^{\mathrm{b}-1}$ and $\mathbf{S}^{\mathrm{w}-1}$ to the parts $\mathrm{PA_1O}$ and $\mathrm{OA_2P}$ of the circuit respectively. The closure failure in the reference lattice, using the FS/RH convention, is $\mathrm{Q_2Q_1} = \mathrm{OQ_1} - \mathrm{OQ_2} = (\mathbf{S}^{\mathrm{b}-1} - \mathbf{S}^{\mathrm{w}-1})\boldsymbol{p}$. This is the net Burgers vector of stress annihilators crossing the interfacial vector $\boldsymbol{p}$:

$$\boldsymbol{B} = (\mathbf{S}^{\mathrm{b}-1} - \mathbf{S}^{\mathrm{w}-1})\boldsymbol{p}. \tag{2.1}$$

Equation (2.1) was first derived by Frank (1950) for grain boundaries and it was generalized to heterophase boundaries by Bilby (1955). It is known as the Frank–Bilby equation. Note that the Burgers vector $\boldsymbol{B}$ is expressed in the coordinate system of the

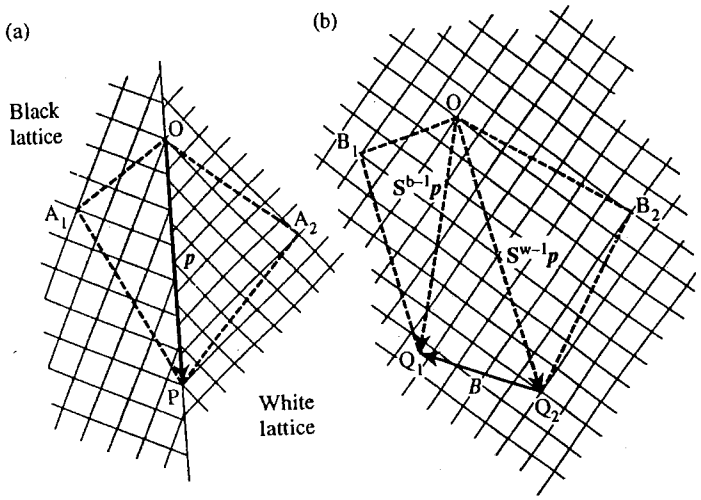

Fig. 2.13 The derivation of the Frank–Bilby equation. (a) A closed right-handed circuit PA_1OA_2P enclosing the interface vector p is mapped in (b) onto a reference lattice where it becomes the path $Q_1B_1OB_2Q_2$ with closure failure Q_2Q_1. (From Christian (1981).)

reference lattice. For example, if the black lattice is selected as the reference lattice, eqn (2.1) becomes

$$\boldsymbol{B} = (\mathbf{E} - \mathbf{S}^{w-1})\boldsymbol{p}, \tag{2.2}$$

where $\mathbf{E}$ is the identity matrix. We shall derive the more popular 'Frank formula' for grain boundaries from eqn (2.1) in Section 2.5.

If the net dislocation content $\boldsymbol{B}$ did not exist in the interface, the vectors $\mathbf{S}^{b-1}\boldsymbol{p}$ and $\mathbf{S}^{w-1}\boldsymbol{p}$ would be brought into parallel alignment in the interface, along $\boldsymbol{p}$, only by straining the black and white lattices elastically. The interface would then be in a state of forced elastic coherence, and it would be associated with a long-range stress field. This state is modelled, as previously, by a uniform and continuous distribution of stress generator dislocations at the interface. The Burgers vector density of this array is the negative of $\boldsymbol{B}$, i.e. $-(\mathbf{S}^{b-1} - \mathbf{S}^{w-1})\boldsymbol{p}$. This is the reason why we identify the dislocations, whose Burgers vector density is predicted by the Frank–Bilby equation, as stress annihilators. The notion of compatibility is defined more precisely in the second derivation of the Frank–Bilby equation which we move on to now.

We begin with the concept of the continuously dislocated state of a lattice. Consider an element of a lattice containing several dislocation lines. The dislocations are discrete objects but we obtain a convenient mathematical description by imagining that the number of dislocation lines of each type tends to infinity while the Burgers vectors of each tends to zero in such a way that the product remains constant. The continuous dislocation distribution that we obtain is characterized by a tensor $\alpha_{ij}(\boldsymbol{r})$, which defines the net Burgers vector in the x_i direction at $\boldsymbol{r}$ of dislocations threading through a surface element of unit area perpendicular to the x_j axis. Let C be a closed curve bounding an area A and let S be any cap ending on C. Conservation of Burgers vector requires that the resultant Burgers vector of dislocations threading through A must equal the resultant Burgers vector of dislocations threading through S. Thus the resultant Burgers vector threading through A is given by

$$b_i = \iint_S \alpha_{ij}\, \mathrm{d}S_j, \tag{2.3}$$

and b_i is independent of the choice of S. Summation over $j = 1, 2, 3$ is implied by the repeated suffix convention in eqn (2.3) and elsewhere in this chapter, except where explicitly stated. When we have a continuous distribution of dislocations there is no longer 'good lattice' in which to make a Burgers circuit in order to define the resultant Burgers vector. Bilby *et al.* (1955) showed how this difficulty may be overcome by making use of a local correspondence between the real lattice and a reference lattice. As we have already discussed in Section 1.7 the same difficulty arises in defining the Burgers vectors of interfacial dislocations in densely spaced arrays.

At any point of the real lattice choose three independent basis vectors, $\boldsymbol{a}_i^{\mathrm{c}}$, which correspond to a set of basis vectors, $\boldsymbol{a}_i^{\mathrm{r}}$, of the reference lattice. The local vectors $\boldsymbol{a}_i^{\mathrm{c}}$ may be regarded as being generated from the reference vectors $\boldsymbol{a}_i^{\mathrm{r}}$ at each point of the lattice by a local deformation:

$$\boldsymbol{a}_i^{\mathrm{c}} = D_{ij}\, \boldsymbol{a}_j^{\mathrm{r}}. \tag{2.4}$$

The components D_{ij} vary from point to point in the lattice. Clearly it is necessary that throughout the dislocated lattice we consistently relate the same crystallographic vectors $\boldsymbol{a}_i^{\mathrm{c}}$ to the reference vectors $\boldsymbol{a}_i^{\mathrm{r}}$. The vectors $\boldsymbol{a}_i^{\mathrm{c}}$ define local variations in the lattice, although to an observer moving in the real lattice the local $\boldsymbol{a}_i^{\mathrm{c}}$ vectors are everywhere parallel, and any two parallel vectors, defined by reference to the local lattice, have the same $\boldsymbol{a}_i^{\mathrm{c}}$ components.

Let $\hat{\boldsymbol{e}}_i$ be a set of fixed orthonormal vectors. With respect to a Cartesian frame aligned along the $\hat{\boldsymbol{e}}_i$ a displacement in the real lattice from x_i to $x_i + \mathrm{d}x_i$ can be written as the vector $\mathrm{d}x_i\hat{\boldsymbol{e}}_i$. If C is a small closed circuit in the real lattice we have

$$\int_C \mathrm{d}x_i \hat{\boldsymbol{e}}_i = \boldsymbol{0}. \tag{2.5}$$

Let the vectors $\boldsymbol{d}_i$ be obtained from the vectors $\hat{\boldsymbol{e}}_i$ by the local deformation $\mathbf{D}$, i.e. $\boldsymbol{d}_i = \mathbf{D}_{ij}\hat{\boldsymbol{e}}_j$. Then eqn (2.5) becomes

$$\int_C \mathrm{d}x_i \mathrm{D}_{ij}^{-1}\, \boldsymbol{d}_j = \boldsymbol{0}. \tag{2.6}$$

We now require the closure failure of the corresponding circuit in the reference lattice. Each vector $\boldsymbol{d}_k$ of the real lattice, is replaced by its corresponding vector, $\hat{\boldsymbol{e}}_k$, in the reference lattice, and the closure failure giving the net Burgers vector of the distribution encircled by C is the vector sum of the reference lattice displacements, i.e.

$$\boldsymbol{b} = -\int_C \mathrm{d}x_i D_{ij}^{-1}\, \hat{\boldsymbol{e}}_{\mathrm{j}}. \tag{2.7}$$

The minus sign is inserted in eqn (2.7) to be consistent with the FS/RH convention (Hirth and Lothe 1982). In order to compare directly with eqn (2.3) we use Stokes' theorem to transform the line integral in eqn (2.7) into a surface integral over any cap S having C as its limit. Stokes' theorem may be stated as follows:

$$\int_C f_i \mathrm{d}x_i = \iint_S \varepsilon_{ijk} \frac{\partial f_k}{\partial x_j}\, \mathrm{d}S_i, \tag{2.8}$$

where f_i is a differentiable vector function, ε_{ijk} is the permutation tensor of eqn (1.12), and dS_i denotes the ith component of the unit normal to the surface multiplied by the element of area dS. Applying Stokes' theorem to eqn (2.7), by identifying f_i with $D_{ij}^{-1}\hat{\boldsymbol{e}}_j$, we obtain

$$\begin{aligned}\boldsymbol{b} &= -\int\int_S \varepsilon_{imn}\frac{\partial D_{nj}^{-1}}{\partial x_m}\hat{\boldsymbol{e}}_j\,dS_i \\ &= -\int\int_S \varepsilon_{jmn}\frac{\partial D_{ni}^{-1}}{\partial x_m}\hat{\boldsymbol{e}}_i\,dS_j.\end{aligned} \tag{2.9}$$

Comparing eqns (2.3) and (2.9) we see that

$$\alpha_{ij} = -\varepsilon_{jmn}\frac{\partial D_{ni}^{-1}}{\partial x_m}. \tag{2.10}$$

This equation shows us how to evaluate the dislocation tensor at each point in the continuously dislocated lattice even though there is no good material to construct an ordinary Burgers circuit. Imagine the reference lattice is cut into small volume elements, each of which is then given the local deformation D_{ij}. If the separate elements can be glued back together contiguously, without any holes or overlapping regions, so at to form a continuous lattice in ordinary space, the deformations are said to be *compatible*, and a continuous deformation field exists. Small lattice vectors about a point in the real lattice may be written as $dy_i\boldsymbol{d}_i$, where dy_i is a system of local coordinates based on the vectors $\boldsymbol{d}_i$. Since $\boldsymbol{d}_i = D_{ij}\hat{\boldsymbol{e}}_j$, the relation between the local and reference coordinates may be obtained from $dy_i\boldsymbol{d}_i = dy_iD_{ij}\hat{\boldsymbol{e}}_j = dx_j\hat{\boldsymbol{e}}_j$, implying that

$$dx_i = D_{ij}dy_j,\ dy_i = D_{ji}^{-1}dx_j. \tag{2.11}$$

In order for the deformation field D_{ij} to be compatible it is necessary and sufficient that the values of y_i at any point Q may be found from their values at any other point P by integrating $dy_i = D_{ji}^{-1}dx_j$ along *any* path from P to Q. For the integral to be independent of the path from P to Q it is necessary and sufficient that

$$\frac{\partial D_{ni}^{-1}}{\partial x_k} = \frac{\partial D_{ki}^{-1}}{\partial x_n}. \tag{2.12}$$

We see from eqn (2.10) that this corresponds to zero dislocation density. Thus *the condition for compatibilility is the absence of dislocations*. Conversely, when the local deformations of the separate volume elements are not compatible, dislocations are required to fit these elements together.

Now suppose that we have a continuous distribution of dislocations specified by the tensor α_{ij} and concentrate all the dislocations into a shell of thickness t so that α_{ij} vanishes outside the shell. Let t tend to zero and α_{ij} tend to infinity in such a way that the product $t\alpha_{ij}$ remains finite and tends to β_{ij}. β_{ij} is called the *surface dislocation tensor*. This limiting process means that the deformation field D_{ij} is constant outside the shell and equal to $(D^{\mathrm{b}})_{ij}$ and $(D^{\mathrm{w}})_{ij}$ above and below the shell. The deformation field changes from $(D^{\mathrm{b}})_{ij}$ to $(D^{\mathrm{w}})_{ij}$ through the shell. Consider a Burgers circuit that is intersected by the shell as shown in Fig. 2.14. The Burgers vector of the circuit can be written as $b_i = -\int_c(dy_i - dx_i)$ since this is just the negative of the difference in the circuits in the real and reference lattices. Using eqn (2.11) this may be rewritten as

$$b_i = -\int_C(\delta_{ij} - D_{ji})\,dy_j \tag{2.13}$$

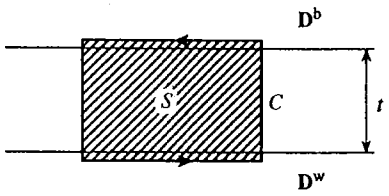

Fig. 2.14 The circuit C enclosing the shaded area S which intersects a shell of thickness t containing, and parallel to, the final interface. Across the shell the deformation tensor changes from $\mathbf{D}^b$ above to $\mathbf{D}^w$ below.

where the the circuit C is carried out in the real lattice, as in Fig. 2.14. Using Stokes' theorem this line integral may be converted into a surface integral:

$$b_i = \int\int_S \varepsilon_{jkn} \frac{\partial D_{ni}}{\partial y_k} \mathrm{d}S_j, \tag{2.14}$$

where the surface S is any surface bounded by the circuit C. Choosing the shaded area in Fig. 2.14 as the surface S and noting that, for small t,

$$\frac{\partial D_{ni}}{\partial y_k} = \frac{(D^b)_{ni} - (D^w)_{ni}}{t} n_k, \tag{2.15}$$

we find that

$$b_i = \int\int_S \varepsilon_{jkn} \frac{(D^b)_{ni} - (D^w)_{ni}}{t} n_k \, \mathrm{d}S_j, \tag{2.16}$$

and therefore

$$\beta_{ij} = \lim_{t \to 0}(t\alpha_{ij}) = \varepsilon_{jkn}((D^b)_{ni} - (D^w)_{ni})n_k. \tag{2.17}$$

It is important to note that $\mathbf{D}^b$ and $\mathbf{D}^w$ gave the relations between the basis vectors of the black and white lattices and the reference lattice, whereas $\mathbf{S}^b$ and $\mathbf{S}^w$ transformed the components of a reference lattice vector into those of a vector in the black and white lattices. Therefore $\mathbf{S}^{b-1} = (\mathbf{D}^b)^t$ and $\mathbf{S}^{w-1} = (\mathbf{D}^w)^t$ (see Section 1.3.2) and eqn (2.17) may be rewritten as follows:

$$\beta_{ij} = \varepsilon_{jkn}((\mathbf{S}^{b-1})_{in} - (\mathbf{S}^{w-1})_{in})n_k. \tag{2.18}$$

Now consider the resultant Burgers vector of dislocations which cross a small area of the shell defined by the vector $\boldsymbol{p}$ and the vector thickness $t\hat{\boldsymbol{n}}$. The normal to this area has components $\mathrm{d}S_j = t\varepsilon_{jab}p_a n_b$ and substituting this in eqn (2.16) we obtain

$$\begin{aligned} b_i &= \varepsilon_{jkn} \frac{(\mathbf{D}^b)_{ni} - (\mathbf{D}^w)_{ni}}{t} n_k t\varepsilon_{\mathrm{jab}} p_a n_b \\ &= \varepsilon_{jkn}\varepsilon_{jab}((\mathbf{D}^b)_{ni} - (\mathbf{D}^w)_{ni})p_a n_b n_k \\ &= (\delta_{ka}\delta_{nb} - \delta_{kb}\delta_{na})((\mathbf{D}^b)_{ni} - (\mathbf{D}^w)_{ni})p_a n_b n_k \\ &= ((\mathbf{D}^b)_{ni} - (\mathbf{D}^w)_{ni})p_n \\ &= ((\mathbf{S}^{b-1})_{in} - (\mathbf{S}^{w-1})_{in})p_n, \end{aligned} \tag{2.19}$$

where we have used $\boldsymbol{p}\cdot\hat{\boldsymbol{n}} = 0$, which follows when $t \to 0$. Thus we have rederived the Frank–Bibly equation, eqn (2.1). The derivation shows explicitly that the Burgers vector density given by eqn (2.1) is such as to make the black and white lattices compatible in the interface.

From eqns (2.16) and (2.17) we see that the surface dislocation tensor β_{ij} gives the ith component of the resultant Burgers vector of dislocation lines cutting unit length in the surface perpendicular to the jth direction. The interface may be thought of as a single entity called a *surface dislocation*, characterized by the tensor β_{ij}. The tensor β_{ij} is the analogue for a surface dislocation of the Burgers vector for a line dislocation. Moreover, whereas a line dislocation may be defined as a line discontinuity separating areas in the slip plane where the amount of slip is different, a surface dislocation is a surface discontinuity separating volumes of material where the lattice deformation is different. This concept, which was introduced by Bilby (1955), is central to the crystallographic theory of martensitic transformations and deformation twinning developed by Bullough and Bilby (1956).

2.4 COMMENTS ON THE FRANK-BILBY EQUATION AND THE DISLOCATION CONTENT OF AN INTERFACE

The Frank–Bilby equation is the cornerstone of many attempts to account for the line defects that are observed in the electron microscope at grain boundaries and especially at heterophase boundaries. In this section we shall discuss some complicating aspects of the theory in more detail.

The first point to note is that it is a continuum theory. The nature of the adjoining black and white crystal or DSC lattices is taken into account only in the choices of unit cells that are assumed to be related to some unit cell of the reference lattice. These choices establish $\mathbf{S}^{\mathrm{b}}$ and $\mathbf{S}^{\mathrm{w}}$, and together with the interface normal they determine the surface dislocation tensor in eqn (2.18). The point group and translational symmetries of the adjoining crystals are not built into the theory, and the surface dislocation tensor is not invariant with respect to these symmetry operations. For example, if $\mathbf{S}^{\mathrm{b}}$ is replaced by where $\mathbf{U}^{\mathrm{b}}\mathbf{S}^{\mathrm{b}}$, where $\mathbf{U}^{\mathrm{b}}$ is a point group operation of the black lattice, or a unimodular matrix which effects a change in the unit cell of the black lattice to be related to the reference lattice, the surface dislocation tensor changes in general. Yet the dichromatic pattern is completely unaffected by this replacement (see Section 1.5.4), and therefore the atomic structure of the interface is unaffected also.

The reason why the theory is not invariant with respect to different choices of $\mathbf{U}^{\mathrm{b}}$ (or $\mathbf{U}^{\mathrm{w}}$) is clear from an examination of the Burgers circuit construction in Fig. 2.13. Each $\mathbf{U}^{\mathrm{b}}$ produces a different circuit $\mathrm{Q_1B_1O}$ in the reference lattice, and hence a different closure failure $\mathrm{Q_2Q_1}$. The fact that the infinite lattices generated with and without $\mathbf{U}^{\mathrm{b}}$ are equivalent, in type and orientation, is not reflected automatically by the theory. As an example, consider a 'grain boundary' obtained by a 120° rotation about a [111] axis in a cubic lattice. Since the [111] axis has three-fold symmetry this large-angle boundary is nothing more than a perfect single crystal, yet it would be described by a high-density of crystal lattice dislocations on the 'boundary plane'. The origin of the ambiguity in the dislocation description of an interface can be traced back to eqn (2.4) which defines the local deformation D_{ij}. This is the device that Bilby *et al.* (1955) introduced to define a Burgers vector in a continuously dislocated lattice. In eqn (2.4) D_{ij} may be replaced by $U_{ik}^{-1}D_{kj}$ where $\mathbf{U}$ is a unimodular matrix that describes local point symmetry operations of the dislocated crystal, or effects different choices of unit cell

vectors $\boldsymbol{c}_i$. To a local observer in the dislocated crystal **U** is a constant matrix, but to an external observer **U** is a function of position. The dislocation tensor α_{ij} in eqn (2.10) is thus also affected by different choices of **U**.

There is an infinite number of unimodular matrices and therefore *there is an infinite number of dislocation descriptions of a particular interface.* However, *all* dislocation descriptions of a particular interface are *descriptions of a unique physical object* with a particular atomic structure and energy in its fully relaxed state, and in an *exact* theory, involving full atomic relaxation, all these descriptions would yield identical atomic structures, energies, and elastic fields!

The classic example of this unsatisfactory aspect of dislocation models of interfaces is the symmetrical tilt grain boundary. The relationship between the crystal lattices may be described as (i) a rotation about an axis in the boundary plane as in the usual tilt boundary description, (ii) a simple shear on the boundary plane, as in a deformation twin, or (iii) as a 180° rotation about the boundary normal, corresponding to a 180° twist boundary. This is illustrated in Fig. 2.15. There is an infinity of other descriptions. According to (i) the resultant crystal lattice dislocation content of the boundary consists of a single array of edge dislocations, with Burgers vectors normal to the boundary plane. Since the crystal lattices are fully compatible with each other on the shear plane, i.e. the boundary plane, there is no resultant dislocation content in the boundary for the second description. In the third description the boundary would be described by a dense network of screw dislocations forming a 180° twist boundary. Again, the same atomic structure would be produced after full relaxation of the boundary, for all these boundary models, that is, the final boundary structure would be independent of the route taken to generate it geometrically.

As a specific example, consider again the (111) $\Sigma = 3$ twin boundary illustrated previously in Figs 2.8 and 2.11. There we assumed that the transformation, **T**, relating the crystal lattices was a shear parallel to (111). Hence the section of boundary along AB in Fig. 2.11(b) was devoid of any dislocation content. On the other hand, the segment parallel to $(11\bar{2})$ along CD in Fig. 2.11(c) possessed the crystal lattice dislocation content shown. If instead we now assume that the transformation, **T**, relating the crystal lattices is a rotation of $\cos^{-1}\frac{1}{3} \simeq 70.5°$ around $[1\bar{1}0]$, and follow the procedure shown in Fig. 2.5, we obtain the crystal lattice dislocation structures shown along AB and CD in Figs 2.16(a,b) for these two boundary segments. Very different dislocation structures are therefore obtained for these identical physical objects.

We are therefore faced with the rather unsatisfactory question of whether any of the possible dislocation descriptions is in some sense preferable to all the others. It is tempting to adopt as the 'best' description the one which corresponds to the smallest dislocation content, since this would presumably be the simplest. But, according to this criterion, the best description of a symmetrical tilt boundary would correspond to zero dislocation content regardless of the tilt angle. However, at small tilt angles experimental observations reveal an array of discrete line singularities which can be identified as crystal lattice edge dislocations corresponding to description (i) above. The presence of these line singularities cannot be accounted for by description (ii), and their origin would have to be attributed to some form of local relaxation in the boundary, which does not relieve any incompatibility. We emphasize that both descriptions apply to the same physical object consisting of atoms arranged in a particular configuration.

Cases where there is justification for choosing a particular $\mathbf{S}^b$ and $\mathbf{S}^w$ occur when migration of the interface leads to a change of shape of the bicrystal as a result of the conservative motion of interfacial dislocations, as discussed in Chapter 9 (see Table 9.2).

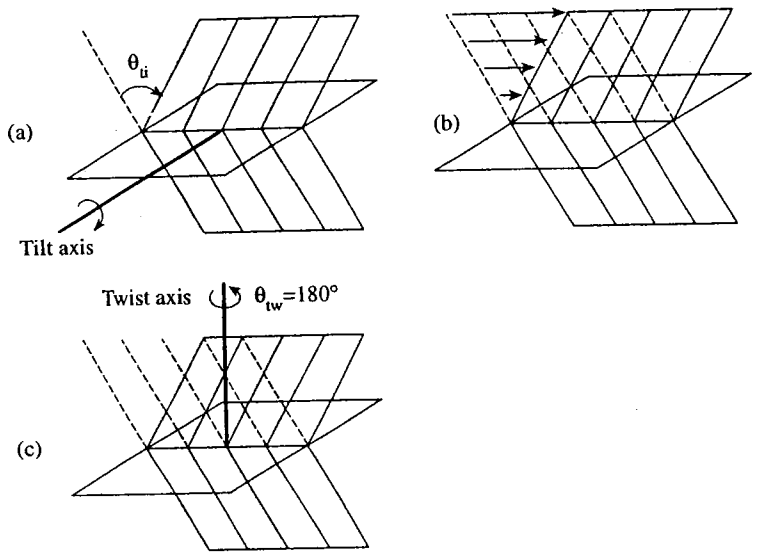

Fig. 2.15 Diagram showing that a symmetric tilt boundary may be regarded as either (a) a tilt boundary of misorientation θ_{ti}, or (b) a deformation twin boundary created by a simple shear on the boundary plane, or (c) a 180° twist boundary.

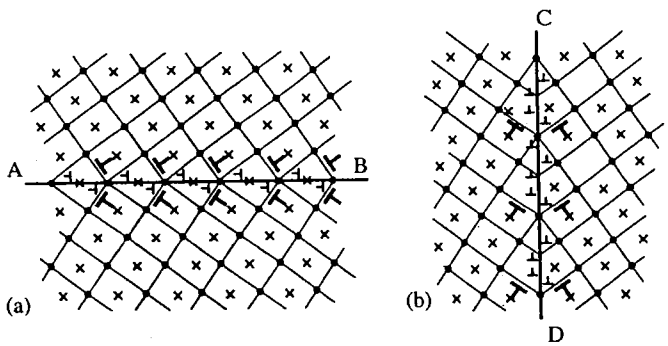

Fig. 2.16 (a) The (111) twin boundary shown in Fig. 2.11(b) and 2.12(a) regarded as a symmetric tilt boundary of misorientation ≃70.5°. The $(11\bar{2})$ boundary shown in Figs 2.11(c) and 2.12(d) is now regarded as a symmetric tilt boundary of misorientation ≃70.5°. Note the differences in the dislocation descriptions for the same interfaces.

In that case $\mathbf{S}^b$ and $\mathbf{S}^w$ describe how planes and directions of one lattice are transformed (at least locally) at the interface into planes and directions of the other lattice. This is the case in martensitic transformations and deformation twinning, where there is a local correspondence between unit cells of either crystal that is determined by local atomic movements as the interface migrates. It is also the case in the glissile motion of a small-angle tilt grain boundary as discussed in Section 9.2.1.1. The success of the crystallographic theory of martensite (Bullough and Bilby 1956) is to determine $\mathbf{S}^b$ and $\mathbf{S}^w$, the macroscopic shape change, the Burgers vector content of the interface, and the interface plane self-consistently (see Section 9.2.1.3).

We have described one source of ambiguity in the dislocation description of an interface arising from the infinity of descriptions of $\mathbf{S}^b$ and $\mathbf{S}^w$ for a given choice of reference lattice. Another source of ambiguity is the choice of reference structure. An example has already been given in Section 2.2 where a comparison was made of the dislocation descriptions that are derived for a grain boundary using either a single crystal or a bicrystal as the reference structure. Useful reference structures are often interfaces in which one or two directions are nearly commensurate in both crystal lattices enabling near-CSLs to be generated. In many cases, especially for heterophase interfaces, a variety of possible choices of a near-CSL exists (Balluffi *et al.* 1982). However, the appropriate choice of reference structure is the one for which the experimentally observed dislocations in the interface have Burgers vectors of the corresponding reference lattice. But since Frank–Bilby theory does not address atomic relaxation processes it cannot predict the appropriate choice.

Finally, we emphasize that the Burgers vector content $\boldsymbol{B}$, eqn (2.1), is the sum of the Burgers vectors of all dislocations crossing a vector $\boldsymbol{p}$ lying in the interface. Consistent with the continuum nature of the theory the vector $\boldsymbol{B}$ is not discretized into Burgers vectors of crystal lattice dislocations or DSC dislocations. Such a discretization is dedendent on the relaxation processes within the interface which are beyond Frank–Bilby theory. Some further aspects of this problem are discussed in Section 2.8. Any such discretization is of little practical interest if the density of dislocations is so large that their cores overlap. In this situation it may be more useful to think of the whole interface as a surface dislocation characterized by a surface dislocation tensor, eqn (2.18).

2.5 FRANK'S FORMULA

For a grain boundary, where the two adjoining lattices are related by a rotation, $\mathbf{S}^b$ and $\mathbf{S}^w$ in the Frank–Bilby equation may be replaced by rotation matrices $\mathbf{R}^b$ and $\mathbf{R}^w$:

$$\boldsymbol{B} = (\mathbf{R}^{b-1} - \mathbf{R}^{w-1})\boldsymbol{p}. \tag{2.20}$$

Using the rotation formula, eqn (1.9), where $\mathbf{R}^b$ corresponds to a rotation of θ^b about $\hat{\boldsymbol{\rho}}^b$ and $\mathbf{R}^w$ to a rotation of θ^w about $\hat{\boldsymbol{\rho}}^w$, we obtain

$$\begin{aligned}\boldsymbol{B} = \boldsymbol{p}(\cos\theta^b - \cos\theta^w) - \sin\theta^w(\boldsymbol{p}\times\hat{\boldsymbol{\rho}}^w) + \sin\theta^b(\boldsymbol{p}\times\hat{\boldsymbol{\rho}}^b)\\ + (1-\cos\theta^b)(\hat{\boldsymbol{\rho}}^b\cdot\boldsymbol{p})\hat{\boldsymbol{\rho}}^b - (1-\cos\theta^w)(\hat{\boldsymbol{\rho}}^w\cdot\boldsymbol{p})\hat{\boldsymbol{\rho}}^w.\end{aligned} \tag{2.21}$$

Frank showed that this formula is simplified considerably if the reference lattice is taken to be the median lattice. The black and white lattices are obtained from the median lattice by equal and opposite rotations of $\theta/2$ about a common axis $\hat{\boldsymbol{\rho}}$. Setting $\hat{\boldsymbol{\rho}}^b = \hat{\boldsymbol{\rho}}^w = \hat{\boldsymbol{\rho}}$ and $\theta^w = -\theta^b = \theta/2$ in eqn (2.21) we obtain

$$\boldsymbol{B} = 2\sin(\theta/2)(\boldsymbol{p}\times\hat{\boldsymbol{\rho}}), \tag{2.22}$$

which is known as Frank's formula. The modulus of $|\boldsymbol{B}|$ varies, in general, as $\boldsymbol{p}$ varies in orientation in the boundary plane. If γ is the angle between $\hat{\boldsymbol{\rho}}$ and $\boldsymbol{p}$ then

$$|\boldsymbol{B}| = 2\sin(\theta/2)|\boldsymbol{p}|\sin\gamma, \tag{2.23}$$

where

$$\sin\gamma = \{\sin^2\mu\sin^2\varphi + \cos^2\varphi\}^{\frac{1}{2}}, \tag{2.24}$$

and φ is the angle between the rotation axis $\hat{\boldsymbol{\rho}}$ and the boundary normal $\hat{\boldsymbol{n}}$ and μ is the angle between the projection of $\hat{\boldsymbol{\rho}}$ onto the boundary plane and $\boldsymbol{p}$ (see Fig. 2.17). The maximum value of $|\boldsymbol{B}|$, $|\boldsymbol{B}|_{\max}$, is thus obtained when $\sin\mu = \pm 1$:

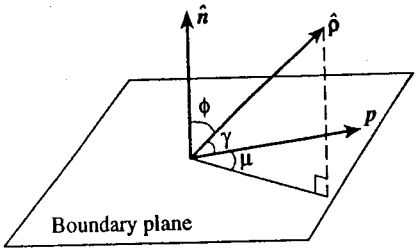

Fig. 2.17 The terms used in eqns (2.23) and (2.24).

$$|\boldsymbol{B}|_{\max} = 2\sin(\theta/2)\,|\boldsymbol{p}|. \tag{2.25}$$

The minimum value, $|\boldsymbol{B}|_{\min}$, is obtained when $\sin\mu = 0$:

$$|\boldsymbol{B}|_{\min} = 2\sin(\theta/2)\,|\boldsymbol{p}|\cos\varphi. \tag{2.26}$$

From eqn (2.25) we see that $|\boldsymbol{B}|_{\max}$ increases monotonically with misorientation θ. For a pure tilt boundary $|\boldsymbol{B}|$ varies between zero for $\boldsymbol{p}$ along the tilt axis and $|\boldsymbol{B}|_{\max}$ for $\boldsymbol{p}$ perpendicular to the tilt axis. For a pure twist boundary $|\boldsymbol{B}|$ is equal to $|\boldsymbol{B}|_{\max}$ for all orientations of $\boldsymbol{p}$.

2.6 THE O-LATTICE

The O-lattice (Bollmann 1970) is a further construction which has been widely used in analysing the dislocation structure of interfaces. Although the O-lattice was developed independently of the Frank–Bilby theory it turns out that they are very closely related. Indeed, the equation that defines the O-lattice may be regarded as a quantized form of the Frank–Bilby equation, in which the vectors $\boldsymbol{B}$ and $\boldsymbol{p}$ are discrete rather than continuous. The principle underlying the O-lattice is the belief that optimal structures are produced in interfaces in regions centred on points where the two lattices adjoining the interface 'match'. The definition of 'matching' that has been developed in the context of the O-lattice will be given shortly. We have already defined the CSL (Section 1.5.4) as the one-, two-, or three-dimensional lattice of common lattice sites which may be produced by two interpenetrating crystal lattices at particular relative orientations. If the two lattices adjoining the interface produce a CSL then the lattice points of the CSL in the interface are one example of points where the two adjoining lattices are said to 'match' each other. However, a CSL exists only in rather special circumstances, e.g. at certain misorientations between identical lattices, the values of which depend on the lattice symmetry, or when there are equal lattice parameters in the case of differing crystal lattices. If we take two arbitrary crystal lattices, with an arbitrary orientation between them, the chances are there will be no CSL. However, Bollmann (1970) showed that other more general points of lattice matching may be defined. If it is imagined that the two adjoining lattices interpenetrate, there are points in space which occupy equivalent positions in the unit cells of the two lattices. More precisely, if for any cell of one lattice the internal coordinates of a point, expressed as fractions of the cells edges, are identical with the fractional coordinates of the same point measured relative to a cell of the other lattice, the point is a point of 'lattice matching' and it is called an O-point. The set of all O-points constitutes the O-lattice which, as seen below, may be a point, line or planar lattice. Also, as seen below, such a lattice will always exist regardless of the misorientation

between the two interpenetrating lattices. The O-lattice may therefore be thought of as a generalization of the concept of the CSL. In the particular case where a CSL exists, the CSL is a sublattice of the O-lattice.

Consider the case where we are working in the framework of a single crystal reference system, and the two lattices adjoining the interface are black and white crystal lattices, not necessarily of the same type. To find the O-lattice we imagine that the two crystal lattices are interpenetrating. The sites of the white lattice are denoted by the infinite set of vectors $\{\boldsymbol{R}^{\mathrm{w}}\}$. We take the white lattice as the reference lattice and consider an arbitrary point with coordinates $\boldsymbol{r}^{\mathrm{w}}$ expressed in the frame of the white lattice. The coordinates of this point are transformed into the coordinates with respect to the black lattice by the transformation $\boldsymbol{r}^{\mathrm{b}} = \mathbf{S}^{\mathrm{b}}\boldsymbol{r}^{\mathrm{w}}$. Thus, if $\boldsymbol{r}^{\mathrm{w}}$ and $\boldsymbol{r}^{\mathrm{b}}$ have the same internal cell coordinates then the point is an O-point. But if that is true then $\boldsymbol{r}^{\mathrm{b}}$ and $\boldsymbol{r}^{\mathrm{w}} + \boldsymbol{R}^{\mathrm{w}}$ have the same internal cell coordinates. Thus the general condition for an O-point is the following:

$$\boldsymbol{r}^{\mathrm{b}} = \boldsymbol{r}^{\mathrm{w}} + \boldsymbol{R}^{\mathrm{w}}$$

where

$$\boldsymbol{r}^{\mathrm{b}} = \mathbf{S}^{\mathrm{b}}\boldsymbol{r}^{\mathrm{w}}. \tag{2.27}$$

Then $\boldsymbol{r}^{\mathrm{b}}$ is an O-point, $\boldsymbol{R}^{\mathrm{o}}$. Equation (2.27) is illustrated in Fig. 2.18. Eliminating $\boldsymbol{r}^{\mathrm{w}}$ from Eqn. (2.27) we obtain an explicit equation for the O-points:

$$(\mathbf{E} - \mathbf{S}^{\mathrm{b}-1})\boldsymbol{R}^{\mathrm{o}} = \boldsymbol{R}^{\mathrm{w}} \tag{2.28}$$

or

$$\boldsymbol{R}^{\mathrm{o}} = (\mathbf{E} - \mathbf{S}^{\mathrm{b}-1})^{-1}\boldsymbol{R}^{\mathrm{w}}. \tag{2.29}$$

Equation (2.29) is the defining equation of the O-lattice. By substituting for $\boldsymbol{R}^{\mathrm{w}}$ the three base vectors of the (reference) white lattice in turn, the columns of the matrix $(\mathbf{E} - \mathbf{S}^{\mathrm{b}-1})^{-1}$define the corresponding base vectors of the O-lattice. The matrix $(\mathbf{E} - \mathbf{S}^{\mathrm{b}-1})$ may be of rank 3,2 or 1. When it is of rank 3 the solutions $\boldsymbol{R}^{\mathrm{o}}$ represent a lattice of points in three dimensions. This is the case when all three eigenvalues of $\mathbf{S}^{\mathrm{b}}$ are not unity, as occurs at most heterophase boundaries, where there is not a

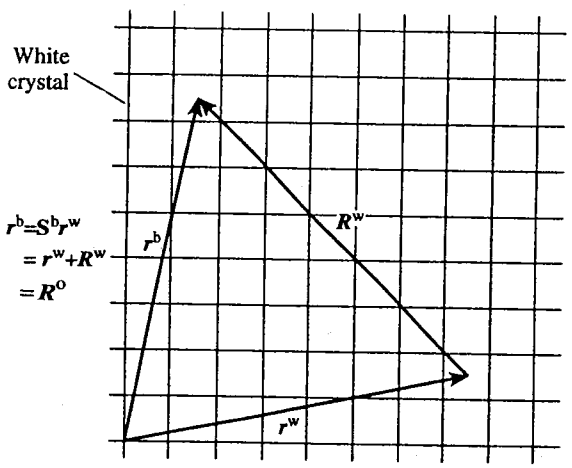

Fig. 2.18 The derivation of the O-lattice equation, eqns (2.27)–(2.29).

coincidental relationship between the lattice parameters of the two crystal lattices. When the matrix is of rank 2 the O-lattice becomes a lattice of lines, called O-lines. The lines are parallel to the eigenvector of $\mathbf{S}^{\mathrm{b}}$ corresponding to the eigenvalue equal to unity. For example, if the black and white lattices are identical, apart from a rotation $\mathbf{R}^{\mathrm{b}} = \mathbf{S}^{\mathrm{b}}$, where $\mathbf{R}^{\mathrm{b}}$ represents a rotation of θ^{b} about $\hat{\boldsymbol{\rho}}^{\mathrm{b}}$, then the O-lines are parallel to $\hat{\boldsymbol{\rho}}^{\mathrm{b}}$. Thus, for grain boundaries the O-lattice may always be described as a lattice of O-lines by choosing to describe the relationship between the lattices as a rotation. In a plane normal to $\hat{\boldsymbol{\rho}}^{\mathrm{b}}$ the rotation matrix may be represented by a 2×2 matrix, which is of rank 2:

$$\mathbf{R}^{\mathrm{b}} = \begin{pmatrix} \cos\theta & -\sin\theta \\ \sin\theta & \cos\theta \end{pmatrix} \tag{2.30}$$

and

$$(\mathbf{E} - \mathbf{R}^{\mathrm{b}-1})^{-1} = \begin{pmatrix} \frac{1}{2} & \frac{1}{2}\cot\frac{1}{2}\theta \\ -\frac{1}{2}\cot\frac{1}{2}\theta & \frac{1}{2} \end{pmatrix}. \tag{2.31}$$

It follows from eqns (2.29) and (2.31) that the basis vectors of the O-lattice vary continuously with the misorientation θ. Since CSL sites are coincidences of lattice sites with internal cell coordinates (0,0,0) it follows that CSL sites are also O-points but not all O-points are CSL sites. At irrational orientations where there is no CSL the O-lattice continues to exist. If one of the eigenvalues of $\mathbf{S}^{\mathrm{b}}$ is equal to unity the transformation $\mathbf{S}^{\mathrm{b}}$ is described as an invariant line strain for obvious reasons. If $\mathbf{S}^{\mathrm{b}}$ is an invariant plane strain there are two eigenvalues of $\mathbf{S}^{\mathrm{b}}$ that are equal to unity and then the matrix $(\mathbf{E} - \mathbf{S}^{\mathrm{b}-1})$ becomes of rank 1. The O-lattice then becomes a lattice of parallel planes, called O-planes. A general invariant plane strain $\mathbf{S}^{\mathrm{b}}$ is represented by

$$(\mathbf{S}^{\mathrm{b}})_{ij} = \delta_{ij} + e_i n_j, \tag{2.32}$$

where $\boldsymbol{e}$ is a constant vector and $\hat{\boldsymbol{n}}$ is normal to the invariant plane. Thus, if $\boldsymbol{p}$ is any vector lying in the invariant plane then $(\mathbf{S}^{\mathrm{b}})_{ij} p_j = p_i$ confirming that $\boldsymbol{p}$ is invariant under the transformation. The inverse of $\mathbf{S}^{\mathrm{b}}$ is represented by

$$(\mathbf{S}^{\mathrm{b}-1})_{ij} = \delta_{ij} - \frac{e_i n_j}{1 + e_k n_k}, \tag{2.33}$$

as may be confirmed directly by forming $(\mathbf{S}^{\mathrm{b}-1})_{ij}(\mathbf{S}^{\mathrm{b}})_{jk} = \delta_{ik}$. Then $(\mathbf{E} - \mathbf{S}^{\mathrm{b}-1})$ becomes

$$\delta_{ij} - (\mathbf{S}^{\mathrm{b}-1})_{ij} = \frac{e_i n_j}{1 + e_k n_k}, \tag{2.34}$$

which is a matrix of rank 1, as can be seen by writing out its determinant, Δ:

$$\Delta = e_1 e_2 e_3 n_1 n_2 n_3 \begin{vmatrix} 1 & 1 & 1 \\ 1 & 1 & 1 \\ 1 & 1 & 1 \end{vmatrix}. \tag{2.35}$$

Another, and equally important, interpretation of the O-lattice is that it is the lattice of possible origins for the relation $\boldsymbol{r}^{\mathrm{b}} = \mathbf{S}^{\mathrm{b}} \boldsymbol{r}^{\mathrm{w}}$. To show this consider a shift of origin to the O-lattice point $\boldsymbol{R}^{\mathrm{o}}$. The relation $\boldsymbol{r}^{\mathrm{b}} = \mathbf{S}^{\mathrm{b}} \boldsymbol{r}^{\mathrm{w}}$ becomes

$$\begin{aligned} \boldsymbol{r}^{\mathrm{b}} - \boldsymbol{R}^{\mathrm{o}} &= \mathbf{S}^{\mathrm{b}} \boldsymbol{r}^{\mathrm{w}} - \boldsymbol{R}^{\mathrm{o}} \\ &= \mathbf{S}^{\mathrm{b}} (\boldsymbol{r}^{\mathrm{w}} - \mathbf{S}^{\mathrm{b}-1} \boldsymbol{R}^{\mathrm{o}}) \\ &= \mathbf{S}^{\mathrm{b}} (\boldsymbol{r}^{\mathrm{w}} + \boldsymbol{R}^{\mathrm{w}} - \boldsymbol{R}^{\mathrm{o}}), \end{aligned} \tag{2.36}$$

where we have used eqn (2.29). This is of the original form $\boldsymbol{r}^{b} = \mathbf{S}^{b}\boldsymbol{r}^{w}$ but corresponding points of the two crystals are changed. Thus point $\boldsymbol{r}^{b}$ was derived from point $\boldsymbol{r}^{w}$ before the shift of origin but is now derived from the point $\boldsymbol{r}^{w} + \boldsymbol{R}^{w}$, measured from the first origin.

So far we have not attributed any physical significance to the O-points other than to say that they are points of generalized crystal lattice coincidence. It is evident from eqn (2.29) that the O-lattice depends on the choice of the description $\mathbf{S}^{b}$ of the relationship between the crystal lattices. For a given pair of crystal lattices, at a particular relative orientation, alternative specifications of $\mathbf{S}^{b}$ correspond to choosing alternative unit cells from either lattice. Mathematically, this is achieved by pre- and post-multiplying $\mathbf{S}^{b}$ by unimodular matrices. It is, therefore, not surprising that the O-lattice changes with different selections of $\mathbf{S}^{b}$ because the cells, with respect to which the internal cell coordinates are measured, change when an alternative $\mathbf{S}^{b}$ is selected. Only the coincident crystal lattice sites, when they exist, are invariant with respect to alternative specifications of $\mathbf{S}^{b}$.

In order to make further progress it is necessary to introduce a *physical assumption*. We create an interface by defining a cut plane through the O-lattice and discarding black crystal lattice sites on one side of the cut and white crystal lattice sites on the other. It is then assumed that if an O-element (point, line, or plane) exists in the interface then it is a region of 'good fit' meaning that it is energetically favourable. The O-points are described as points of geometric registry between the crystal lattices. There is no rigorous justification for these assertions, or even a clear idea of what they mean in terms of atomic arrangements, but some intuitive reasoning may be offered.

If we take the trivial case where the black and white crystal lattices are identical with no misorientation forming a single (grey) crystal lattice then the 'interfacial energy' associated with any plane in the lattice is obviously zero. The O-lattice for this trivial case is a continuum extending throughout the crystal lattice since every point has the same internal cell coordinates in the 'black and white lattices'. As soon as we introduce a misorientation between the crystal lattices, or we deform one crystal lattice, the continuum of O-points is destroyed and we have an O-lattice. At small misorientations or deformations the O-lattice is coarse and it becomes finer as the misorientation or the lattice deformation increase in magnitude. This seems paradoxical, because it suggests that we discontinuously change from a state of perfect matching (the single crystal) to a state of widely spaced regions of matching (small misorientations or deformations) to a state of improved matching at higher misorientations or deformations. The resolution to the paradox is that we have ignored relaxation within the interface. At small misorientations or deformations we can reasonably expect to see discrete lattice dislocations in the interface. Since the O-points are assumed to be associated with regions of good fit within the interface we expect to see one O-point between each successive pair of dislocations. Therefore the average spacing of dislocations along a particular direction within the interface should correspond to the O-lattice spacing in that direction. Thus, if we assume that the relaxation within the interface introduces *localized* dislocations then at small misorientations or deformations there are large regions of relatively good fit separated by small regions of bad fit at the dislocation cores. Although the spacing of the O-points is large at small misorientations or deformations it is assumed that the energy of the interface derives mainly from the relatively small regions of misfit between the O-points. If we assume this argument may be extrapolated to higher angles or deformations we conclude that the energy of the interface increases as the average spacing of the dislocations decreases, which is equivalent to the O-lattice spacing. We see that it is not essential to understand precisely what is meant by saying that an O-point

represents a point of geometric registry or good fit, because all that it implies is that *between the O-points* there is an accumulating disregistry which, it is assumed, is concentrated into dislocations approximately midway between them. Put another way, it is the dislocation content of the interface that is physically significant and the O-lattice is merely a geometrical construction to obtain it.

Following Christian (1981), we shall now make the relationship between the O-lattice and the Frank–Bilby equation for the dislocation content of an interface explict. We separate the different O-elements (points, lines, or planes) by Wigner–Seitz cell walls. On constructing the interface by sectioning the O-lattice, as described above, the intersections of the Wigner–Seitz cell walls are identified with line discontinuities within the interface which are called 'mathematical dislocations'. Each O-lattice point may be considered as the origin for the relation $\boldsymbol{r}^{\mathrm{b}} = \mathbf{S}^{\mathrm{b}}\boldsymbol{r}^{\mathrm{w}}$ within its own cell. When a cell wall is crossed the relation between corresponding lattice points changes by the vector $\boldsymbol{R}^{\mathrm{w}}$ which is the difference vector between two reference lattice points. We saw in eqn (2.29) that $(\mathbf{E} - \mathbf{S}^{\mathrm{b}-1})\boldsymbol{R}^{\circ} = \boldsymbol{R}^{\mathrm{w}}$. By identifying $\boldsymbol{R}^{\circ}$ with $\boldsymbol{p}$, and $\boldsymbol{B}$ with $-\boldsymbol{R}^{\mathrm{w}}$, this is identical to the Frank–Bilby equation, eqn (2.1), where $\mathbf{S}^{\mathrm{w}} = \mathbf{E}$. The only difference between eqn (2.29) and the Frank–Bilby equation is that the continuous variables $\boldsymbol{p}$ and $\boldsymbol{B}$ are quantized in the O-lattice equation equation because the discreteness of the black and white crystal lattices has been taken into account in the O-lattice treatment but not in the Frank–Bilby treatment. Bollmann calls the discrete dislocations that are defined by eqn (2.29) *primary* dislocations. They are distinguished by having Burgers vectors that are lattice vectors of either crystal.

The physical assumption that the dislocation content of the interface is minimized is equivalent to maximizing the spacing of O-elements within the interface. This suggests a criterion for selecting a description of the relationship $\mathbf{S}^{\mathrm{b}}$ from among the infinity of possible description of $\mathbf{S}^{\mathrm{b}}$ which maximizes the size of the one-, two-, or three-dimensional unit cell of the O-lattice. We have already remarked (Section 2.4), however, that this criterion is unsatisfactory when it is applied to symmetrical tilt boundaries. In that case the simple shear description gives an O-plane lattice with the boundary plane coinciding with one of the O-planes. As before, there are no dislocations required by such a description of the interface, and therefore at small angles of misorientation, where line defects possessing dislocation character are seen experimentally, the criterion does not lead to the most useful description.

Unlike the mathematical dislocations, whose positions are defined by the O-lattice cell walls, the physical dislocations are not, in general, uniformly spaced along the interface. The physical spacings are determined by the discreteness of the crystal lattice. For example, if the average spacing of the dislocations is $2\frac{1}{2}a$ this will be the spacing of the mathematical dislocations but the physical dislocations will be spaced alternately by $2a$ and $3a$.

Consider next the case where we are using a bicrystal reference structure and the two relevant lattices are the $\mathrm{DSC}^{\mathrm{w}}$ and $\mathrm{DSC}^{\mathrm{b}}$ lattices. These two DSC lattices form an O-lattice, which is sometimes called an O2-lattice, given by

$$(\mathbf{E} - \mathbf{D}^{\mathrm{b}-1})\boldsymbol{R}^{\circ} = \mathbf{R}^{\mathrm{DSC^w}}. \tag{2.37}$$

Here we take the $\mathrm{DSC}^{\mathrm{w}}$ lattice as the reference lattice, and $\mathbf{D}^{\mathrm{b}}$ is the transformation which generates the $\mathrm{DSC}^{\mathrm{b}}$ lattice from the $\mathrm{DSC}^{\mathrm{w}}$ lattice. The dislocations between successive O-elements of the O2-lattice have Burgers vectors of the $\mathrm{DSC}^{\mathrm{w}}$ lattice and they are called secondary dislocations. The Wigner–Seitz construction may be applied in the same way to the O2-lattice to determine the patches of good DSC lattice matching, i.e. the patches where continuity of the DSC lattice across the interface is maintained.

There have been numerous applications of the O-lattice theory to interpreting observed line defect contrast at grain and interphase boundaries in the electron microscope. Both primary and secondary dislocation arrays have been identified and characterized, and it is remarkable how successful the theory has been considering its simplicity and the rather unsatisfactory physical assumptions it contains.

One weak point of the theory is of course the physical assumption that determines the choice of the description of $\mathbf{S}^b$. Precisely the same problem arose in the Frank–Bilby theory, and there we concluded that the only rigorous way to decide the most appropriate description was to observe the motion of atoms as the interface migrated. In the O-lattice case the most appropriate description of $\mathbf{S}^b$ (or $\mathbf{D}^b$) has another interpretation. It is the description which most accurately describes the pattern of local relaxation responsible for the network of dislocations with Burgers vectors $\boldsymbol{R}^w$ (or $\boldsymbol{R}^{DSC^w}$). Thus, at a small-angle grain boundary we would choose the disorientation description for $\mathbf{S}^b$ because this most simply describes the local changes in misorientation that occur between successive dislocations in the interface. As Bollmann has pointed out the O-lattice is effectively a first approximation at describing the relaxation pattern within the interface. If a different $\mathbf{S}^b$ is selected then a different relaxation pattern will be derived. The trick is to *guess* the description of $\mathbf{S}^b$ (or $\mathbf{D}^b$) which most closely approximates the local relaxations within the interface. This is not always straightforward as demonstrated by the experimental observations of Goodhew *et al.* (1976). Those authors found that the dislocation structure of small-angle (1–5°) (110) twist boundaries in gold could be explained by an O-lattice construction only if the transformation relating the two crystal lattices varied with position in the boundary plane: in some regions it was a simple rotation whereas in others it was a rotation plus a translation. This simply amounts to saying that the actual dislocation structure is dictated by minimization of the boundary energy, and since the O-lattice construction is geometrical in nature it may or may not predict the correct structure.

2.7 THE GEOMETRY OF DISCRETE DISLOCATION ARRAYS IN INTERFACES

2.7.1 The general interface

In this section we assume that a description of the relationship between the lattices which adjoin the interface has been selected, and that the interface is free of stresses at long range. The Burgers vector density of stress annihilator dislocations in the interface is assumed to be represented by i independent sets of discrete dislocations, the jth set with Burgers vector $\mathbf{b}_j$, line vector $\hat{\boldsymbol{\xi}}_j$, and spacing d_j. The question we address is the following: given the set of Burgers vectors $\boldsymbol{b}_j$ what are the line directions $\hat{\boldsymbol{\xi}}_j$ and spacings d_j? This problem was first considered by Frank (1950), Read (1953), and Hirth and Lothe (1982), who considered grain boundaries, and more recently the heterophase interface problem was addressed by Sargent and Purdy (1975) and Knowles (1982). We shall follow the approach of Knowles (1982) for heterophase interfaces. Our analysis includes grain boundaries as the special case where the relationship between the crystal lattices is often a pure rotation.

Our starting point is the Frank–Bilby equation, eqn (2.1):

$$\not{\boldsymbol{B}} = (\mathbf{S}^{b-1} - \mathbf{S}^{w-1})\boldsymbol{p}, \tag{2.1}$$

Recall that $\mathbf{S}^b$ and $\mathbf{S}^w$ are the affine transformations that generate the black and white crystal lattices from some reference lattice, and $\boldsymbol{B}$ is the sum of the Burgers vector of

stress annihilator dislocations crossing the interfacial vector $\boldsymbol{p}$. Since $\boldsymbol{B}$ is expressed in the reference lattice we assume that the discrete Burgers vectors of the dislocations, into which $\boldsymbol{B}$ is assumed to decompose, are lattice vectors of the reference lattice. That is, we assume that $\boldsymbol{B}$ may be written as

$$\boldsymbol{B}(\boldsymbol{p}) = \sum_{j=1}^{i} c_j(\boldsymbol{p})\boldsymbol{b}_j, \tag{2.38}$$

where the sum is taken over the i sets of discrete dislocations that are assumed to exist in the interface, and the vectors $\boldsymbol{b}_j$ are assumed to be lattice vectors of the reference lattice, although they are not necessarily primitive vectors. However, it is quite possible for the dislocations to dissociate into partial dislocations forming complex networks in the interface involving stacking faults. Such an eventuality cannot be predicted by this geometrical theory which can treat only the average Burgers vector content crossing a macroscopic vector $\boldsymbol{p}$ in the interface and its decomposition into assumed discrete Burgers vectors. To account for this eventuality we must consider local interactions among the i predicted sets of dislocations, and this will be discussed briefly in Section 2.8.

Let $\mathbf{W} = \mathbf{S}^{b-1} - \mathbf{S}^{w-1}$ and consider the decomposition of $\boldsymbol{B}$ described by eqn (2.38). Let $\hat{\boldsymbol{n}}$ be the interface normal, pointing from the white crystal into the black. Let N_j be a vector lying in the interface, normal to the sense vector $\hat{\boldsymbol{\xi}}_j$ of the dislocations with Burgers vector $\boldsymbol{b}_j$, and of length equal to the reciprocal of the spacing d_j:

$$N_j = \frac{\hat{\boldsymbol{n}} \times \hat{\boldsymbol{\xi}}_j}{d_j}. \tag{2.39}$$

The number of dislocations intersected by a vector $\boldsymbol{p}$ is $N_j \cdot \boldsymbol{p}$, and a dislocation cut by $\boldsymbol{p}$ is counted as a positive contribution to $\boldsymbol{B}$ if $\boldsymbol{p} \times \hat{\boldsymbol{n}}$ has a positive component along $\hat{\boldsymbol{\xi}}_j$. It follows that $c_j(\boldsymbol{p})$ in eqn (2.38) is equal to $N_j \cdot \boldsymbol{p}$, and therefore

$$\boldsymbol{B} = \sum_{j=1}^{i} (N_j \cdot \boldsymbol{p})\boldsymbol{b}_j = \mathbf{W}\boldsymbol{p}. \tag{2.40}$$

Our task is to find the line directions $\hat{\boldsymbol{\xi}}_j$ and spacings d_j given $\mathbf{W}$ and the Burgers vectors $\boldsymbol{b}_j$.

The first point to observe is that if there are more than three sets of dislocations in eqn (2.40), i.e. $i > 3$, then the i Burgers vectors $\boldsymbol{b}_1, \boldsymbol{b}_2, \boldsymbol{b}_3, \ldots \boldsymbol{b}_i$ are linearly dependent. In that case there is no unique solution. In the general case three independent Burgers vectors are required to satisfy eqn (2.40), and if there are less than three then only certain special types of interface may be described. In this section we consider the general case of $i = 3$ and solve eqn (2.40) for the N_j, $j = 1, 2, 3$. In general we cannot assume that $|\mathbf{W}| \neq 0$, since $\mathbf{W}$ may be of rank 2 or 1. Writing out enq (2.40) in full we have

$$(N_1 \cdot \boldsymbol{p})\boldsymbol{b}_1 + (N_2 \cdot \boldsymbol{p})\boldsymbol{b}_2 + (N_3 \cdot \boldsymbol{p})\boldsymbol{b}_3 = \mathbf{W}\boldsymbol{p} \tag{2.41}$$

and multiplying both sides by $\boldsymbol{b}_2 \times \boldsymbol{b}_3$ we obtain

$$(N_1 \cdot \boldsymbol{p})(\boldsymbol{b}_1 \cdot \boldsymbol{b}_2 \times \boldsymbol{b}_3) = \mathbf{W}\boldsymbol{p} \cdot (\boldsymbol{b}_2 \times \boldsymbol{b}_3). \tag{2.42}$$

In particular if $\boldsymbol{p}$ is parallel to $\hat{\boldsymbol{\xi}}_1$ we have $N_1 \cdot \boldsymbol{p} = 0$ and therefore

$$\mathbf{W}\hat{\boldsymbol{\xi}}_1 \cdot \boldsymbol{b}_1^* = 0 \tag{2.43}$$

where $\boldsymbol{b}_1^*$ is a reciprocal Burgers vector defined by

$$b_1^* = \frac{b_2 \times b_3}{b_1 \cdot b_2 \times b_3}. \tag{2.44}$$

Similar formulae hold for $\hat{\xi}_2$ and $\hat{\xi}_3$ and b_2^* and b_3^*. Now $\mathbf{W}\hat{\xi}_1 \cdot b_1^* = \hat{\xi}_1 \cdot \mathbf{W}^t b_1^*$, where $\mathbf{W}^t$ is the transpose of $\mathbf{W}$, and therefore $\hat{\xi}_1$ is perpendicular to both $\mathbf{W}^t b_1^*$ and $\hat{n}$. Therefore $\hat{\xi}_1$ is parallel to $(\mathbf{W}^t b_1^*) \times \hat{n}$ and

$$N_1 = \frac{\hat{n} \times \hat{\xi}_1}{d_1} = \frac{\hat{n} \times ((\mathbf{W}^t b_1^*) \times \hat{n})}{d_1 \left| (\mathbf{W}^t b_1^*) \times \hat{n} \right|}. \tag{2.45}$$

Multiplying both sides of eqn (2.41) by b_1^*, for any interfacial vector p, we obtain

$$(N_1 \cdot p) = \mathbf{W}p \cdot b_1^* \tag{2.46}$$

and substituting eqn (2.45) into eqn (2.46) we find that

$$d_1 = 1/\left| (\mathbf{W}^t b_1^*) \times \hat{n} \right| \tag{2.47}$$

and

$$N_1 = \mathbf{W}^t b_1^* - (\hat{n} \cdot \mathbf{W}^t b_1^*)\hat{n} \tag{2.48}$$

with

$$\hat{\xi}_1 = \frac{((\mathbf{W}^t b_1^*) \times \hat{n})}{\left| (\mathbf{W}^t b_1^*) \times \hat{n} \right|}. \tag{2.49}$$

Equations (2.47)–(2.49) represent the solution to the task we set ourselves. Equation (2.48) states that N_1 is the projection of $\mathbf{W}^t b_1^*$ onto the interface plane. These formulae hold regardless of the rank of $\mathbf{W}$. But in the particular case where the rank of $\mathbf{W}$ is equal to three the inverse of $\mathbf{W}$ exists and eqn (2.41) may be rewritten as follows:

$$(N_1 \cdot p)\mathbf{W}^{-1} b_1 + (\mathbf{N}_2 \cdot p)\mathbf{W}^{-1} b_2 + (N_3 \cdot p)\mathbf{W}^{-1} b_3 = p. \tag{2.50}$$

The vectors $\mathbf{W}^{-1} b_j$, are recognized as O-lattice vectors (see eqn (2.29)) and the lattice formed from them is a point O-lattice. Setting $a_1^o = \mathbf{W}^{-1} b_1$, $a_2^o = \mathbf{W}^{-1} b_2$, $a_3^o = \mathbf{W}^{-1} b_3$ as the basis vectors of the O-lattice, eqn (2.50) becomes

$$(N_1 \cdot p)a_1^o + (N_2 \cdot p)a_2^o + (N_3 \cdot p)a_3^o = p. \tag{2.51}$$

Setting p parallel to $\hat{\xi}_1$, so that $N_1 \cdot p = 0$, and multiplying by $a_2^o \times a_3^o$ we obtain

$$\hat{\xi}_1 \cdot (a_2^o \times a_3^o) = 0. \tag{2.52}$$

Thus $\hat{\xi}_1$ is perpendicular to $a_1^{o*} = (a_2^o \times a_3^o)/(a_1^o \cdot a_2^o \times a_3^o)$ and $\hat{n}$:

$$\hat{\xi}_1 = \frac{a_1^{o*} \times \hat{n}}{\left| a_1^{o*} \times \hat{n} \right|}. \tag{2.53}$$

Substituting this expression for $\hat{\xi}_1$ into eqn (2.39) and using $(N_1 \cdot p) = p \cdot a_1^{o*}$, which follows from eqn (2.51) by multiplying both sides by a_1^{o*}, we deduce that

$$N_1 = a_1^{o*} - (a_1^{o*} \cdot \hat{n})\hat{n} \tag{2.54}$$

and

$$d_1 = 1/\left| a_1^{o*} \times \hat{n} \right|. \tag{2.55}$$

Equation (2.54) states that N_1 is the projection of a_1^{o*} onto the interface plane. Equations (2.53), (2.54), and (2.55) are equivalent to eqns (2.49), (2.48), and (2.47) if

$$\mathbf{W}^{\mathrm{t}}\boldsymbol{b}_1^* = \boldsymbol{a}_1^{\circ *}, \tag{2.56}$$

for $|\mathbf{W}| \neq 0$, and similar relations hold for $\boldsymbol{a}_2^{\circ *}$ and $\boldsymbol{a}_3^{\circ *}$. We shall prove that this relation holds by showing that it is consistent with $\boldsymbol{a}_1^{\circ} \cdot \boldsymbol{a}_1^{\circ *} = 1$ and $\boldsymbol{a}_2^{\circ} \cdot \boldsymbol{a}_1^{\circ *} = \boldsymbol{a}_3^{\circ} \cdot \boldsymbol{a}_1^{\circ *} = 0$. Using the definition $\boldsymbol{a}_1^{\circ}$ we obtain:

$$\boldsymbol{a}_1^{\circ} \cdot \boldsymbol{a}_1^{\circ *} = (\mathbf{W}^{-1}\boldsymbol{b}_1) \cdot (\mathbf{W}^{\mathrm{t}}\boldsymbol{b}_1^*),$$

which in component form becomes

$$(a_1^{\circ})_i (a_1^{\circ *})_i = \mathrm{W}_{ij}^{-1} (b_1)_j \mathrm{W}_{ki} (b_1^*)_k. \tag{2.57}$$

Performing the sum on i, and using $W_{ki} W_{ij}^{-1} = \delta_{kj}$, we obtain

$$\boldsymbol{a}_1^{\circ} \cdot \boldsymbol{a}_1^{\circ *} = \boldsymbol{b}_1 \cdot \boldsymbol{b}_1^* = 1. \tag{2.58}$$

Similarly, $\boldsymbol{a}_2^{\circ} \cdot \boldsymbol{a}_1^{\circ *}$ becomes

$$\boldsymbol{a}_2^{\circ} \cdot \boldsymbol{a}_1^{\circ *} = (\mathbf{W}^{-1}\boldsymbol{b}_2) \cdot (\mathbf{W}^{\mathrm{t}}\boldsymbol{b}_1^*),$$

which in component form reads

$$(a_2^{\circ})_{\mathrm{i}} (a_1^{\circ *})_{\mathrm{i}} = W_{ij}^{-1} (b_2)_j W_{ki} (b_1^*)_k. \tag{2.59}$$

Performing the sum on i again we deduce that

$$\boldsymbol{a}_2^{\circ} \cdot \boldsymbol{a}_1^{\circ *} = \boldsymbol{b}_2 \cdot \boldsymbol{b}_1^* = 0. \tag{2.60}$$

Similarly $\boldsymbol{a}_3^{\circ} \cdot \boldsymbol{a}_1^{\circ *}$ may also be shown to be zero. This proves that eqn (2.56) is correct.

If we now add a fourth set of dislocations, with specified Burgers vector $\boldsymbol{b}_4$, line sense $\hat{\boldsymbol{\xi}}_4$, and spacing d_4, we find that the N_i change, where $i = 1, 2, 3$, by $-(\boldsymbol{b}_4 \cdot \boldsymbol{b}_i^*)N_4$. As before, $N_4 = \hat{\boldsymbol{n}} \times \hat{\boldsymbol{\xi}}_4 / d_4$. A fourth set of dislocations may be produced by local interactions between the first three sets of dislocations.

To *summarize*, eqns (2.47) and (2.49) give the spacings and line directions of the three independent sets of dislocations in an interface with normal $\hat{\boldsymbol{n}}$ for an arbitrary choice of the matrix $\mathbf{W}$. In the particular case where the rank of $\mathbf{W}$ equals 3 these equations are equivalent to eqns (2.55) and (2.53), which are expressed in terms of reciprocal lattice vectors of the corresponding point O-lattice.

2.7.2 Application to a grain boundary with arbitrary geometrical parameters

Consider a grain boundary requiring three independent sets of dislocations to describe the stress annihilator dislocation content. We have already seen that if the adjoining lattices are related by a rotation, and if the median lattice is selected as the reference lattice, the Burgers vector content has a particularly simple form:

$$\boldsymbol{B} = 2(\boldsymbol{p} \times \hat{\boldsymbol{\rho}}) \sin(\theta/2). \tag{2.22}$$

Here the black and white lattices are created from a median lattice by equal and opposite rotations of $\theta/2$ about the axis $\hat{\boldsymbol{\rho}}$. At small angles one would generally choose the median lattice to be a crystal lattice with an orientation half way between the two crystal lattices. In that case the Burgers vectors $\boldsymbol{b}_i$ are lattice vectors of the crystal lattice and the discrete dislocations are primary dislocations. The angle θ is interpreted as the total boundary misorientation. At large angles one could choose another large-angle boundary as the reference structure, and regard the black and white crystal lattices as being generated by equal and opposite rotations from their orientations in this reference structure. In that

case the dislocations are of the secondary type, and the Burgers vectors are lattice vectors of the DSC lattice of the reference boundary. The angle θ is interpreted as the misorientation from the large-angle boundary reference structure. Thus,

$$2\sin(\theta/2)\,(\boldsymbol{p}\times\hat{\boldsymbol{\rho}}) = \sum_{i=1}^{3}(N_i\cdot\boldsymbol{p})\boldsymbol{b}_i, \tag{2.61}$$

and after multiplying both sides with respect to $\boldsymbol{b}_j^*$ we deduce

$$2\sin(\theta/2)\boldsymbol{b}_j^*\cdot(\boldsymbol{p}\times\hat{\boldsymbol{\rho}}) = N_j\cdot\boldsymbol{p}. \tag{2.62}$$

In particular, setting $\boldsymbol{p} = \hat{\boldsymbol{\xi}}_j$ we find that $\hat{\boldsymbol{\xi}}_j$ is perpendicular to $\hat{\boldsymbol{\rho}}\times\boldsymbol{b}_j^*$. Therefore,

$$\hat{\boldsymbol{\xi}}_j = \frac{(\hat{\boldsymbol{\rho}}\times\boldsymbol{b}_j^*)\times\hat{\boldsymbol{n}}}{\left|(\hat{\boldsymbol{\rho}}\times\boldsymbol{b}_j^*)\times\hat{\boldsymbol{n}}\right|}, \tag{2.63}$$

and

$$N_j = 2(\hat{\boldsymbol{\rho}}\times\boldsymbol{b}_j^* - [\hat{\boldsymbol{n}}\cdot(\hat{\boldsymbol{\rho}}\times\boldsymbol{b}_j^*)]\hat{\boldsymbol{n}})\sin(\theta/2), \tag{2.64}$$

$$d_j = \frac{1}{2\sin(\theta/2)\left|(\hat{\boldsymbol{\rho}}\times\boldsymbol{b}_j^*)\times\hat{\boldsymbol{n}}\right|}. \tag{2.65}$$

Equations (2.63) and (2.65) give the line directions and spacings of the three sets of dislocations with Burgers vectors $\boldsymbol{b}_1$, $\boldsymbol{b}_2$, and $\boldsymbol{b}_3$ required to represent the Burgers vector content of a grain boundary with arbitrary geometrical parameters. Note that all vectors are expressed in the coordinate frame of the median lattice.

2.7.3 Grain boundaries containing one and two sets of dislocations

We have seen that in general we need three non-coplanar Burgers vectors of discrete dislocations to account for the Burgers vector content of a grain boundary with arbitrary geometrical parameters. In this section we ask what kinds of boundaries may be formed from just one or two independent sets of dislocations and still satisfy Frank's formula.

If there is *only one set of dislocations*, with Burgers vector $\boldsymbol{b}$, then Frank's formula becomes

$$2(\boldsymbol{p}\times\hat{\boldsymbol{\rho}})\sin(\theta/2) = (N\cdot\boldsymbol{p})\boldsymbol{b}. \tag{2.66}$$

Therefore $\boldsymbol{b}$ is perpendicular to $\boldsymbol{p}$ and $\hat{\boldsymbol{\rho}}$ regardless of the orientation of $\boldsymbol{p}$ within the boundary plane. Thus, $\boldsymbol{b}$ must be perpendicular to the boundary plane, and $\hat{\boldsymbol{\rho}}$ must lie in the boundary plane. Thus the boundary is a tilt boundary. It is emphasized that these vectors are expressed in the median lattice. If the normal to the boundary plane, $\hat{\boldsymbol{n}}$, is a mirror plane of the median lattice the boundary is of the symmetric tilt type, otherwise it is an asymmetric tilt boundary. Setting $\boldsymbol{p}$ parallel to $\hat{\boldsymbol{\xi}}$ we further deduce that $\hat{\boldsymbol{\xi}}\times\hat{\boldsymbol{\rho}} = 0$ and therefore the dislocation lines are parallel to the rotation axis. The spacing, d, of the dislocation lines is given by

$$d = |\boldsymbol{b}|/2\sin(\theta/2) \tag{2.67}$$

If there are *two independent sets of dislocations* there are just two types of boundary that may be formed, and we shall consider them in turn. Both types of boundary satisfy Frank's formula:

$$2(\boldsymbol{p}\times\hat{\boldsymbol{\rho}})\sin(\theta/2) = (N_1\cdot\boldsymbol{p})\boldsymbol{b}_1 + (N_2\cdot\boldsymbol{p})\boldsymbol{b}_2. \tag{2.68}$$

Multiplying both sides by $\boldsymbol{b}_1 \times \boldsymbol{b}_2$ we deduce

$$\boldsymbol{p}\cdot\hat{\boldsymbol{\rho}} \times (\boldsymbol{b}_1 \times \boldsymbol{b}_2) = 0. \tag{2.69}$$

The first way of satisfying this equation is for $\hat{\boldsymbol{\rho}} \times (\boldsymbol{b}_1 \times \boldsymbol{b}_2)$ to be perpendicular to $\boldsymbol{p}$. Since this has to be true for any $\boldsymbol{p}$ lying in the boundary plane it can be satisfied only if $\hat{\boldsymbol{\rho}} \times (\boldsymbol{b}_1 \times \boldsymbol{b}_2)$ is parallel to the boundary normal. Thus $\hat{\boldsymbol{\rho}}$ and $(\boldsymbol{b}_1 \times \boldsymbol{b}_2)$ lie in the boundary plane and the boundary is a tilt boundary. Setting $\boldsymbol{p}$ parallel to $\hat{\boldsymbol{\rho}}$ in eqn (2.68) we find

$$(N_1\cdot\hat{\boldsymbol{\rho}})\boldsymbol{b}_1 + (N_2\cdot\hat{\boldsymbol{\rho}})\boldsymbol{b}_2 = 0. \tag{2.70}$$

Since $\boldsymbol{b}_1$ and $\boldsymbol{b}_2$ are not parallel, by assumption, it follows that $N_1\cdot\hat{\boldsymbol{\rho}}$ and $N_2\cdot\hat{\boldsymbol{\rho}}$ are zero and hence $\hat{\boldsymbol{\xi}}_1$ and $\hat{\boldsymbol{\xi}}_2$ are parallel to $\hat{\boldsymbol{\rho}}$. The asymmetric tilt boundary to which this case corresponds is sketched schematically in Fig. 2.3. To find the spacings, d_1 and d_2, of the dislocations we set $\hat{\boldsymbol{\xi}}_1 = \hat{\boldsymbol{\xi}}_2 = \hat{\boldsymbol{\rho}}$ and $\boldsymbol{p} = \hat{\boldsymbol{\rho}} \times \hat{\boldsymbol{n}}$ in eqn (2.68):

$$-2\sin(\theta/2)\hat{\boldsymbol{n}} = \frac{\boldsymbol{b}_1}{d_1} + \frac{\boldsymbol{b}_2}{d_2}. \tag{2.71}$$

Therefore,

$$\frac{d_1}{d_2} = -\frac{(\boldsymbol{b}_1 \times \hat{\boldsymbol{n}})\cdot(\boldsymbol{b}_1 \times \boldsymbol{b}_2)}{(\boldsymbol{b}_2 \times \hat{\boldsymbol{n}})\cdot(\boldsymbol{b}_1 \times \boldsymbol{b}_2)}. \tag{2.72}$$

Substituting this into eqn (2.71) and multiplying both sides by $\hat{\boldsymbol{n}}$ we obtain

$$d_1 = \frac{(\boldsymbol{b}_2\cdot\hat{\boldsymbol{n}})(\boldsymbol{b}_1 \times \hat{\boldsymbol{n}})\cdot(\boldsymbol{b}_1 \times \boldsymbol{b}_2) - (\boldsymbol{b}_1\cdot\hat{\boldsymbol{n}})(\boldsymbol{b}_2 \times \hat{\boldsymbol{n}})\cdot(\boldsymbol{b}_1 \times \boldsymbol{b}_2)}{2\sin(\theta/2)(\boldsymbol{b}_2 \times \hat{\boldsymbol{n}})\cdot(\boldsymbol{b}_1 \times \boldsymbol{b}_2)}$$

and

$$d_2 = \frac{(\boldsymbol{b}_1\cdot\hat{\boldsymbol{n}})(\boldsymbol{b}_2 \times \hat{\boldsymbol{n}})\cdot(\boldsymbol{b}_1 \times \boldsymbol{b}_2) - (\boldsymbol{b}_2\cdot\hat{\boldsymbol{n}})(\boldsymbol{b}_1 \times \hat{\boldsymbol{n}})\cdot(\boldsymbol{b}_1 \times \boldsymbol{b}_2)}{2\sin(\theta/2)(\boldsymbol{b}_1 \times \hat{\boldsymbol{n}})\cdot(\boldsymbol{b}_1 \times \boldsymbol{b}_2)}. \tag{2.73}$$

The second type of boundary that satisfies eqn (2.69) is that where $\hat{\boldsymbol{\rho}}$ is parallel to $\boldsymbol{b}_1 \times \boldsymbol{b}_2$. Setting $\hat{\boldsymbol{\rho}} = \boldsymbol{b}_1 \times \boldsymbol{b}_2/|\boldsymbol{b}_1 \times \boldsymbol{b}_2|$ in eqn (2.68) we obtain

$$\frac{2\sin(\theta/2)}{|\boldsymbol{b}_1 \times \boldsymbol{b}_2|}[(\boldsymbol{p}\cdot\boldsymbol{b}_2)\boldsymbol{b}_1 - (\boldsymbol{p}\cdot\boldsymbol{b}_1)\boldsymbol{b}_2] = (N_1\cdot\boldsymbol{p})\boldsymbol{b}_1 + (N_2\cdot\boldsymbol{p})\boldsymbol{b}_2. \tag{2.74}$$

Since this must hold for any vector $\boldsymbol{p}$ in the boundary it follows that

$$N_1\cdot\boldsymbol{p} = \frac{2\sin(\theta/2)}{|\boldsymbol{b}_1 \times \boldsymbol{b}_2|}(\boldsymbol{p}\cdot\boldsymbol{b}_2),$$

and

$$N_2\cdot\boldsymbol{p} = -\frac{2\sin(\theta/2)}{|\boldsymbol{b}_1 \times \boldsymbol{b}_2|}(\boldsymbol{p}\cdot\boldsymbol{b}_1). \tag{2.75}$$

Setting $\boldsymbol{p}$ parallel to $\hat{\boldsymbol{\xi}}_1$ and $\hat{\boldsymbol{\xi}}_2$ in turn we deduce that $\hat{\boldsymbol{\xi}}_1\cdot\boldsymbol{b}_2 = \hat{\boldsymbol{\xi}}_2\cdot\boldsymbol{b}_1 = 0$. Thus,

$$\hat{\boldsymbol{\xi}}_1 = \frac{\boldsymbol{b}_2 \times \hat{\boldsymbol{n}}}{|\boldsymbol{b}_2 \times \hat{\boldsymbol{n}}|},$$

and

$$\hat{\xi}_2 = \frac{\boldsymbol{b}_1 \times \hat{\boldsymbol{n}}}{|\boldsymbol{b}_1 \times \hat{\boldsymbol{n}}|}. \tag{2.76}$$

Therefore N_1 becomes

$$N_1 = \frac{\boldsymbol{b}_2 - (\hat{\boldsymbol{n}}\cdot\boldsymbol{b}_2)\hat{\boldsymbol{n}}}{|\boldsymbol{b}_2 \times \hat{\boldsymbol{n}}|\, d_1},$$

whereas

$$N_2 = -\frac{\boldsymbol{b}_1 - (\hat{\boldsymbol{n}}\cdot\boldsymbol{b}_1)\hat{\boldsymbol{n}}}{|\boldsymbol{b}_1 \times \hat{\boldsymbol{n}}|\, d_2}. \tag{2.77}$$

Substituting $\boldsymbol{p} = N_1$ and $\boldsymbol{p} = N_2$ in turn into eqn (2.75) and using eqn (2.77) for N_1 and N_2 we find that

$$d_1 = \frac{|\boldsymbol{b}_1 \times \boldsymbol{b}_2|}{2\sin(\theta/2)\,|\boldsymbol{b}_2 \times \hat{\boldsymbol{n}}|}$$

and

$$d_2 = \frac{|\boldsymbol{b}_1 \times \boldsymbol{b}_2|}{2\sin(\theta/2)\,|\boldsymbol{b}_1 \times \hat{\boldsymbol{n}}|}. \tag{2.78}$$

Thus,

$$N_1 = \frac{\boldsymbol{b}_2 - (\hat{\boldsymbol{n}}\cdot\boldsymbol{b}_2)\hat{\boldsymbol{n}}}{|\boldsymbol{b}_1 \times \boldsymbol{b}_2|} 2\sin(\theta/2)$$

and

$$N_2 = -\frac{\boldsymbol{b}_1 - (\hat{\boldsymbol{n}}\cdot\boldsymbol{b}_1)\hat{\boldsymbol{n}}}{|\boldsymbol{b}_1 \times \boldsymbol{b}_2|} 2\sin(\theta/2). \tag{2.79}$$

When $\hat{\boldsymbol{n}}$ is parallel to $\boldsymbol{b}_1 \times \boldsymbol{b}_2$ we have a pure twist boundary because $\hat{\boldsymbol{\rho}}$ is then parallel to $\boldsymbol{b}_1 \times \boldsymbol{b}_2$. Then,

$$N_1 = \frac{\boldsymbol{b}_2}{|\boldsymbol{b}_1 \times \boldsymbol{b}_2|} 2\sin(\theta/2)$$

and

$$N_2 = -\frac{\boldsymbol{b}_1}{|\boldsymbol{b}_1 \times \boldsymbol{b}_2|} 2\sin(\theta/2). \tag{2.80}$$

Therefore, we see that the vectors N_1 and N_2 for boundaries of arbitrary $\hat{\boldsymbol{n}}$ in eqn (2.79) are the projections onto that boundary of the N_1 and N_2 for the pure twist boundary. Hence, it may be shown (Frank 1950, Hirth and Lothe 1982) that the dislocation grid for a boundary of arbitrary $\hat{\boldsymbol{n}}$ is just the projection onto it of the dislocation grid of the pure twist boundary. The dislocation structures of all boundaries of this type therefore consist simply of two families of intersecting dislocations.

2.7.4 Epitaxial interfaces

An epitaxial interface is formed when one material (the epilayer) is grown on a thick substrate. If the epilayer has a thickness below some critical value it is energetically favourable for the epilayer to be elastically strained so that a commensurate interface is developed between the epilayer and the substrate. At larger thicknesses a transition occurs in which stress annihilator dislocations are introduced into the interface to relieve the long range stress field in the epilayer. The transition is discussed in Section 2.10.6. In this section we shall confine our attention to the kinds of misfit that may be relieved by the existence of one or two independent sets of stress annihilator dislocations in the interface. We follow the procedure described by Sargent and Purdy (1975), although some of our conclusions are quite different. The purpose is to present an analysis for epitaxial interfaces that is analogous to the analysis of Section 2.7.3 of the types of grain boundaries that may be formed from one or two independent sets of dislocations.

Since the misfit strain is confined largely to the thin epilayer we assume that the reference lattice is the crystal lattice of the substrate. The Frank–Bilby equation is then

$$\boldsymbol{B} = (\mathbf{S}^{-1} - \mathbf{E})\boldsymbol{p} \tag{2.81}$$

where S transforms the components of a vector expressed in the substrate crystal lattice into those of a vector expressed in the crystal lattice of the epilayer. Since the interface is epitaxial we assume that S satisfies $\mathbf{S}\hat{\boldsymbol{n}} = \hat{\boldsymbol{n}}$. This simply ensures that the interface normal is the same direction in both the substrate and deposit lattices.

Let there be only *one set* of crystal lattice dislocations in the interface with Burgers vector $\boldsymbol{b}$ and line sense $\hat{\boldsymbol{\xi}}$, expressed in the substrate lattice. Consider the form of the transformation S that can satisfy the Frank–Bilby equation, eqn (2.1), given this one set of dislocations. We have

$$(\boldsymbol{N}\cdot\boldsymbol{p})\boldsymbol{b} = (\mathbf{S}^{-1} - \mathbf{E})\boldsymbol{p} \tag{2.82}$$

and setting $\boldsymbol{p} = \hat{\boldsymbol{\xi}}$ we deduce that $\mathbf{S}^{-1}\hat{\boldsymbol{\xi}} = \hat{\boldsymbol{\xi}}$. If $\hat{\boldsymbol{\xi}} = [1, 0, 0]$, $\hat{N} = [0, 1, 0]$, and $\hat{\boldsymbol{n}} = [0, 0, 1]$ then $\mathbf{S}^{-1}$ has the form

$$\mathbf{S}^{-1} = \begin{pmatrix} 1 & S_{12}^{-1} & 0 \\ 0 & S_{22}^{-1} & 0 \\ 0 & S_{32}^{-1} & 1 \end{pmatrix}. \tag{2.83}$$

Setting $\boldsymbol{p} = \boldsymbol{N}$ in eqn (2.82) we deduce that $N^2\boldsymbol{b} = (\mathbf{S}^{-1} - \mathbf{E})\boldsymbol{N}$ and therefore $S_{12}^{-1} = b_1/d$, $S_{22}^{-1} = b_2/d + 1$, $S_{32}^{-1} = b_3/d$.

For pure edge dislocations with $\boldsymbol{b}\cdot\hat{\boldsymbol{n}} = 0$ then $b_1 = 0$, $b_2 = b$, $b_3 = 0$, and $\mathbf{S}^{-1}$ describes a tetragonal distortion:

$$\mathbf{S}^{-1} = \begin{pmatrix} 1 & 0 & 0 \\ 0 & (b/d + 1) & 0 \\ 0 & 0 & 1 \end{pmatrix}. \tag{2.84}$$

For pure edge dislocations with $\boldsymbol{b}\cdot\boldsymbol{N} = 0$ then $b_1 = 0$, $b_2 = 0$, $b_3 = b$, and $\mathbf{S}^{-1}$ describes a simple shear normal to the interface plane:

$$\mathbf{S}^{-1} = \begin{pmatrix} 1 & 0 & 0 \\ 0 & 1 & 0 \\ 0 & b/d & 1 \end{pmatrix}. \tag{2.85}$$

For pure screw dislocations $b_1 = b, b_2 = 0, b_3 = 0$, and $\mathbf{S}^{-1}$ describes a simple shear in the interface plane:

$$\mathbf{S}^{-1} = \begin{pmatrix} 1 & b/d & 0 \\ 0 & 1 & 0 \\ 0 & 0 & 1 \end{pmatrix}. \tag{2.86}$$

Consider now the form of the transformation $\mathbf{S}$ that is possible when *two independent sets of dislocations* are present in the interface. Let the Burgers vectors of the two sets be $\boldsymbol{b}_1$ and $\boldsymbol{b}_2$ and let the line senses be $\hat{\boldsymbol{\xi}}_1$ and $\hat{\boldsymbol{\xi}}_2$. The Frank–Bilby equation becomes:

$$(N_1 \cdot p)\boldsymbol{b}_1 + (N_2 \cdot p)\boldsymbol{b}_2 = (\mathbf{S}^{-1} - \mathbf{E})p. \tag{2.87}$$

Setting p equal to $\hat{\boldsymbol{\xi}}_1$ and $\hat{\boldsymbol{\xi}}$ in turn we deduce that

$$(N_2 \cdot \hat{\boldsymbol{\xi}}_1)\boldsymbol{b}_2 = (\mathbf{S}^{-1} - \mathbf{E})\hat{\boldsymbol{\xi}}_1 \tag{2.88}$$

and

$$(N_1 \cdot \hat{\boldsymbol{\xi}}_2)\boldsymbol{b}_1 = (\mathbf{S}^{-1} - \mathbf{E})\hat{\boldsymbol{\xi}}_2 \tag{2.89}$$

Setting $\hat{\boldsymbol{\xi}}_1 = [1, 0, 0]$, $N_1 = [0, 1/d_1, 0]$, $\hat{n} = [0, 0, 1]$, $\hat{\boldsymbol{\xi}}_2 = [\hat{\xi}_{21}, \hat{\xi}_{22}, 0]$, $N_2 = 1/d_2[N_{21}, N_{22}, 0]$, $\boldsymbol{b}_1 = [b_{11}, b_{12}, b_{13}]$ and $\boldsymbol{b}_2 = [\mathbf{b}_{21}, b_{22}, b_{23}]$ and substituting these vectors into eqns (2.88) and (2.89) we find that

$$\mathbf{S}^{-1} = \begin{pmatrix} -\xi_{22}b_{21}/d_2 + 1 & b_{11}/d_1 + \xi_{21}b_{21}/d_2 & 0 \\ -\xi_{22}b_{22}/d_2 & b_{12}/d_1 + \xi_{21}b_{22}/d_2 + 1 & 0 \\ -\xi_{22}b_{23}/d_2 & b_{13}/d_1 + \xi_{21}b_{23}/d_2 & 1 \end{pmatrix}. \tag{2.90}$$

If the two sets of dislocations are pure edge dislocations with Burgers vectors in the plane of the interface, then $\mathbf{S}^{-1}$ has the form:

$$\mathbf{S}^{-1} = \begin{pmatrix} (\sin^2\theta)b_2/d_2 + 1 & -(\sin\theta\cos\theta)b_2/d_2 & 0 \\ -(\sin\theta\cos\theta)b_2/d_2 & 1 + b_1/d_1 + (\cos^2\theta)b_2/d_2 & 0 \\ 0 & 0 & 1 \end{pmatrix}, \tag{2.91}$$

where $b_1 = |\boldsymbol{b}_1|$, $b_2 = |\boldsymbol{b}_2|$, and $\hat{\boldsymbol{\xi}}_2 = [\cos\theta, \sin\theta, 0]$. When the angle θ between the dislocation lines is 90°, $\mathbf{S}^{-1}$ reduces to a diagonal matrix describing two orthogonal tensile strains, of magnitudes b_1/d_1 and b_2/d_2, in the plane of the interface. For θ between 0 and 90°, $\mathbf{S}^{-1}$ is no longer diagonal but it is symmetric. When it is diagonalized it is found to represent two orthogonal principal strains in the plane of the interface of magnitude $(x \pm (x^2 - 4(b_1b_2/d_1d_2)\sin^2\theta)^{\frac{1}{2}})/2$, where $x = b_1/d_1 + b_2/d_2$. However, the directions of these tensile strains no longer coincide with the Burgers vectors $\boldsymbol{b}_1$ and $\boldsymbol{b}_2$. Instead, the two angles between the principal strain axes and $\boldsymbol{b}_1$ are given by

$$\tan\varphi = \tan\theta - \frac{x}{(b_2/d_2)\sin(2\theta)}\left(1 \mp \left[1 - \frac{4b_1b_2\sin^2\theta}{d_1d_2x^2}\right]^{\frac{1}{2}}\right). \tag{2.92}$$

If the two sets of dislocations are pure screw dislocations then $\mathbf{S}^{-1}$ has the form:

$$\mathbf{S}^{-1} = \begin{pmatrix} 1 - \sin\theta\cos\theta\, b_2/d_2 & b_1/d_1 + \cos^2\theta\, b_2/d_2 & 0 \\ -\sin^2\theta\, b_2/d_2 & 1 + \sin\theta\cos\theta\, b_2/d_2 & 0 \\ 0 & 0 & 1 \end{pmatrix}. \tag{2.93}$$

As before $\hat{\boldsymbol{\xi}}_2 = [\cos\theta, \sin\theta, 0]$. $\mathbf{S}^{-1}$ describes a shear transformation in the interface plane, although it is neither pure nor simple in general. The principal strains are $\pm\sqrt{b_1 b_2/d_1 d_2}\sin\theta$ and the angles between the principal directions and $\boldsymbol{b}_1$ are given by

$$\tan\varphi = \frac{\left[\frac{b_2}{d_2}\right]^{\frac{1}{2}}\sin\theta}{\left[\frac{b_2}{d_2}\right]^{\frac{1}{2}}\cos\theta \mp \left[\frac{b_1}{d_1}\right]^{\frac{1}{2}}}. \tag{2.94}$$

2.8 LOCAL DISLOCATION INTERACTIONS

The analysis of the stress annihilator dislocation content of an interface presented thus far takes no account of interactions between the dislocations. The dislocations were all straight, even when they crossed each other, and the spacing of parallel dislocations was constant. We have already remarked that the spacing of parallel dislocations is quantized by the crystal lattice, so that we expect variations in the spacing such that the average spacing is the same as that predicted by the theory. When dislocation lines cross they interact and may form new networks. It is obvious that the decomposition of the net Burgers vector content $\boldsymbol{B}$ into Burgers vectors of discrete dislocations is not unique, and the correct description is the one corresponding to the lowest boundary energy.

The local interactions that arise from dislocations crossing each other depend on their self-energies and interaction energies and thus they depend on the crystal structure and the character of the interface. This has been considered in detail by Amelinckx and Dekeyser (1959) for small-angle grain boundaries in cubic crystals and by Amelinckx (1979). Here we confine ourselves to a few general remarks and refer the reader to Amelinckx and Dekeyser (1959) and Amelinckx (1979) for a more specific treatment. Provided the final dislocation network in the interface still satisfies the Frank–Bilby equation the interface will remain free of long-range stresses.

One possible way of satisfying this condition is for an array of parallel dislocations with Burgers vector $\boldsymbol{b}$, line direction $\hat{\boldsymbol{\xi}}$, and $N = (\hat{\boldsymbol{n}} \times \hat{\boldsymbol{\xi}})/d$, to split into two arrays of Burgers vector $\boldsymbol{b}$, line directions $\hat{\boldsymbol{\xi}}_1$ and $\hat{\boldsymbol{\xi}}_2$, and $N_1 = (\hat{\boldsymbol{n}} \times \hat{\boldsymbol{\xi}}_1)/d_1$ and $N_2 = (\hat{\boldsymbol{n}} \times \hat{\boldsymbol{\xi}}_2)/d_2$), such that $N = N_1 + N_2$. This follows from $(N\cdot\boldsymbol{p})\boldsymbol{b} = (N_1\cdot\boldsymbol{p})\boldsymbol{b} + (N_2\cdot\boldsymbol{p})\boldsymbol{b}$ for any interfacial vector $\boldsymbol{p}$, and hence the Frank–Bilby equation is unaffected.

Another way of not affecting the Frank–Bilby equation is by repeating local changes regularly throughout the network, such that the average directions of the dislocations are not altered. These local rearrangements do not change the number of dislocations cut by a large vector $\boldsymbol{p}$ in the interface and thus the Frank–Bilby equation remains satisfied. An example is shown in Fig. 2.19 where a lozenge-shaped network has interacted locally to produce a hexagonal network. The interaction can be visualized as occurring in two steps. In the first, each straight dislocation in the sets 1 and 2 in Fig. 2.19(a) is transformed into a zig-zag configuration conforming to the geometry in Fig. 2.19(b). In the second, segments of dislocations 1 and 2 which overlap react to form segments of new dislocations of type 3 according to the Burgers vector reaction $\boldsymbol{b}^{(1)} + \boldsymbol{b}^{(2)} = \boldsymbol{b}^{(3)}$. If a reaction does not occur the network has a lozenge-shaped mesh, as shown in Fig. 2.19(b). In general, twist grain boundaries are expected to contain hexagonal networks of dislocations except when the lines are within a few degrees of being orthogonal. Whether or not reactions take place is determined by a balance of elastic energies that is considered in detail by Hirth and Lothe (1982).

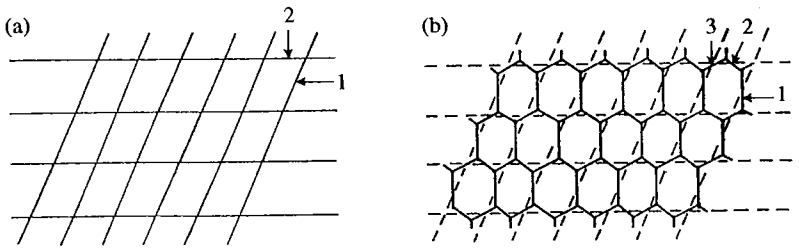

Fig. 2.19 Local interactions in a lozenge–shaped network of two types of dislocation in (a) to produce a hexagonal network of three types of dislocation in (b). (From Hirth and Lothe (1982).)

2.9 TWO EXAMPLES

In this section we shall illustrate the application of the theory of dislocation arrays at interfaces to two heterophase interfaces. In the first example we consider interfaces, produced by diffusion bonding at 1200 °C, between single crystals or polycrystals of Pt and a (001) substrate of NiO, following Shieu and Sass (1990). The interesting feature about some of these interfaces is that there is a misorientation of the f.c.c. crystal axes in addition to the misfit arising from the difference in lattice parameters a^{Pt} and a^{NiO}. In the second example we consider Al–Al_3Ni interfaces in a directionally soldified eutectic alloy, following Knowles and Goodhew (1983*a*, *b*). Those authors determined the line directions of three sets of stress annihilator dislocations within interfaces bounding the Al_3Ni rods and then used the theory in a rather novel way to deduce the transformation relating the Al and Al_3Ni phases and the Burgers vectors of the dislocations.

2.9.1 Pt–NiO interfaces

Shieu and Sass (1990) observed three types of orientation relation between single crystals of Pt, or polycrystalline films of Pt, and a single crystal (001) substrate of NiO. Here we shall confine our attention to the perfect epitaxial orientation ($(001)^{Pt}$ on $(001)^{NiO}$ and $[110]^{Pt}$ parallel to $[110]^{NiO}$) and the 'twist misfit' interface in which the $[110]^{Pt}$ and $[110]^{NiO}$ axes are misoriented by an angle θ. When $\theta = 0$ we recover the perfect epitaxial orientation. For the perfect epitaxial orientation a square network of dislocations was observed with line directions along [110] and $[1\bar{1}0]$ and a spacing of 5.2 ±0.5 nm. At the twist misfit interfaces square arrays of dislocations were also observed but the spacings of the dislocations decreased as θ increased and the line directions changed rapidly from ⟨110⟩. For example, for $\theta = 1.5°$ the measured spacing of the dislocations was 3.8 ± 0.5 nm and the line directions were approximately 25 ° away from ⟨110⟩. An example of the dislocation structure observed in a misoriented interface is shown in Fig. 2.20. Our task is to explain the observed spacings and line directions of the dislocations as a function of θ. Our analysis is similar to that of Shieu and Sass (1990) except that we take the Pt crystal lattice, rather than the NiO lattice, as our reference lattice and we use the Frank–Bilby theory rather than the O-lattice formulation. Our reason for choosing the Pt crystal as the reference is that we believe that the dislocations could lie slightly on the Pt side because NiO is elastically harder. Of course, whether we use the Frank–Bilby theory or the O-lattice theory makes no difference to the predicted line directions and spacings.

We define the misfit parameter α as follows:

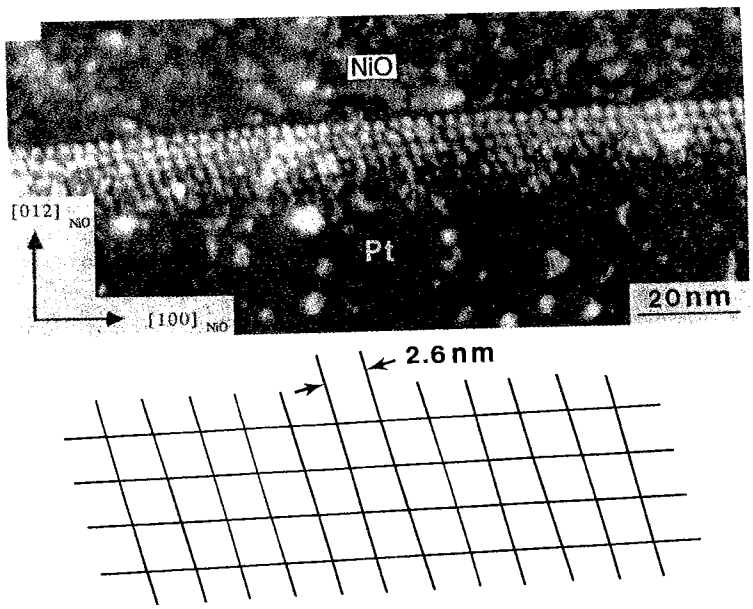

Fig. 2.20 Dark-field electron micrograph of a NiO–Pt interface with a misorientation comprising $\simeq 3.2°$ about the axis normal to the interface and $\simeq 1°$ about the $[1\bar{1}0]$ axis of NiO in the plane of the interface. A network of two sets of dislocations is seen as shown in the schematic diagram. From Shieu and Sass (1990).

$$\alpha = \frac{a^{\mathrm{NiO}} - a^{\mathrm{Pt}}}{a^{\mathrm{Pt}}}. \tag{2.95}$$

The appropriate values of a^{NiO} and a^{Pt} are those at the temperature at which the interfaces were formed, i.e. 1200 °C. Using the value of the lattice parameter for Pt at 20 °C (0.392 39 nm) and the linear thermal expansion coefficient for Pt ($9 \times 10^{-6}\,°\mathrm{C}^{-1}$) we obtain $a^{\mathrm{Pt}} = 0.396\,56$ nm at 1200 °C. The lattice parameter of NiO at 275 °C is 0.419 46 nm, but the linear thermal expansion coefficient is not available. If we assume the thermal expansion coefficient is the same as that of MgO (i.e. $12.8 \times 10^{-6}\,°\mathrm{C}^{-1}$) we obtain $a^{\mathrm{NiO}} = 0.424\,43$ nm at 1200 °C. Therefore at 1200 °C the misfit parameter $\alpha = 0.0703$. In view of the uncertainty about the NiO lattice parameter at 1200 °C it is unreasonable to specify α so precisely and we shall assume $\alpha = 0.07$. If the $[110]^{\mathrm{NiO}}$ axis is misoriented from the $[110]^{\mathrm{Pt}}$ axis by θ then the transformation **S** relating the NiO lattice to the Pt lattice is

$$\mathbf{S} = (1+\alpha)\begin{pmatrix} \cos\theta & -\sin\theta & 0 \\ \sin\theta & \cos\theta & 0 \\ 0 & 0 & 0 \end{pmatrix}, \tag{2.96}$$

and therefore

$$\mathbf{W} = \mathbf{S}^{-1} - \mathbf{E} = \frac{1}{1+\alpha}\begin{pmatrix} 1+\alpha-\cos\theta & -\sin\theta & 0 \\ \sin\theta & 1+\alpha-\cos\theta & 0 \\ 0 & 0 & \alpha \end{pmatrix}. \tag{2.97}$$

We *assume* that the Burgers vectors of the observed dislocations are $\boldsymbol{b}_1 = \frac{1}{2}[110]$ and $b_2 = \frac{1}{2}[1\bar{1}0]$ lattice vectors of the Pt crystal. The Frank–Bilby equation becomes:

$$(N_1 \cdot \boldsymbol{p})\boldsymbol{b}_1 + (N_2 \cdot \boldsymbol{p})\boldsymbol{b}_2 = \mathbf{W}\boldsymbol{p}, \tag{2.98}$$

and multiplying both sides of this equation with $\boldsymbol{b}_1$ and setting $\boldsymbol{p} = \hat{\boldsymbol{\xi}}_1$ we deduce that $\mathbf{W}^t\boldsymbol{b}_1 \cdot \hat{\boldsymbol{\xi}}_1 = 0$. Therefore $\hat{\boldsymbol{\xi}}$ is perpendicular to $\mathbf{W}^t\boldsymbol{b}_1$ and [001], i.e.

$$\hat{\boldsymbol{\xi}}_1 = \frac{[(1 + \alpha - \cos\theta - \sin\theta), -(1 + \alpha - \cos\theta + \sin\theta), 0]}{\sqrt{2(1 + \alpha - \cos\theta)^2 + 2(\sin\theta)^2}}. \tag{2.99}$$

The angle η_1 between $\hat{\boldsymbol{\xi}}_1$ and $\boldsymbol{b}_1$ indicates the edge vs. screw character of the dislocations:

$$\tan\eta_1 = \frac{(1 + \alpha - \cos\theta)}{\sin\theta}. \tag{2.100}$$

We observe that when $\theta = 0$, i.e. at the exact epitaxial interface, the dislocations are of pure edge type, and that the angle η_1 decreases rapidly from 90 ° at small values of θ. For $\theta = 1.5$ ° we obtain $\eta = 70$ °. Similar results are obtained for $\hat{\boldsymbol{\xi}}_2$ and η_2:

$$\hat{\boldsymbol{\xi}}_2 = \frac{[(-1 - \alpha + \cos\theta - \sin\theta), -(1 + \alpha - \cos\theta - \sin\theta), 0]}{\sqrt{2(1 + \alpha - \cos\theta)^2 + 2(\sin\theta)^2}}, \tag{2.101}$$

and $\eta_2 = \eta_1$, so that the dislocations remain orthogonal regardless of θ. Thus, we have shown that the network of $\frac{1}{2}\langle 110\rangle$ dislocations remains orthogonal as the twist angle is varied and that the network is rotated, initially very rapidly, as the twist angle is increased. The estimation that the network rotates by 20 ° when $\theta = 1.5$ ° compares very well with the experimentally observed rotation of 25 ° in view of the extreme sensitivity of η_1 to both α and θ.

The dislocation spacing d_1 is readily found from

$$\frac{\boldsymbol{b}_1}{d_1} = \mathbf{W}\hat{\boldsymbol{n}} \times \hat{\boldsymbol{\xi}}_1, \tag{2.102}$$

which is obtained by setting $\boldsymbol{p} = N_1$ in eqn (2.98). From this we deduce that

$$\begin{aligned} d_1 &= \frac{(1 + \alpha)a^{\mathrm{Pt}}}{\sqrt{2(1 + \alpha + \cos\theta)^2 + 2(\sin\theta)^2}} \\ &= \frac{a^{\mathrm{NiO}}a^{\mathrm{Pt}}}{2[(a^{\mathrm{Pt}})^2 + (a^{\mathrm{NiO}})^2 - 2a^{\mathrm{Pt}}a^{\mathrm{NiO}}\cos\theta)]^{\frac{1}{2}}}. \end{aligned} \tag{2.103}$$

When $\theta = 1.5$ ° we obtain $d_1 = 4.0$ nm, which compares very well with the experimentally observed spacing of 3.8 ± 0.5 nm. At $\theta = 0$ we obtain 4.3 nm, which is somewhat smaller than the experimentally observed spacing of 5.2 ± 0.5 nm.

2.9.2 Al–Al_3Ni eutectic interfaces

Knowles and Goodhew (1983*a*,*b*) studied the dislocation structures of interfaces between Al_3Ni fibres in an Al matrix by transmission electron microscopy. The specimen was produced by directional solidification. Al_3Ni has a complicated orthorhombic structure and the Al matrix has an f.c.c. structure. The [010] axis of the fibres was parallel to the $[1\bar{1}0]$ axis of the matrix and the (111) plane in the matrix was parallel to the (102) plane

in the fibres. There was pronounced faceting of the fibres and three predominant interface planes, which were high index in both fibre and matrix, were observed. It was found that three sets of dislocations appeared in the interfaces, with spacings and directions that varied with the interface normal $\hat{n}$. It was not possible to determine the Burgers vectors of the dislocations experimentally but it was possible to find three vectors r_1, r_2, and r_3 such that for each interface normal the three sets of observed line directions and spacings satisfied

$$\hat{\xi}_i \text{ parallel to } r_i \times \hat{n}$$

and

$$d_i = \frac{1}{|r_i \times \hat{n}|}. \tag{2.104}$$

The significance of this is realized by comparing these equations with eqns (2.47) and (2.49): r_i is to be identified with $\mathbf{W}^t b_i^*$, which is a basis vector of the reciprocal lattice of the O-lattice (see eqn (2.56)). The three r_i were found to be:

$$\begin{aligned} r_1 &= 0.131\,[\cos 63.1\,^\circ, \cos 31.6\,^\circ, \cos 74.7\,^\circ] \\ r_2 &= 0.625\,[\cos 138.7\,^\circ, \cos 130.8\,^\circ, \cos 84.8\,^\circ] \\ r_3 &= 0.151\,[\cos 44.7\,^\circ, \cos 53.4\,^\circ, \cos 68.0\,^\circ] \end{aligned} \tag{2.105}$$

in units of nm^{-1}, using an axis system parallel to the crystal axes in the Al matrix. The problem now is to determine the transformation matrix $\mathbf{W}$ and the set of three b_i which satisfy the three equations

$$r_i = \mathbf{W}^t b_i^*. \tag{2.106}$$

The transformation matrix $\mathbf{W}$ in these equations describes the deviation in the actual relationship between the crystal lattices from some bicrystal reference structure. The Burgers vectors b_i are defined with respect to a corresponding reference lattice. There are two related questions to be answered: what is the appropriate reference structure that defines $\mathbf{W}$ and what are the appropriate Burgers vectors? In principle there is an infinite number of possible reference structures but in practice there are restrictions that may be placed on the solutions in order for them to make physical sense. Knowles and Goodhew (1983b) made the common assumption of the near CSL model for their selection of possible reference structures as described in Section 2.2. According to this model we must seek CSL^w and CSL^b cells (Fig. 2.10(a)) in the matrix and fibre lattices that are almost coincident at the observed orientation relationship between the matrix and fibre lattices. The strain that is required to make them coincident is then the source of the misfit in the interface that gives rise to the observed dislocations, as was the case in Fig. 2.10(b). It seems reasonable to demand that there is at least one near CSL period between successive dislocations. If this were not the case then it would not make sense to describe the dislocations as localizing the misfit from the near CSL reference structure and, therefore, the reason for the existence of the dislocations would disappear. The Burgers vectors are vectors of the reference DSC lattice and it is possible that they are non-primitive vectors, although we would not expect them to be much larger than primitive DSC lattice vectors for reasons of energetics. This restriction was used by Knowles and Goodhew (1983*b*), together with the restriction described earlier for the choice of reference state, to eliminate many possible solutions of eqn (2.106).

Eight possible choices of reference structure were considered by Knowles and Goodhew

(1983b) and all of them involved non-primitive DSC lattice vectors for the $\boldsymbol{b}_i$. The most successful choice of reference state was judged by comparing the predicted and observed spacings of dislocations on the three interface facets. The Burgers vectors of the interfacial dislocations were thus found to be $\boldsymbol{b}_1 = \frac{1}{2}[1\bar{2}1]$, $\boldsymbol{b}_2 = \frac{1}{4}[11\bar{2}]$, and $\boldsymbol{b}_3 = [010]$ with respect to the matrix coordinate system. However, it was necessary to use the lattice parameters of Al and Al_3Ni at an elevated temperature in order to obtain satisfactory agreement. It was assumed that the thermal expansion of Al_3Ni was negligible in comparison with that of Al and the room temperature lattice parameters of Al_3Ni were used. The near coincident unit cell was of a relatively small volume, i.e. $12.5(a^m)^3$ and $4abc$ where a^m is the lattice parameter in the matrix and a,b,c are the lattice parameters in the fibre.

The analysis of Knowles and Goodhew raises the general question of whether the matrix $\mathbf{W}$ can be specified uniquely if we know the Burgers vectors, line directions, and spacings of all dislocations in a particular interface. The answer is *no* because $\boldsymbol{B} = \mathbf{W}\boldsymbol{p}$ may always be replaced by $\boldsymbol{B} = \mathbf{W}\mathbf{I}\boldsymbol{p}$, where $\mathbf{I}$ is an invariant plane strain (see eqn (2.32)), which, by definition, leaves all interface vectors $\boldsymbol{p}$ invariant. Knowles and Goodhew overcame this difficulty by analysing the line directions and spacings of dislocations in non-parallel interfaces.

2.10 ELASTIC FIELDS OF INTERFACES

2.10.1 Introduction

In Section 2.2 we discussed two formulations of the dislocation content of a flat interface that is free of long-range stresses. In Bonnet's formulation the elastic field is modelled by cancelling arrays of stress generator and annihilator dislocations. There is no net dislocation content of the interface. In the Read–Shockley formulation there is a net dislocation content of the interface, which alters the relationship between the crystal lattices from that of some reference structure. We have maintained that the two approaches are equivalent provided there is no stress field far from the interface. In this section we consider the elastic field of such an interface. Each crystal is approximated by an elastic continuum and continuity of displacements and tractions are assumed to be maintained at the interface. The dislocations in the interface are regarded mathematically as source functions which generate the stress field of the interface. In linear elastic theory the field of the interface is given by a linear superposition of the elastic fields of all the dislocations in the interface.

There is no inconsistency in applying the Read–Shockley formulation (see Section 2.2) to the elastic field of a grain boundary. In the absence of externally applied constraints to the bicrystal the distortion field of the dislocations reduces to a pure rotation far from the boundary plane and the strain tensor tends to zero. Since the stress is proportional to the strain it follows that the stress field of the dislocation array should also tend to zero far from the boundary plane. We expect this remark to apply irrespective of whether the elastic constants of the two crystals are the same, or whether isotropic or anisotropic elasticity is assumed. The only condition is that the relationship between the crystal lattices is a pure rotation. In this section we examine whether our expectation is satisfied when linear elasticity is used to model the elastic fields of dislocation arrays in the Read–Shockley formulation. Because we are restricting ourselves to linear elasticity the misorientation must be small. We shall see that our expectation is always satisfied, but in some cases care has to be taken with the boundary conditions far from the interface.

In particular, simply summing the elastic fields of dislocations accommodating a misorientation between crystals of the same structure in anisotropic elasticity, or between crystals with different structures in isotropic or anisotropic elasticity, does not give zero long-range stresses unless care is taken to ensure that no tractions are applied externally to the bicrystal.

The same cannot be said of applying the Read–Shockley formulation to a heterophase interface. The distortion field of the dislocations effects a change in crystal structure, which is not merely a rotation. Since the strain tensor is finite far from the interface it follows that there is a long-range stress field associated with the dislocations. The absence of a long-range stress field in reality can be modelled correctly with interfacial dislocations by using Bonnet's formulation. For example, at an epitaxial interface the uniform state of stress in a thin epilayer (i.e. below the critical thickness) can be modelled by a uniform, continuous distribution of dislocations at the interface. These dislocations are stress generators. Their long-range field is cancelled at large thicknesses by the introduction of discrete stress annihilator dislocations. Thus, both arrays are necessary to describe the stress field of the interface in the absence of long-range stresses.

2.10.2 Stress and distortion fields of grain boundaries in isotropic elasticity

In Section 2.7.2 we saw how a general grain boundary may be modelled by three sets of parallel dislocations, with line directions and spacings given by eqns (2.63) and (2.65). In Section 2.7.3 we discussed the types of grain boundary that may be modelled with just one or two independent sets of dislocations. In this section we obtain expressions for the linear isotropic elastic stress fields of these arrays of dislocations. We assume that the dislocation lines are straight. Local dislocation interactions may violate this assumption and it is then necessary to sum the stress fields of dislocation segments. Although Frank's formula prescribes the net Burgers vector density required to produce a particular relative rotation, it is perhaps not obvious that the sum of the elastic distortions produced by an array of dislocations, with the required net Burgers vector density, effects the required rotation. We demonstrate that this is satisfied in the approximation that $2\sin(\theta/2) \cong \theta$, i.e. in the small-angle regime. Moreover, we demonstrate that long-range stresses when they exist, are consistent with the presence of long-range strains and Hooke's law. The existence of long-range strains implies a change of crystal structure across the interface. To model correctly the absence of long-range stresses at such an interface requires cancelling arrays of stress generator and annihilator dislocations.

Following Hirth and Lothe (1982) we consider an array of straight dislocations parallel to the z-axis, and let the boundary normal be along the x-axis, as shown in Fig. 2.21. Let the Burgers vector have components (b_x, b_y, b_z). We may obtain the stress field of this array of dislocations by considering the stress fields of three components separately and summing them, as shown schematically in Fig. 2.21.

The first array has $\boldsymbol{b} = (b_x, 0, 0)$ and is shown in Fig. 2.21(a). This is the array expected in a symmetric tilt boundary. For an isolated edge dislocation at the origin with Burgers vector $(b_x, 0, 0)$ the displacement, $(u_x, u_y, 0)$, and stress field, τ, at the point (x, y, z) are

$$u_x = \frac{b_x}{2\pi}\left[\tan^{-1}\left(\frac{y}{x}\right) + \frac{xy}{2(1-\nu)(x^2+y^2)}\right] \tag{2.107}$$

$$u_y = -\frac{b_x}{2\pi}\left[\frac{(1-2\nu)}{4(1-\nu)}\ln(x^2+y^2) + \frac{x^2-y^2}{4(1-\nu)(x^2+y^2)}\right] \tag{2.108}$$

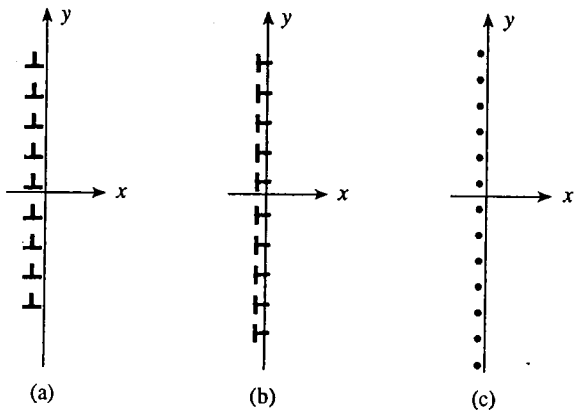

Fig. 2.21 Schematic illustration of the manner in which the linear elastic stress field of an array of dislocations along z with Burgers vector (b_x, b_y, b_z) is broken down into component arrays with Burgers vector (a) $(b_x, 0, 0)$, (b) $(0, b_y, 0)$ and (c) $(0, 0, b_z)$.

$$\tau_{xx} = -\frac{\mu b_x}{2\pi(1-\nu)} \frac{y(3x^2+y^2)}{(x^2+y^2)^2} \tag{2.109}$$

$$\tau_{yy} = \frac{\mu b_x}{2\pi(1-\nu)} \frac{y(x^2-y^2)}{(x^2+y^2)^2} \tag{2.110}$$

$$\tau_{xy} = \frac{\mu b_x}{2\pi(1-\nu)} \frac{x(x^2-y^2)}{(x^2+y^2)^2} \tag{2.111}$$

$$\tau_{zz} = \nu(\tau_{xx}+\tau_{yy}) = -\frac{\mu b_x \nu}{\pi(1-\nu)} \frac{y}{(x^2+y^2)} \tag{2.112}$$

$$\tau_{xz} = \tau_{yz} = 0 \tag{2.113}$$

Here ν is Poisson's ratio. Using eqn (2.109) we deduce that the stress τ_{xx} due to the array of dislocations shown in Fig. 2.21(a) is given by

$$\tau_{xx} = -\frac{\mu b_x}{2\pi(1-\nu)D} \sum_{n=-\infty}^{\infty} \frac{(3X^2+(Y-n)^2)(Y-n)}{(X^2+(Y-n)^2)^2} \tag{2.114}$$

where $X = x/D$, $Y = y/D$, and D is the dislocation spacing. Performing the sum we obtain:

$$\tau_{xx} = -\tau_0 \sin(2\pi Y)(\cosh(2\pi X) - \cos(2\pi Y) + 2\pi X \sinh(2\pi X)) \tag{2.115}$$

where

$$\tau_0 = \frac{\mu b_x}{2D(1-\nu)(\cosh(2\pi X) - \cos 2\pi Y)^2}. \tag{2.116}$$

The other stress components are similarly found using eqns (2.110) and (2.111):

$$\tau_{yy} = -\tau_0 \sin(2\pi Y)(\cosh(2\pi X) - \cos(2\pi Y) - 2\pi X \sinh(2\pi X)) \tag{2.117}$$

$$\tau_{xy} = \tau_0 2\pi X (\cosh(2\pi X)\cos(2\pi Y) - 1). \tag{2.118}$$

At large distances form the boundary, where $x \gg D/2\pi$, the stresses decay exponentially. For example, τ_{xx} behaves as follows:

$$\tau_{xx} \cong -\frac{\mu b_x \sin(2\pi y/D)}{(1-\nu)D}(2\pi x/D)\exp(-2\pi x/D). \tag{2.119}$$

Thus, there are no long-range stresses. Indeed, at $x = 2D$ the the stresses have decayed to approximately 1 per cent of the stress from a single dislocation, in agreement with St Venant's principle. In the boundary plane, where $x = 0$, the ratio of the stress, τ_{xx}, at $(0, y)$ to the stress due to a single dislocation at the origin is equal to $(\pi y/D)\cot(\pi y/D)$. Thus at separations of up to $D/2\pi$ from a given dislocation in the array, more than 90 per cent of the stress τ_{xx} of the array is attributable to the given dislocation.

The second array, Fig. 2.21(b), has $\boldsymbol{b} = (0, b_y, 0)$. The stress fields of this array are given by

$$\tau_{xy} = \tau_0 \sin(2\pi Y)(\cosh(2\pi X) - \cos(2\pi Y) - 2\pi X \sinh(2\pi X)) \tag{2.120}$$

$$\tau_{xx} = -\tau_0 2\pi X(\cosh(2\pi X)\cos(2\pi Y) - 1) \tag{2.121}$$

$$\tau_{yy} = \tau_0[2\sinh(2\pi X)(\cosh(2\pi X) - \cos(2\pi Y)) - 2\pi X(\cosh(2\pi X)\cos(2\pi Y) - 1)] \tag{2.122}$$

As $x \to \pm\infty$ it is seen that τ_{xx} and τ_{xy} tend to zero exponentially, but

$$\tau_{yy} \to \frac{\mu b_y}{D(1-\nu)}\operatorname{sgn}(x), \tag{2.123}$$

where $\operatorname{sgn}(x) = 1$ if $x > 0$ and $\operatorname{sgn}(x) = -1$ if $x < 0$. Therefore, there is a long-range stress field, τ_{yy}, associated with this array of dislocations. This simply means that for a grain boundary to satisfy Frank's formula there must be no net Burgers vector parallel to the boundary plane associated with edge dislocations. For example, for the asymmetric tilt boundary, which can be modelled by two independent arrays of edge dislocations, the components of the Burgers vector densities parallel to the boundary plane cancel, as seen in eqn (2.71). An array of dislocations of the type shown in Fig. 2.21(b) can appear in an epitaxial interface. In that case the stress field far from the interface is cancelled by the stress field of the stress generator array.

The final array, shown in Fig. 2.21(c), is associated with the following stress fields:

$$\tau_{xz} = -\frac{\mu b_z}{2D}\frac{\sin(2\pi Y)}{\cosh(2\pi X) - \cos(2\pi Y)} \tag{2.124}$$

$$\tau_{yz} = \frac{\mu b_z}{2D}\frac{\sinh(2\pi X)}{\cosh(2\pi X) - \cos(2\pi Y)}. \tag{2.125}$$

As $x \to \pm\infty$ it is seen that τ_{xz} decays to zero exponentially but

$$\tau_{yz} \to \frac{\mu b_z}{2D}\operatorname{sgn}(x). \tag{2.126}$$

To derive these formulae we have used the stress field of a single screw dislocation with Burgers vector $(0, 0, b_z)$:

$$\tau_{xz} = -\frac{\mu b_z}{2\pi}\frac{y}{x^2 + y^2}, \tag{2.127}$$

$$\tau_{yz} = \frac{\mu b_z}{2\pi}\frac{x}{x^2 + y^2}, \tag{2.128}$$

$$\tau_{xy} = \tau_{xx} = \tau_{yy} = \tau_{zz} = 0. \tag{2.129}$$

The displacement field for the isolated screw dislocation is:

$$u_z = -\frac{b_z}{2\pi}\tan^{-1}(x/y);\ u_x = u_y = 0. \tag{2.130}$$

Equation (2.126) shows that a single array of screw dislocations in a grain boundary is associated with a long-range shear stress τ_{yz}. In a pure twist boundary this is cancelled by another array of screw dislocations along y. The combined effect of the two arrays of screw dislocations is to produce a rotation about the boundary normal x, and all stress components decay exponentially at large separations from the boundary plane.

The distortion tensor $\mathbf{u}$ is defined by the nine derivatives of the displacements u_x, u_y, u_z:

$$\mathbf{u} = \begin{bmatrix} u_{x,x} & u_{x,y} & u_{x,z} \\ u_{y,x} & u_{y,y} & u_{y,z} \\ u_{z,x} & u_{z,y} & u_{z,z} \end{bmatrix}. \tag{2.131}$$

where $u_{x,y} = \partial u_x/\partial y$, etc. The strain tensor components are symmetric combinations of the distortion tensor, e.g.

$$\left.\begin{aligned} \varepsilon_{xy} &= (u_{x,y} + u_{y,x})/2 \\ \varepsilon_{xx} &= u_{x,x} \end{aligned}\right\} \tag{2.132}$$

whereas the antisymmetric components of $\mathbf{u}$ define the rotation vector, $\boldsymbol{\theta}$, at a point:

$$\left.\begin{aligned} \theta_x &= (u_{y,z} - u_{z,y})/2 \\ \theta_y &= (u_{z,x} - u_{x,z})/2 \\ \theta_z &= (u_{x,y} - u_{y,x})/2. \end{aligned}\right\} \tag{2.133}$$

Consider the long-range distortion field of the array of edge dislocations shown in Fig. 2.21(a). Using eqns (2.107) and (2.108) for the displacement fields u_x and u_y we obtain the distortion tensor far from the interface as follows:

$$\mathbf{u}_a = b_x \operatorname{sgn}(x)/2D \begin{bmatrix} 0 & 1 & 0 \\ -1 & 0 & 0 \\ 0 & 0 & 0 \end{bmatrix}. \tag{2.134}$$

Thus the long-range distortion is a relative rotation of the two grains about the z-axis of b_x/D. This is consistent with Frank's formula because $2\sin(\theta/2) \cong \theta = b_x/D$ in the small-angle limit where linear elastic theory is valid. It is also consistent with the absence of any strains and hence any stresses far from the interface.

The long-range distortion field of the dislocation array shown in Fig. 2.21(b) is given by:

$$\mathbf{u}_b = b_y \operatorname{sgn}(x)/2D \begin{bmatrix} \mathrm{f} & 0 & 0 \\ 0 & 1 & 0 \\ 0 & 0 & 0 \end{bmatrix} \tag{2.135}$$

where

$$f = -\nu/(1-\nu) \tag{2.136}$$

This represents a relative tetragonal distortion of b_y/D along the y-axis, and a Poisson contraction of fb_y/D along x. Hooke's law for an isotropic medium may be stated as follows:

$$\left.\begin{aligned}
\tau_{xx} &= 2\mu\varepsilon_{xx} + \lambda e \\
\tau_{yy} &= 2\mu\varepsilon_{yy} + \lambda e \\
\tau_{zz} &= 2\mu\varepsilon_{zz} + \lambda e \\
\tau_{xy} &= 2\mu\varepsilon_{xy} \\
\tau_{yz} &= 2\mu\varepsilon_{yz} \\
\tau_{zx} &= 2\mu\varepsilon_{zx}.
\end{aligned}\right\} \tag{2.137}$$

where

$$\lambda = 2\nu\mu/(1-2\nu) \tag{2.138}$$

and

$$e = \varepsilon_{xx} + \varepsilon_{yy} + \varepsilon_{zz} \tag{2.139}$$

When the long-range disortions, eqn (2.135), are substituted into Hooke's law, using eqn (2.132), we recover the long-range stress τ_{yy}, given by eqn (2.123), and all other stress components are zero.

The long-range distortion field of the array shown in Fig. 2.21(c) is given by:

$$\mathbf{u}_c = b_z \operatorname{sgn}(x)/2D \begin{bmatrix} 0 & 0 & 0 \\ 0 & 0 & 1 \\ 0 & 0 & 0 \end{bmatrix}. \tag{2.140}$$

The presence of a long-range shear distortion is consistent with the long-range stress τ_{yz}, given by eqn (2.126).

Any grain boundary composed of sets of straight dislocations can be analysed using the equations we have given for the stress and distortion fields for the three components of the Burgers vector. Although a given set of dislocations may be associated with a long-range stress field the combination of all sets must be free of long-range stresses if the boundary satisfies Frank's formula.

2.10.3 Grain boundary energies

Read and Shockley (1950) used dislocation theory to analyse grain boundary energies in the isotropic elastic approximation. In this section we shall derive their celebrated formula for small-angle grain boundaries.

Consider a small-angle symmetric tilt boundary, which is composed of a wall of edge dislocations of spacing D. We saw in the previous section that the stress field of each dislocation extends a distance of roughly D. Thus, the energy per unit length of each dislocation is approximately given by

$$E_d \cong \frac{\mu b^2}{4\pi(1-\nu)} \ln(D/r_o) + E_c. \tag{2.141}$$

The core radius of the dislocation is r_o and E_c is the energy per unit length of the dislocation core. Expressing r_o as αb, where α is a constant of the order of unity for a crystal lattice dislocation, and using $\theta \cong b/D$, the energy per unit area of the boundary becomes

$$\sigma \cong \sigma_o \theta (A - \ln \theta) \tag{2.142}$$

where

$$\sigma_o = \frac{\mu b}{4\pi(1-\nu)} \tag{2.143}$$

$$A = \frac{4\pi(1-\nu)E_c}{\mu b^2} - \ln \alpha. \tag{2.144}$$

The parameter σ_o involves only the elastic constants while the parameter A involves unknown quantities about the dislocation cores, namely the core energy and radius.

Although this derivation is rather intuitive it contains the essential physics. We shall follow a derivation presented by Read (1953) which can be readily extended to show that the same form of σ can be expected even when the boundary contains several arrays of dislocations. Consider the symmetric tilt boundary again. The bicrystal is divided into parallel strips centred on each dislocation as shown in Fig. 2.22. Let the energy associated with each strip be E_{strip}. This energy can be divided into an elastic strain energy, E_s, and a core energy, E_c:

$$E_{strip} = E_s + E_c. \tag{2.145}$$

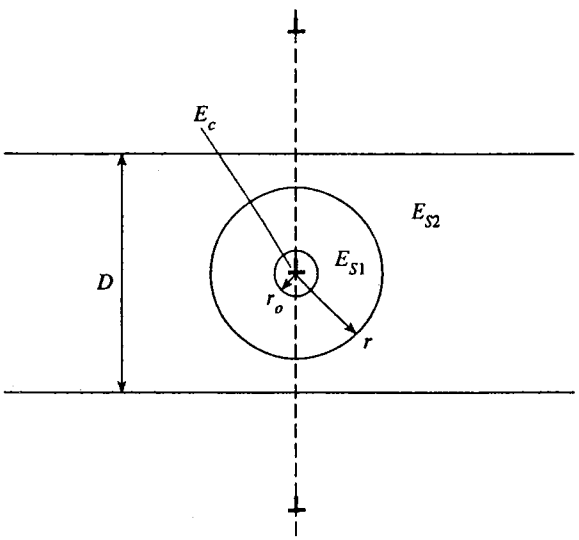

Fig. 2.22 The calculation of grain boundary energy. The array of dislocations, with spacing D, is divided into strips of width D. The elastic strain energy is divided into a contribution, E_{s1}, in a cylindrical region of radius r around the dislocation line, and the energy, E_{s2}, in the volume of the strip outside this region. The core energy, E_c, is confined to the cylindrical region of radius r_o.

The strain energy E_s is further divided into the elastic strain energy, E_{s1}, in a cylindrical region around the dislocation line and the energy in the volume of the strip outside this region, E_{s2} (see Fig. 2.22). The radius of the cylindrical region is $r = cD$, where the constant $c < 1$ must be large enough to ensure $cD \gg r_o$ and small enough for the stress field inside the cylinder to be approximately equal to that of the enclosed dislocation alone.

Suppose the boundary misorientation decreases by $d\theta$, leading to increases in D and r given by:

$$-d\theta/\theta = dD/D = dr/r. \tag{2.146}$$

We now consider the changes in the three contributions to the energy of the strip, dE_c, dE_{s1}, and dE_{s2}. Provided the dislocation spacing D is large enough we can reasonably expect the change in the dislocation core energy, dE_c, to be zero. Consider dE_{s2}. The volume of the strip increases but the elastic energy density decreases because the dislocations are further apart. We now show that these two effects cancel so that $dE_{s2} = 0$. The elastic energy density varies as the square of the elastic strain. The elastic strain in this region varies as b/D. Thus the elastic strain energy in this region is proportional to $1/D^2$. On the other hand, the area of a cylindrical element of area varies as D^2. Thus, the elastic strain energy E_{s2} is invariant when D changes: $dE_{s2} = 0$.

Consider dE_{s1}. The stress in this region depends only on the included dislocation and therefore the elastic energy density does not change. But the area of the region increases from that of a cylinder of radius cD to a cylinder of radius $c(D + dD)$. The elastic stress field in the increased area is that of the included dislocation. The self-energy of a dislocation is equal to the work done on the slip plane in a virtual process in which the dislocation is created by introducing a relative displacement equal to $\boldsymbol{b}$ across a cut on the slip plane. The work is done against the shear stress acting on the slip plane and in the slip direction. The increase in the radius of the cylinder by $dr = cdD$ increases the area of the slip plane by dr per unit length of dislocation. During the virtual process the stress at any point rises from its initial value of zero to its final value of $\tau_o b/r$, so that the work done on the part of the slip plane dr is $\frac{1}{2}\tau_o b^2 dr/r$ of creating the dislocation. τ_o is uniquely determined by the elastic constants of the material and this expression for the stress is valid provided $r \gg b$ and it remains valid even in anisotropic elasticity. Therefore,

$$dE_{strip} = dE_{s1} = \tfrac{1}{2}\tau_o b^2 dr/r = -\tfrac{1}{2}\tau_o b^2 d\theta/\theta. \tag{2.147}$$

Integration of this expression results in the following:

$$E_{strip} = \tfrac{1}{2}\tau_o b^2 (A - \ln\theta). \tag{2.148}$$

A is an integration constant. The energy per unit area of the boundary is E_{strip}/D, or

$$\sigma = \tfrac{1}{2}\tau_o b\theta (A - \ln\theta), \tag{2.149}$$

which is identical to eqn (2.142).

If the boundary contains more than one array of dislocations we have to take account of the interactions between the arrays. But the above analysis shows that the interaction energy can contribute only to the elastic strain energy terms E_{s1} for each array. The above argument may thus be repeated for each array separately, and the interaction energy absorbed into the constants of integration. The result is that σ has the form of

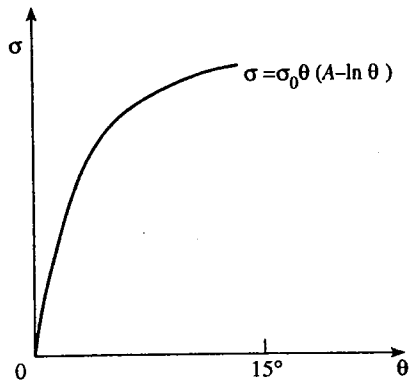

Fig. 2.23 A sketch of the energy, σ, of a small–angle grain boundary as a function of the misorientation, θ, according to eqn (2.142).

eqn (2.142) for each array and therefore the resultant boundary energy still has the form of eqn (2.142). We conclude, therefore, that the predicted variation of σ with θ has the same form for all small-angle grain boundaries. This form is sketched in Fig. 2.23. It is seen that as $\theta \to 0$ the boundary energy shows a cusp.

The derivation assumes that the dislocations are uniformly spaced, but this is possible only when the dislocation spacing corresponds to some crystal repeat distance. Thus, uniformly spaced dislocations occur only at particular misorientations. For intermediate angles the irregularities in the dislocation spacings introduce additional terms in the energy. For a small deviation $\delta\theta$ from the nearest rational angle $\theta = 1/m$ (for rotations about ⟨001⟩ axes in cubic crystals), the extra energy is of order

$$\frac{-\sigma_0 \delta\theta}{m} \ln \delta\theta. \tag{2.150}$$

As $\delta\theta \to 0$ the slope of the σ versus θ curve becomes infinite and the rational angles $\theta = 1/m$ correspond to cusps in the true σ versus θ curve. Thus we obtain the σ versus θ curve that is sketched in Fig. 2.24. The broken line represents eqn (2.142), and at each rational orientation there is small cusp corresponding to the term described by (2.150). The 'strength' of these minor cusps is proportional to $1/m$, and thus we expect deeper cusps at boundaries with smaller dislocation spacings. However, as the dislocation spacing decreases the whole theory becomes doubtful.

The energy term (2.150) may be interpreted as the energy arising from an additional array of dislocations with Burgers vector b/m, superimposed on an array of uniformly spaced dislocations with Burgers vector b. In this picture the non-uniformities in the spacings of the dislocations near $\theta = 1/m$ are modelled by new dislocations with Burgers vector b/m superimposed on the boundary of orientation $\theta = 1/m$. We recognize the new dislocations as secondary dislocations of the $\theta = 1/m$ reference state. Thus, secondary dislocations are equivalent to non-uniformities in the spacings of primary dislocations. Tertiary dislocations are equivalent to non-uniformities in the spacings of secondary dislocations, and so on. We call the cusps caused by primary and secondary dislocations primary and secondary cusps.

The agreement between the predicted σ versus θ curve, eqn (2.142), for primary cusps, i.e. small-angle grain boundaries, and experimental results is very good, as seen in Fig. 5.20. The agreement is in some cases too good since it extends to quite large angles where the linear elastic theory must break down. The existence of secondary cusps at

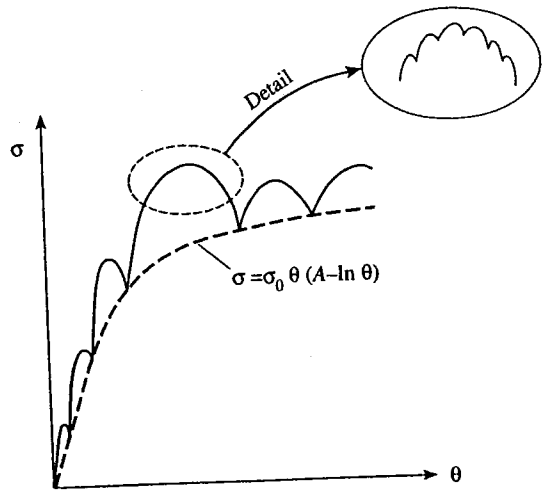

Fig. 2.24 A sketch of the energy, σ, of a small–angle grain boundary as a function of the misorientation, θ, according to the Read–Shockley analysis. Primary cusps occur at those orientations where dislocations are uniformly spaced, where the energy is given by the Read–Shockley formula, eqn (2.142), shown by the dashed line. Further, secondary, cusps exist on the primary cusps and so on.

rational grain boundary orientations has been much more controversial, and was reviewed by Sutton and Balluffi (1987). These cusps are often very shallow and may disappear altogether at finite temperatures. Entropic contributions to the boundary free energy are ignored in the Read–Shockley analysis. Their chief effect is to delocalize secondary dislocation cores and thereby weaken the elastic fields of the dislocations. We shall return to this subject in Section 2.13.3.

An interesting *empirical* observation has been made by Wolf (1989) concerning a Read–Shockley type formula for large-angle grain boundaries. Wolf carried out computer simulations of relaxed grain boundary energies at 0 K for several series of boundaries. In each series the mean boundary plane was constant and either the tilt or the twist angle was varied systematically. Thus, in each series only one of the five macroscopic degrees of freedom was varied. Certain features of the σ versus θ curves were found to be common to all the curves: there were no major cusps except at the endpoints of the $\sigma(\theta)$ curve, and $\sigma(\theta)$ was found to be a smooth function of θ, with vanishing slope in the middle of the misorientation range between the cusps at either end (see Fig. 2.25). Wolf found that the Read–Shockley formula with θ replaced by $\sin\theta$ could be fitted to all the calculated σ versus θ curves very well throughout the entire misorientation range:

$$\sigma(\theta) = \sigma_0 \sin\theta(A - \ln(\sin\theta)). \tag{2.151}$$

The parameters σ_0 and A were varied to give the best fit to the calculated values of $\sigma(\theta)$. However, it was also necessary to take account of crystal symmetry, if the rotation axis were a symmetry axis, by suitable scaling of θ, and also to adjust the endpoints of the fitted $\sigma(\theta)$ curve if they corresponded to grain boundaries rather than the perfect crystal.

There does not appear to be any theoretical justification that can be given for eqn (2.151). Frank's formula indicates that at large angles θ should be replaced by $2\sin(\theta/2)$ and not $\sin\theta$, but then $\sigma(\theta)$ would not have the required property of vanishing

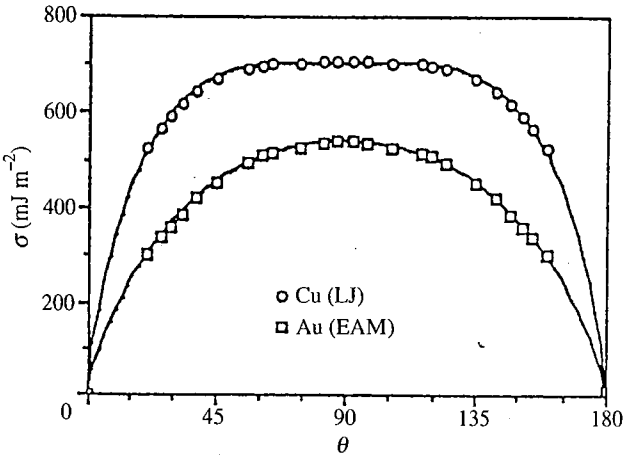

Fig. 2.25 Computed energies, σ, of (001) twist grain boundaries in Cu and Au using Lennard-Jones and embedded atom potentials respectively. The misorientation, θ, has been multiplied by 2. (From Wolf (1989).)

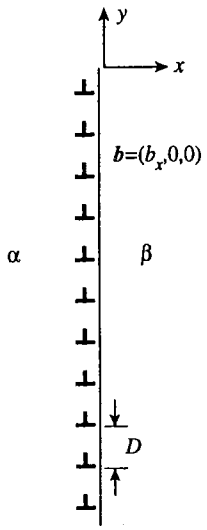

Fig. 2.26 Schematic illustration of a symmetric tilt boundary comprising an array of edge dislocations with Burgers vector $\boldsymbol{b} = (b_x, 0, 0)$, and spacing D, between two phases α and β.

slope at $\theta = 90°$. The usefulness of eqn (2.151) is that it suggests that large-angle grain boundary energies may be determined from the energies of small-angle boundaries by an *empirical* extrapolation. Further discussion of grain boundary energies in the framework of the structural unit model is given in Section 4.3.1.8.

2.10.4 Stress fields of heterophase interfaces in isotropic elasticity

Consider an array of edge dislocations forming a flat, symmetric tilt boundary between two phases α and β, as shown in Fig. 2.26. The array of dislocations produces an elastic field which we shall consider in this section in the isotropic elastic approximation. This

field is in addition to any other strain field that existed in the bicrystal prior to the introduction of the dislocation array. As far as the Frank–Bilby equation is concerned the interface is effectively a grain boundary because the dislocations accommodate a misorientation between the two crystals. Indeed, the application of Frank's formula to the array of edge dislocations is exactly the same as for a symmetric tilt grain boundary. The misorientation between the crystals should be independent of their elastic constants because it depends only on the magnitude, b_x, of the Burgers vector of the dislocations and on their spacing, D. Thus, the misorientation produced by the dislocation array is given by $\theta_z \cong 2\sin(\theta_z/2) = b_x/D$. This is the misorientation we expect to obtain from the elastic field of the dislocation array, and it is perhaps not obvious how this result is independent of the elastic constants.

In order for the elastic distortion field of the dislocation array to satisfy Frank's formula it is necessary that there are no net surface tractions far from the interface. Otherwise the net surface tractions will have to be balanced by externally applied forces to maintain equilibrium. Such applied loads will lead to distortions, in addition to those prescribed by Frank's formula. It is perhaps surprising that this rather obvious condition has sometimes been overlooked and consequently a great deal of confusion has resulted. For example, Chou and Lin (1975) found that simply summing the stress fields of the dislocations comprising the array produced finite stresses infinitely far from the interface. They concluded (erroneously) that such tilt walls could not be mechanically stable in heterophase interfaces. Hirth *et al.* (1979) showed that their result was consistent with Frank's formula being violated by the elastic field and showed how an elastic field consistent with Frank's formula could be obtained. It follows that symmetric tilt walls of dislocations are indeed mechanically stable in heterophase interfaces. We shall follow the analysis of Hirth *et al.* (1979).

We begin with the formulae derived by Nakahara *et al.* (1972) for the displacement field of a single edge dislocation with Burgers vector $[b_x, 0, 0]$ in an α/β interface. These formulae are the heterophase analogues of eqns (2.107) and (2.108). They are:

$$u_x^\alpha = \frac{\mu^\beta K^{\beta\alpha} b_x}{\pi\mu^\alpha}\frac{xy}{x^2+y^2} + \frac{b_x(1+K^{\alpha\beta}-K^{\beta\alpha})}{2\pi}\tan^{-1}(y/x) \tag{2.152}$$

$$u_y^\alpha = \frac{(K^{\alpha\beta}+K^{\beta\alpha}-1)b_x}{4\pi}\ln(x^2+y^2) + \frac{\mu^\beta K^{\beta\alpha} b_x}{2\pi\mu^\alpha}\frac{y^2-x^2}{x^2+y^2} \tag{2.153}$$

where

$$K^{\alpha\beta} = \mu^\beta[\mu^\beta + \kappa^\beta\mu^\alpha]^{-1}, \tag{2.154}$$

and

$$\kappa^\alpha = 3 - 4\nu^\alpha. \tag{2.155}$$

Here Poisson's ratio has been denoted by ν. The corresponding formulae in the β phase are obtained by interchanging the α and β superscripts. Using these formulae we can calculate the rotations far from the interface of the α and β phases about the tilt axis, z. We obtain the following rotation of the α phase relative to the β phase:

$$\theta_z = \frac{b_x}{D}\left[1 + \tfrac{1}{2}(\mu^\beta - \mu^\alpha)\{K^{\beta\alpha}/\mu^\alpha - K^{\alpha\beta}/\mu^\beta\}\right]. \tag{2.156}$$

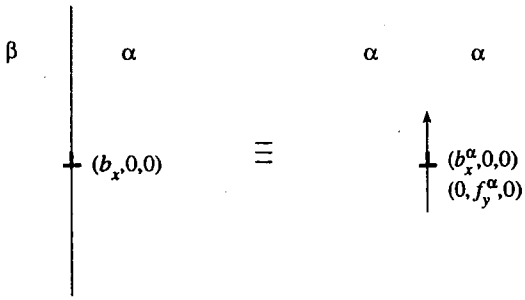

Fig. 2.27 A dislocation with Burgers vector $(b_x, 0, 0)$ between two phases α and β is equivalent to a dislocation with Burgers vector $(b_x^\alpha, 0, 0)$ and a line force $(0, f_y^\alpha, 0)$ in an infinite medium of the α phase.

It is clear that Frank's formula is not satisfied unless $\mu^\beta = \mu^\alpha$. Using eqns (2.152)–(2.153) it can be shown that the long-range stresses τ_{xx} and τ_{yy} arising from the array of edge dislocations are zero in both phases. However, the long-range stress τ_{xy} tends to the following value at long range:

$$\tau_{xy}^\alpha = \tau_{xy}^\beta = \frac{b_x}{D}\left[\mu^\alpha K^{\alpha\beta} - \mu^\beta K^{\beta\alpha}\right]. \tag{2.157}$$

The key to understanding the origin of this long-range stress field is a result due to Dundurs and Sendeckyj (1965). They noted the existence of net tractions in each half-crystal associated with an interfacial dislocation. The tractions are equal in magnitude and opposite in sign in the two half crystals, giving no net force on the dislocation. This means that in each half-space the field of an interfacial dislocation may be represented by that of an infinite medium dislocation (i.e. as though the other half-space had the same elastic constants) that is coincident with a line of force, as shown schematically in Fig. 2.27. More precisely, the elastic field in the α phase of an isolated interfacial dislocation with Burgers vector $(b_x, 0, 0)$ is equivalent to that of an infinite medium dislocation with Burgers vector $(b_x^\alpha, 0, 0)$ and an infinite medium line force $(0, f_y^\alpha, 0)$ given by

$$b_x^\alpha = b_x[1 - K^{\beta\alpha} + K^{\alpha\beta}] \tag{2.158}$$

$$f_y^\alpha = 2b_x[\mu^\beta K^{\beta\alpha} - \mu^\alpha K^{\alpha\beta}]. \tag{2.159}$$

In the β phase the Burgers vector $(b_x^\beta, 0, 0)$ and line force $(0, f_y^\beta, 0)$ describing the elastic field are given by

$$b_x^\beta = b_x[1 - K^{\alpha\beta} + K^{\beta\alpha}] \tag{2.160}$$

$$f_y^\beta = -f_y^\alpha. \tag{2.161}$$

In the α-phase the displacements arising from the line of force, given by eqn (2.159), are as follows:

$$u_x^\alpha = \frac{f_y^\alpha}{2\pi\mu^\alpha(\kappa^\alpha + 1)}\frac{xy}{x^2 + y^2} \tag{2.162}$$

$$u_y^\alpha = \frac{-f_y^\alpha}{4\pi\mu^\alpha(\kappa^\alpha + 1)}\left[\kappa^\alpha \ln(x^2 + y^2) + \frac{x^2 - y^2}{x^2 + y^2}\right]. \tag{2.163}$$

When these displacements are added to those of the infinite medium dislocation, given by eqns (2.107)–(2.108) with Burgers vector given by eqn (2.158), we obtain the displacements of the interfacial dislocation given by eqns (2.152)–(2.153). Thus, we have proved the equivalence of the field of an interfacial dislocation to the field of an infinite medium dislocation and an infinite medium line of force.

It has already been shown in eqns (2.114)–(2.119) that an array of infinite medium dislocations, forming a symmetric tilt boundary, has no long-range stress field. Therefore the source of the long-range stress field found in eqn (2.157) must be the lines of force at the interface. The net tractions on a cut normal to the x-axis are readily evaluated using eqns (2.162)–(2.163) and found to be $-\frac{1}{2}f_y^\alpha$ in the α phase ($x > 0$) and $\frac{1}{2}f_y^\alpha$ in the β phase ($x < 0$). These tractions are independent of the position of the cut plane along x in each phase. The shear stress, τ_{xy}^α, they generate is equal to $-\frac{1}{2}f_y^\alpha/D$ which is exactly equal to the long range shear stress of the array of interfacial dislocations given in eqn (2.157).

In a finite bicrystal mechanical equilibrium requires that the long-range shear stress τ_{xy}^α is balanced by externally applied forces. In other words the bicrystal is *not* in equilibrium unless forces are applied to it externally. This is to be expected because Frank's formula is not satisfied, as seen in eqn (2.156). With no constraints applied to the surface of a finite bicrystal the long-range shear stress τ_{xy}^α is cancelled by an image stress $-\tau_{xy}^\alpha$. The image stress produces uniform simple shears, parallel to the interface, of $-\tau_{xy}^\alpha/\mu^\alpha$ and $-\tau_{xy}^\alpha/\mu^\beta$, in the α and β phases respectively. These simple shears introduce a change of orientation of the α phase relative to the β phase equal to:

$$\tau_{xy}^\alpha\left[\frac{1}{2\mu^\alpha}-\frac{1}{2\mu^\beta}\right]=\frac{b_x}{2D}(\mu^\beta-\mu^\alpha)\left[\frac{K^{\alpha\beta}}{\mu^\beta}-\frac{K^{\beta\alpha}}{\mu^\alpha}\right] \tag{2.164}$$

Adding this to θ_z in eqn (2.156) we see that elimination of the long-range shear stress field results in Frank's formula being satisfied. In this final relaxed state the elastic field of the dislocation array in the α phase may be thought of as a superposition of three fields: (i) the field of an array of infinite medium dislocations with effective Burgers vector $(b_x^\alpha, 0, 0)$, (ii) the field of an array of infinite medium line forces with forces per unit length $(0, f_y^\alpha, 0)$, (iii) a uniform simple shear parallel to the interface of $-\tau_{xy}^\alpha/\mu^\alpha$ to cancel the long-range shear stress generated by the array of line forces. The field in the β phase is the same except that quantities associated with the α phase are replaced by those associated with the β phase. It is interesting to note that the effective Burgers vectors b_x^α and b_x^β depend on the elastic constants of the two phases. Therefore the rotations of the two phases are not equal in magnitude, in contrast to the grain boundary case, although their relative rotation is the same as in the grain boundary case.

To *summarize*, the elastic field of the heterophase interface does satisfy Frank's formula when the adjoining crystals are free of net surface tractions. This is physically sensible because we can always imagine that the α/β interface is created by bonding together the surfaces of two stress free α and β phases with a relative misorientation of $\theta = b_x/D$. Then, according to St Venant's principle the stress field of the interface should decay over a distance comparable to D from the interface. The relaxation of the long-range stresses does not introduce any further incompatibilities into the interface. This may be seen in two ways. First, the average effective Burgers vector, $(b_x^\alpha + b_x^\beta)/2$, is equal to b_x. Secondly, the long-range shear stresses are relieved by uniform simple shear strains parallel to the interface, leaving the interface invariant. These two statements hold also in the anisotropic elastic case.

Finally, we note that the difficulty we encountered with long-range tractions far

from the interface does not arise if cancelling arrays of stress generator and annihilator dislocations are used to model the elastic field of the interface.

2.10.5 Dislocation arrays at interfaces in anisotropic elasticity

Although the analysis is more involved it can be shown (Hirth *et al.* 1979) that the conclusions of the previous section apply in the anisotropic elastic case as well. The anisotropic elastic field of an interface dislocation in an infinite bicrystal may be represented by a sum of two fields in each half-space. The first is that of a dislocation with an effective Burgers vector in an infinite medium of the half-space. There are no net surface tractions on any plane associated with an infinite medium dislocation. The second is a line of force coinciding with the dislocation. Barnett and Lothe (1974) generalized the result of Dundurs and Sendeckyj (1965) to give an expression for the line force in anisotropic elasticity. There are net surface tractions acting on planes parallel to the interface due to these lines of force at the interface. Furthermore, Frank's formula is not satisfied by the interface so long as the net surface tractions are not relaxed. In a finite bicrystal with no surface constraints the surface tractions of the dislocation array are cancelled by image stresses. The strains associated with these image stresses leave the interface invariant and do not, therefore, introduce any further incompatibilities into the interface. In the final relaxed state of the finite unconstrained bicrystal Frank's formula is satisfied and there are no net tractions acting any plane parallel to the interface.

Alternatively, and arguably more conveniently, the anisotropic elastic field can always be modelled by cancelling arrays of stress generator and annihilator dislocations. The net tractions produced by the two arrays cancel automatically and the condition of no stresses far from the interface is guaranteed.

2.10.6 Isotropic elastic analysis of epitaxial interfaces

Frank and van der Merwe (1949) presented an elastic stress analysis of an epilayer grown on a flat substrate with a slightly different lattice parameter. Their one-dimensional analysis was extended to two dimensions by Jesser and Kuhlmann-Wilsdorf (1967). The essence of the analysis is to demonstrate that once the thickness of the epilayer exceeds a certain critical value it becomes energetically favourable to introduce crystal lattice stress annihilator dislocations at the interface, and thereby relieve the elastic strain energy.

For simplicity we consider cubic lattices for the substrate and epilayer, with lattice parameters a^s and a^e. The interface is assumed to be on a (001) plane in each crystal. The 'misfit' is defined as

$$f = (a^e - a^s)/a^s \tag{2.165}$$

and represents the elastic strain in the [100] and [010] directions in the interface if the two lattices are in perfect registry. In this elastically strained state the interface contains an array of coherency dislocations and is fully coherent, as in Fig. 2.6b. This condition is sometimes described as 'commensurate' or a 'state of forced elastic coherence'. The epilayer has a free surface and the surface tractions must be zero. Since the epilayer is much thinner than the substrate we assume that the strain is all taken up in the epilayer. The epilayer is thus in a state of biaxial stress, which in isotropic elasticity is given by

$$\sigma = 2\mu \frac{(1+\nu)}{(1-\nu)} f \tag{2.166}$$

where μ and ν are the shear modulus and Poisson ratio in the epilayer. The biaxial stress state may therefore be modelled by two uniform, continuous distributions of stress generator, coherency dislocations with Burgers vector densities equal to $[f00]$ and $[0f0]$. The elastic strain energy of the epilayer, per unit area, is

$$E_{el} = 2\mu \frac{(1+\nu)}{(1-\nu)} f^2 h, \tag{2.167}$$

where h is the film thickness. Since this increases linearly with h there must be a critical thickness at which it becomes energetically favourable to introduce anticoherency stress annihilator dislocations. To find this critical thickness we first calculate the energy of the interface when a fraction of the misfit is relieved by stress annihilator dislocations. We assume the stress annihilator dislocations form a square array, with Burgers vector b and spacing D. The remaining elastic strain ε is given by

$$\varepsilon = f - b/D. \tag{2.168}$$

The energy of the dislocation array, per unit area, is

$$E_d = 2 \times \frac{\mu b^2}{4\pi(1-\nu)D} \ln\left[\frac{eh}{r_o}\right] \tag{2.169}$$

where r_o is the core radius of the stress annihilator dislocations, and the factor of 2 arises from the existence of two orthogonal sets of edge dislocations. By putting h inside the logarithm of eqn (2.169) we have assumed that the film thickness is less than the spacing of the stress annihilators. The total energy, per unit area, of the film is obtained by adding E_d to E_{el} with ε in place of f in eqn (2.167):

$$E = 2\mu \frac{(1+\nu)}{(1-\nu)} \varepsilon^2 h + \frac{\mu b(f-\varepsilon)}{2\pi(1-\nu)} \ln\left[\frac{eh}{r_o}\right]. \tag{2.170}$$

For a given film thickness the total energy is minimized for a value of $\varepsilon = \varepsilon_o$, given by

$$\varepsilon_o = \frac{b}{8\pi(1+\nu)h} \ln\left[\frac{eh}{r_o}\right]. \tag{2.171}$$

If ε_o is larger than f then all the misfit is accommodated elastically with no stress annihilators at the interface. If ε_o is less than f then some of the misfit is relaxed by stress annihilators, the spacing of which is given by

$$D = b/(f - \varepsilon_o). \tag{2.172}$$

The critical film thickness, h_c, at which it is energetically favourable for the first stress annihilator to be introduced is obtained by setting ε_o equal to f:

$$h_c = \frac{b}{8\pi(1+\nu)f} \ln\left[\frac{eh_c}{r_o}\right]. \tag{2.173}$$

This is an implicit relation for h_c. We note that it depends on the value assumed for the core radius, r_o, and the Burgers vector, b, of the stress annihilators. There is thus some uncertainty about the value of h_c. But perhaps the most important limitation of this analysis is that it has ignored the question of where the dislocations come from. Matthews and Blakeslee (1974) pointed out that in order to introduce dislocations there has to be a mechanism for doing so. Thus, the Frank–van der Merwe criterion is a necessary but not sufficient condition for stress annihilators to be introduced. For all these reasons

comparison of eqn (2.173) with experimental measurements is problematic. Observed values of h_c are generally larger than those of eqn (2.173), partly because of the insensitivity of the experimental techniques employed and partly for kinetic reasons.

Matthews and Blakeslee (1974) developed a somewhat different criterion for the introduction of stress annihilator dislocations at the interface. They suggested that the dislocations are generated by the glide of existing dislocations which 'thread' through the substrate and epilayer. Other mechanisms have been proposed in recent years: see Hirsch (1991) for a review. In order to move a threading dislocation the force on it has to be sufficient to overcome the line tension of the interfacial dislocations. This criterion again leads to a critical epilayer thickness at which stress annihilators appear, and Willis *et al.* (1990) have shown that, at equilibrium, it is identical to the critical thickness predicted by Frank and van der Merwe. Willis *et al.* argue that apparent differences between the two treatments are due entirely to the use of different approximations to the energy of a single dislocation. Furthermore, Jain *et al.* (1992) criticize both the Frank–van der Merwe and Matthews–Blakeslee analyses because they consider h_c to be determined by the stress at which a *single* stress annihilator dislocation is introduced into the coherent interface. Jain *et al.* argue instead that if an *array* of stress annihilator dislocations is introduced at the transition from the coherent to the semicoherent states not only is a lower energy equilibrium state achieved but also the criterion for h_c is altered qualitatively. In practice, however, the new criterion does not predict a value of h_c which is very different from the values predicted by the Frank–van der Merwe and Matthew–Blakeslee analyses. The validity of the criticism from a theoretical point of view depends on whether stress annihilator dislocations enter the coherent interface one at a time or in unison in the form of an array. This is very difficult to establish experimentally. But as theory of the *equilibrium state* of the interface the treatment by Jain *et al.* is a significant improvement on the earlier models.

2.10.7 Stress fields of precipitates and non-planar interfaces

Eshelby (1957) considered the elastic fields of ellipsoidal precipitates. He noted that the elastic field could be modelled by thinking of the interface surrounding the precipitate as a Somigliana dislocation (see Section 1.7). Although this observation was made in 1957 it is only in recent years that it has been exploited. Bonnet *et al.* (1985) have given elastic solutions for Somigliana dislocations that are particularly useful in modelling the elastic fields of faceted precipitates. As noted by those authors it allows morphologies of precipitates other than ellipsoidal to be treated with relative ease, including precipitates with corners such as cubes. For example, for the cubic morphology the elastic field is calculated by summing the separate contributions of the six faces of the cube, each of which is treated as a Somigliana dislocation defined by a square cut. If the relaxation at each face of the cube gives rise to a rigid body translation of the matrix with respect to the precipitate then there will be Volterra dislocations at the twelve edges of the cube to account for the changes in translation vector between adjoining facets. The elastic fields of these dislocations can then be added to those of the Somigliana dislocations to get the total elastic field of the precipitate. As Bonnet (1988) has demonstrated the elastic fields of quite complex, non-planar heterophase interfaces may be modelled by using appropriate distributions of Somigliana and Volterra dislocations. However, such an analysis is dependent on detailed information from high-resolution electron microscopy of the strain at the interface (see Bonnet (1988)). Specifically, the distribution of dislocations and their degree of localization is essential to formulate the elastic problem.

2.11 DEGREE OF LOCALIZATION OF THE CORES OF INTERFACIAL DISLOCATIONS

2.11.1 Introduction

Until now we have assumed that discrete dislocations in an interface are line defects with Burgers vector densities that are localized within the plane of the interface. But any dislocation has a tendency to delocalize the distribution of its Burgers vector density in order to reduce the energy of its elastic strain field. On the other hand this spreading of the dislocation core will generally disrupt the structure of the surrounding material and so tend to raise the energy of the system. A dislocation will therefore delocalize to the point where these two opposing tendencies are in balance. In addition, the analyses of the elastic fields of interfacial dislocations discussed in Section 2.10 were based on the assumption of a linear elastic continuum for both the interface and the adjoining crystals. In this approximation the stress and strain become singular at the core of each dislocation. But in reality these singularities are relieved by relaxations within the core because at smaller length scales the discrete atomic structure of the medium cannot be ignored, and the approximation of linear elasticity breaks down. Important questions to raise at this point are therefore the following: (i) to what extent are the cores of interfacial dislocations localized? and (ii) how are their stress–strain fields affected by the degree of localization?

If a perfect interfacial dislocation has a Burgers vector that is a non-primitive lattice vector of the reference lattice it may be able to reduce its elastic energy by *dissociating* into two, or more, interfacial dislocations with smaller (primitive) Burgers vectors. This phenomenon is described in Sections 9.2.2.2 and 12.4.3.1. Of course it may be regarded as a form of core delocalization. However, we are not concerned with this phenomenon here: instead, we are concerned with the degree of localization of an interfacial dislocation which is unable to dissociate into discrete dislocations with finite Burgers vectors of the reference crystal or DSC lattices.

For such a dislocation embedded in an interface it is easily seen that the Burgers vector density parallel to the interface may delocalize preferentially in the plane of the interface, if the interface has a relatively low resistance to a change in the translational disposition, parallel to the interface, of the two adjoining crystals. In such a case this portion of the Burgers vector density will have a tendency to spread out in the interface, thereby shearing the interface locally. The resistance of the interface to this disruptive shearing process, averaged over the whole interfacial area, is measured by the slope of the γ-surface, which is the surface representing the ground state energy of the interface as a function of an imposed, rigid-body translation, t, parallel to the interface (Vitek 1968). As discussed in Section 4.3.1.1, when the interface has a periodic structure the γ-surface is a periodic function with the periodicity of the c.n.i.d. (defined in Section 1.5.7). Therefore, the γ-surface of a periodic interface has maxima and minima in general, and the interface will then encounter some resistance to a change in its translational state from the ground state configuration. It follows that the cores of dislocations lying in such an interface are localized in directions parallel to the interface to some extent at least. The degree of localization depends on the slope of the γ-surface.

As the c.n.i.d. decreases in size the γ-surface tends to become flatter, as shown in Section 4.3.1.1. In the limit when the area of the c.n.i.d. is reduced to zero, as happens in the case of a quasiperiodic interface, the γ-surface becomes flat. In that case there is no resistance on average to changes in the translational state of the interface, in the ground state. Therefore, in the ground state, a dislocation inserted into such an interface

will tend to undergo complete delocalization of its Burgers vector density parallel to the interface plane. In that case, the stress and strain fields due to the component of the Burgers vector density parallel to the interface will vanish. However, it is emphasized that the γ-surface measures the *average* resistance to a change of the rigid-body translation of one crystal relative to the other parallel to the interface. The *local* resistance may vary considerably from one region of the interface to another, such that the average resistance is zero. Therefore there may be an activation barrier for the core delocalization to take place, with the result that localized dislocation cores may persist until sufficient thermal activation has been supplied. A discussion of such delocalization processes at elevated temperatures is given in section 12.4.3.2.

The degree of localization of the Burgers vector density normal to the boundary plane is determined by the cohesive forces acting across the interface plane. Provided the interface is stable with respect to cleavage, as is generally the case, there will always be a force tending to localize this Burgers vector density irrespective of the form of the γ-surface.

On the basis of the above, we expect wide variations in the degree to which the cores of interfacial dislocations are delocalized in the ground state. For widely spaced crystal lattice dislocations in small-angle grain boundaries the situation should be similar to that for isolated lattice dislocations. However, as the spacing is reduced, the situation will change as discussed below in Section 2.11.2. For dislocations in large-angle boundaries large variations will occur, depending on the presence, or absence, of periodicity and the form of the γ-surface, and kinetic factors which control the extent to which the interface attains the ground state. These variations will be associated with corresponding variations in the surrounding stress and strain fields.

We have already argued that the localization of the Burgers vector density parallel to the interface may decrease as the temperature is raised at a quasiperiodic interface. Even at a periodic interface the degree of core localization may vary with temperature because the γ-surface is expected to vary with temperature. At a finite temperature it is the free energy of the interface, rather than the internal energy, which determines the γ-surface. As discussed in Section 3.9 the vibrational entropy of the boundary leads, effectively, to a softening of the interatomic forces acting in the material. In addition the enhanced anharmonicity of the atomic environment of a grain boundary in metals, compared with the bulk, leads to an increased thermal expansion which further weakens the cohesive forces across the boundary plane (see Section 4.3.1.10). In that case the ground state of the interface may change with temperature from one which supports localized Burgers vector densities parallel to the interface to one that does not. However, experimental evidence, cited in Section 2.12.2, indicates that for at least a range of grain boundaries in Al, the change in the γ-surface with temperature is not sufficient to lead to significant delocalization.

In the following sections we describe the results of a number of calculations of the detailed core structure of interfacial dislocations at 0 K. They range from results obtained by analytical methods using simple lattice theories (Section 2.11.2) to those obtained by computer simulation using interatomic force models (Section 2.11.3).

2.11.2 Lattice theories of dislocation arrays

2.11.2.1 *Introduction*

In this section we describe analytic models in which the dislocation core region is treated discretely using simple assumed force laws. These indude the Peierls–Nabarro (Peierls

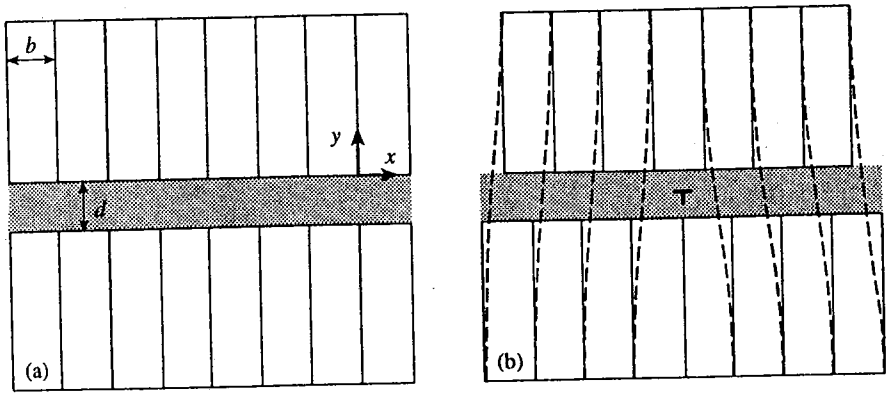

Fig. 2.28 To illustrate the Peierls–Nabarro model for an edge dislocation. In (a) we see two semi-infinite crystals, modelled as elastic continua, separated by an inelastic slab of width d. A dislocation with Burgers vector b, equal to the spacing of the lattice planes in (a), is introduced into the inelastic slab in (b).

1940; Nabarro 1947; Hirth and Lothe 1982) and van der Merwe (1950) models. These more realistic models remove the elastic singularity at the core and provide information about the degree of localization of the core. In addition, they yield expressions for the surrounding stress and strain fields which differ somewhat from those obtained using the elastic continuum approximation.

The idea underlying the Peierls–Nabarro and van der Merwe models is that the core is allowed to spread within an inelastic slab, as sketched in Fig. 2.28 for an edge dislocation. The inelastic slab is bonded to elastic continua on either side of it. Far from the dislocation core the two faces of the slab are displaced relative to one another by the Burgers vector of the dislocation. The object of the model is to determine how rapidly this relative displacement is accumulated through the core. A force law is defined within the inelastic slab which reflects the crystal lattice periodicity and is matched to the elastic constants at small strains. By constructing a force law with this periodicity we are restricting the models to small-angle interfaces containing crystal lattice dislocations. If we wanted to develop analogous models or secondary dislocation arrays at large-angle grain boundaries we would have to construct force laws with appropriate periodicities. In that case it is much less obvious what elastic constants should be fitted in the boundary core region. A balance of forces is established at the boundaries of the inelastic and elastic regions. The inelastic region tries to localize the core as much as possible while the elastic strain field energy in the adjacent continua favours an infinitely wide core. At the force balance the core has a finite width and the elastic singularity is removed.

Van der Merwe (1950) considered models for epitaxial interfaces and grain boundaries of the twist and symmetric tilt types. Bullough and Tewary (1979) presented a Peierls–Nabarro-type model of a symmetric tilt boundary. In this section we introduce the principles of such models by briefly describing the Peierls–Nabarro model for an isolated edge dislocation. We then discuss a symmetric tilt boundary treated by a Peierls–Nabarro model and then by a van der Merwe model. There seems little point in a thorough exposition of these models since their deficiencies are well known. In particular the close proximity of the elastic continua to the dislocation cores and the uncertainty in the inelastic force laws make these models of qualitative interest only.

2.11.2.2 *Peierls–Nabarro model for an isolated edge dislocation*

An edge dislocation is introduced into the crystal by the following imaginary process, which is illustrated in Fig. 2.28. First, the crystal is cleaved along the slip plane, Fig. 2.28(a). One lattice plane, spacing b, is removed from the upper half-crystal, Fig. 2.28(b). The lattice planes are no longer in registry across the cleavage plane. The disregistry of the bottom half-plane with respect to the top one is $\varphi(x) = b/2$ $(x > 0)$ and $\varphi(x) = -b/2$ $(x < 0)$, Fig. 2.28(b). The two half crystals are rebonded and displacements $u(x, y)$ are introduced by relaxation. The displacements are assumed to be antisymmetric about the plane $y = 0$: $u(x, -\varepsilon) = -u(x, \varepsilon)$. The disregistry is now

$$\left.\begin{aligned} \varphi(x) &= 2u(x, -\varepsilon) + b/2 \quad (x > 0) \\ \varphi(x) &= 2u(x, -\varepsilon) - b/2 \quad (x < 0) \end{aligned}\right\} \tag{2.174}$$

with the boundary conditions $u(\infty, -\varepsilon) = -u(-\infty, -\varepsilon) = -b/4$. These boundary conditions ensure that the disregistry is zero far from the core. For brevity we shall write $u(x)$ for $u(x, -\varepsilon)$, so that $u(x)$ refers to the displacement of the bottom surface. The two surfaces above and below $y = 0$ in Fig. 2.28(b) are now assumed to interact by an inelastic force law. In a local disregistry approximation the force law is given by the negative of the gradient of the γ-surface. That is, the restoring force at x, where the disregistry is $\varphi(x)$, is given by the negative of the slope of the γ-surface at a constant disregistry equal to $\varphi(x)$. The approximation consists of ignoring additional terms arising from the coexistence of a continuous set of disregistries in the dislocation core.

The restoring force has the periodicity of the crystal lattice, which is equal to b in the direction of the Burgers vector. Thus the simplest form of the restoring force is

$$\tau_{xy} = A \sin\left[\frac{2\pi\varphi}{b}\right] \tag{2.175}$$

where A is a constant. Substituting eqn (2.174) for $\varphi(x)$ we obtain

$$\tau_{xy} = -A \sin\left[\frac{4\pi u}{b}\right]. \tag{2.176}$$

We may think of this as the first term of an infinite Fourier series representation of τ_{xy}. The constant A is determined, as in the Frenkel model of the theoretical shear strength, by requiring that Hooke's law is satisfied, for small displacements u. Hence in the isotropic elastic approximation we have

$$\tau_{xy} = 2\mu\varepsilon_{xy} = \frac{\mu\varphi}{d} = A\frac{2\pi\varphi}{b} \tag{2.177}$$

where d is the interplanar spacing. It is noted that the shear is inhomogeneous here since it is applied only across one pair of lattice planes. Thus, the equalities in eqn (2.177) are not exact, but approximate, since they apply only in the case of a homogeneous shear ε_{xy}. In this approximation we obtain

$$\tau_{xy} = -\frac{\mu b}{2\pi d} \sin\left[\frac{4\pi u}{b}\right]. \tag{2.178}$$

We now consider the dislocation to be represented by a continuous distribution of dislocations along x, with a Burgers vector density $\rho(x)$. The meaning of $\rho(x)$ is that $\rho(x)\mathrm{d}x$ is the Burgers vector lying between x and $x + \mathrm{d}x$. From eqn (2.174) we have

$$\rho(x) = -2\frac{du}{dx}, \tag{2.179}$$

and

$$b = \int_{-\infty}^{\infty} \rho(x)\, dx = -2\int_{-\infty}^{\infty} \frac{du}{dx} dx. \tag{2.180}$$

The shear stress produced on the plane $y = 0$ by this continuous distribution of dislocations at $(x, 0)$ is given by

$$\tau_{xy}(x, 0) = -\frac{\mu}{2\pi(1-\nu)} \mathbb{P}\int_{-\infty}^{\infty} \frac{\rho(x')}{(x-x')}\, dx' = \frac{\mu}{\pi(1-\nu)} \mathbb{P}\int_{-\infty}^{\infty} \frac{(du/dx)_{x=x'}}{(x-x')}\, dx' \tag{2.181}$$

where $\mathbb{P}$ denotes the principal value of the integral. Combining eqns (2.178) and (2.181) we obtain the following integral equation for the displacements $u(x)$:

$$\mathbb{P}\int_{-\infty}^{\infty} \frac{(du/dx)_{x=x'}}{(x-x')} dx = \frac{b(1-\nu)}{2d} \sin\left(\frac{4\pi u}{b}\right) \tag{2.182}$$

for which the solution is

$$u(x) = -\frac{b}{2\pi} \tan^{-1}\left(\frac{x}{\zeta}\right) \tag{2.183}$$

where

$$\zeta = \frac{d}{2(1-\nu)}. \tag{2.184}$$

Equation (2.183) satisfies the boundary conditions that $u(\infty) = -u(-\infty) = -b/4$. In addition $u(\zeta) = -b/8 = \frac{1}{2}u(\infty)$. We may define 2ζ as the width of the dislocation since in the region $-\zeta < x < \zeta$ the disregistry is greater than one half of its maximum value.

The Burgers vector density has the form of a Lorentzian:

$$\rho(x) = \frac{b}{\pi} \frac{\zeta}{x^2 + \zeta^2} \tag{2.185}$$

Using this Burgers vector density and the standard expressions for the stress field of an isolated edge dislocation (eqns (2.109)–(2.113)) expressions may be derived for the Peierls–Nabarro edge dislocation by integration. It is found that the stress field of the dislocation is no longer singular, the singularity being removed by the finite width of the dislocation core.

2.11.2.3 *Peierls–Nabarro model for a symmetrical tilt boundary*

Consider a symmetrical tilt boundary as sketched in Fig. 2.29. The Peierls–Nabarro model for this boundary was considered by Bullough (1955) (see Bullough and Tewary 1979). The model consists of a vertical stack of infinite elastic plates, each of thickness D and separated by inelastic slabs of thickness d. The dislocations are assumed to delocalize within the inelastic slabs. The aim is to derive the variation of the dislocation core widths with the boundary misorientation. The problem reduces to the equilibrium of a single elastic plate, with its centre at the origin, whose surfaces are subjected to the displace-

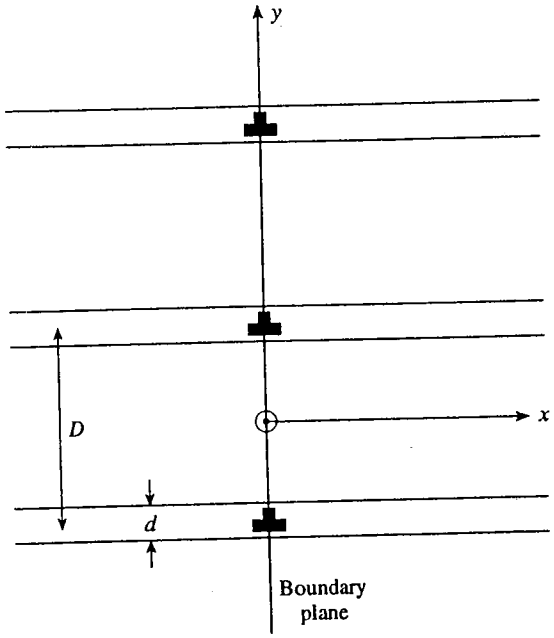

Fig. 2.29 Peierls–Nabarro model of a symmetric tilt boundary. The dislocation spacing is D and the thickness of each inelastic slab is d. (From Bullough and Tewary (1979).)

ments $u(x)$ and $-u(x)$. The same restoring force law, eqn (2.178) is assumed to act across each inelastic slab. The elastic shear stress is obtained from eqn (2.118) by setting $Y = 0$:

$$\tau_{xy}(x, D/2) = -\frac{\mu}{D(1-\nu)} \int_{-\infty}^{\infty} \frac{\pi(t-x)/D}{\sinh^2[\pi(t-x)/D]} \frac{\mathrm{d}u}{\mathrm{d}t} \mathrm{d}t. \tag{2.186}$$

At equilibrium this stress balances the stress from eqn (2.178):

$$\sin\frac{4\pi u(x)}{b} = -\frac{2\pi d/b}{D(1-\nu)} \int_{-\infty}^{\infty} \frac{\pi(t-x)/D}{\sinh^2[\pi(t-x)/D]} \frac{\mathrm{d}u}{\mathrm{d}t} \mathrm{d}t. \tag{2.187}$$

Note that when $D \to \infty$ this equation reverts to eqn (2.182) for an isolated edge dislocation. Although an exact solution to eqn (2.187) has proved elusive an approximate solution, that is quite adequate for misorientations up to about 5°, has been given by Bullough. Bullough's solution is the following:

$$u(x) = \frac{b}{2\pi} \tan^{-1}\left[\frac{\sinh(\pi x/\delta)}{\sin(\pi\varepsilon/\delta)}\right] \tag{2.188}$$

where ε and δ are defined by

$$\begin{aligned} D &= \delta - 2\varepsilon \\ \tan(\pi\varepsilon/\delta) &= b\pi/2\delta(1-\nu). \end{aligned} \tag{2.189}$$

The dislocation core width is obtained from eqn (2.189) as follows:

$$2\zeta = \frac{2\delta}{\pi} \sinh^{-1}\left[\sin\left(\frac{\pi\varepsilon}{\delta}\right)\right]. \tag{2.190}$$

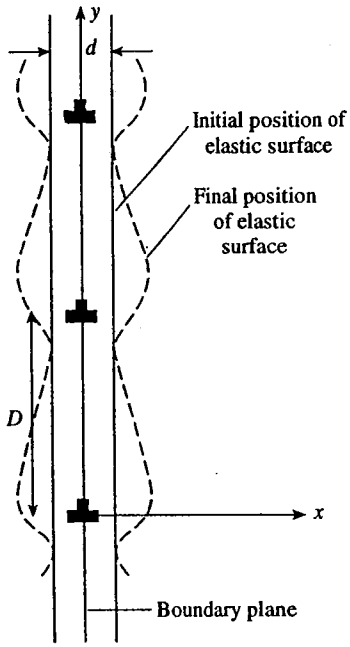

Fig. 2.30 Van der Merwe model of a symmetric tilt boundary. The dislocation spacing is D and the inelastic slab, of thickness d, is now in the boundary plane. The dashed line shows the final shape of the surfaces of the adjoining elastic continua, once the elastic relaxation has taken place. (From Bullough and Tewary (1979).)

It follows from eqn (2.190) that the core width decreases as the dislocation spacing D decreases, i.e. as the tilt angle increases. This is the main result of the model. One of the consequences is that it predicts that the stress required to move the boundary by dislocation glide increases as the misorientation increases.

2.11.2.4 *The van der Merwe model for a symmetrical tilt boundary*

Once the boundary misorientation exceeds a few degrees there is no longer sufficient good material between the dislocation cores for the Peierls–Nabarro model to be applicable. The van der Merwe model (van der Merwe 1950) may be used to model the boundary when the non-Hookean relaxations are confined largely to the boundary plane. Thus the model consists of two elastic half-spaces separated by an inelastic slab of thickness d in the boundary plane (see Fig. 2.30). The object of the model is to study the core relaxation in the boundary plane as a function of the tilt angle. A key difference between this model and the Peierls–Nabarro model is that the restoring force acting between the elastic slabs is tensile. It is again approximated by a sinusoidal force, although in reality it is not a periodic function of the relative separation of the elastic half-spaces. We shall not discuss the model in detail here but state its main results. Figure 2.30 shows the periodic displacement relaxations for the symmetrical tilt boundary. It is seen that each dislocation has a wider core on the compressive side of the dislocation than on the tensile side, as would be expected from the anharmonicity of atomic interactions. The displacement field $u(y)$ is given by

$$u(y) = b/4 + \frac{b}{2\pi}\tan^{-1}\left[A \sin Y/(1 - A\cos Y)\right] \tag{2.191}$$

where

$$\left.\begin{aligned} A &= \sqrt{1+\beta^2} - \beta \\ Y &= 2\pi y/D \\ \beta &= \frac{\pi b(1-2\nu)}{2D(1-\nu)} \cong \frac{\pi(1-2\nu)}{2(1-\nu)}\theta. \end{aligned}\right\} \tag{2.192}$$

As the boundary misorientation increases and the dislocation cores approach each other the compressive field of one dislocation becomes closer to the tensile field of the dislocation above it. The width of the dislocation cores in the boundary plane therefore increases as the boundary misorientation increases.

2.11.3 Atomistic models using computer simulation and interatomic forces

Numerous calculations of the atomic core structures of interfacial dislocations (especially secondary dislocations) have been made using computer simulation techniques and interatomic force laws. We cite here a few examples that illustrate some of the points that were made in Section 2.11.2.1. The cores of secondary edge dislocations with $\boldsymbol{b}$ normal to the boundary plane are found to be highly localized (see Section 4.3.1.8). This result may be expected because of the large cohesive forces acting across the boundary. The cores of some relaxed secondary edge dislocations with $\boldsymbol{b}$ parallel to the interface have already been shown in Fig. 1.20 and 1.21. These cores are seen to be localized as indicated by the pattern of distortion of the DSC lattices, which is easily detected. The localization of these cores is expected because the c.n.i.d.s for these interfaces are quite large and therefore significant variations of the interfacial energy can occur as a function of the relative translation of the adjoining crystals parallel to the interface. On the other hand, Bristowe (1986) has found considerable variation of the degree of localization of a number of secondary screw dislocations in [001] twist boundaries in f.c.c. metals represented by different interatomic force models. Some results are shown in Fig. 2.31, where the calculated width of an isolated secondary screw dislocation in a $\Sigma = 5$ boundary is shown using four different interatomic force laws. It was found that the degree of delocalization tended to increase for a force law which gave a γ-surface with a smaller slope, as expected. Similarly, it was found that the degree of delocalization tended to increase as the size of the c.n.i.d. decreased, which is also expected because the range of values of σ decreases as the c.n.i.d. decreases in size.

2.12 EXPERIMENTAL OBSERVATIONS OF ARRAYS OF INTERFACIAL DISLOCATIONS

2.12.1 Mainly room-temperature observations

There have been many observations, by transmission electron microscopy, of arrays of dislocations at homophase and heterophase interfaces at room temperature. In Section 2.9 we discussed the application of the Frank–Bilby analysis to two experimental observations of dislocation arrays at heterophase interfaces. Despite the large number of experimental studies there have been only a few instances in which the Burgers vectors of the dislocations have been positively identified from the image contrast. As pointed out by Forwood and Clarebrough (1985) the conditions under which the usual $\boldsymbol{g}\cdot\boldsymbol{b} = 0$

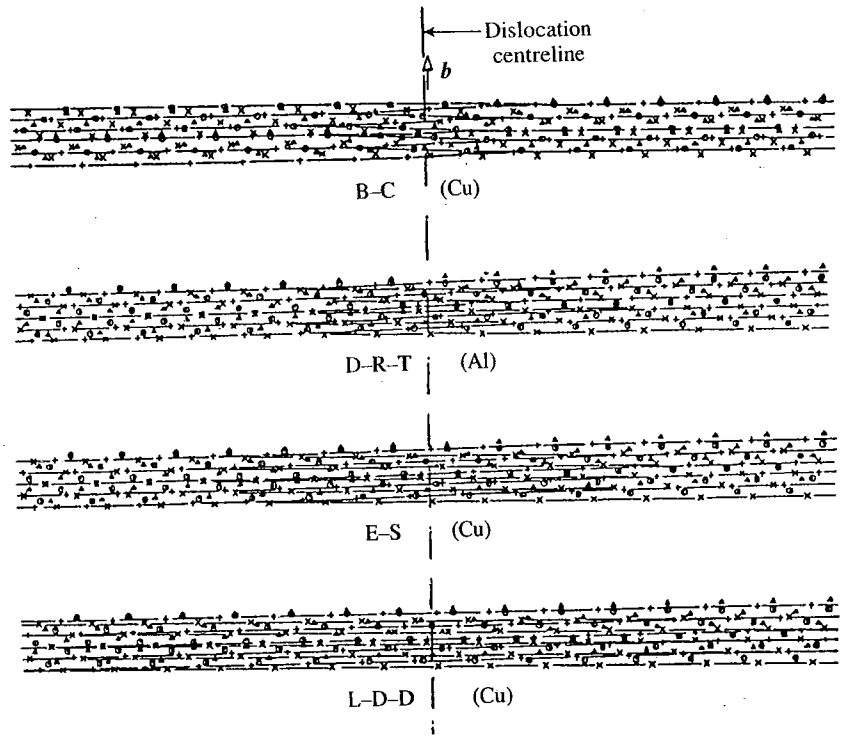

Fig. 2.31 Relaxed structures of an isolated screw dislocation in a $\Sigma = 5(001)$ twist boundary computed at 0 K with 4 different potentials for f.c.c. metals. The horizontal lines show the (310) planes in the plane of the boundary. The width of the dislocation increases from the top of the series to the bottom. (From Bristowe (1986).)

criteria for determining the Burgers vector of a dislocation are more restrictive for interfacial dislocations than they are for a dislocation in the bulk crystal. Frequently the Burgers vectors have been inferred from the measured misorientation from an assumed reference state and the spacings of the dislocations, e.g. Schober and Balluffi (1970), Bollmann *et al.* (1972), Clark and Smith (1978), Knowles and Goodhew (1983a), and Babcock and Balluffi (1987). In this section we shall not present a catalogue of all such observations, which would fill a book in itself. Instead we focus on those observations which have a direct bearing on the theory that we have described in this chapter.

Schober and Balluffi (1970) and Tan *et al.* (1975) observed square grids of line contrast in certain (001) twist grain boundaries in gold (see Fig. 2.32), by transmission electron microscopy. The grain boundaries were manufactured by bonding together two (001) films of gold at selected misorientations. Misorientations close to 0, $2\tan^{-1}\frac{1}{7}$ $2\tan^{-1}\frac{1}{5}$, $2\tan^{-1}\frac{1}{4}$, $2\tan^{-1}\frac{1}{3}$ were studied, corresponding to boundaries vicinal to $\Sigma = 1$, 25, 13, 17, and 5 respectively. The lines of contrast were assumed to correspond to dislocations with Burgers vectors of the appropriate DSC lattices. The observed average dislocations spacings were found to satisfy Frank's formula:

$$d = |\boldsymbol{b}|/2\sin(\Delta\theta/2) \tag{2.193}$$

where $\Delta\theta$ is the measured misorientation from the nearby exact coincidence site lattice orientation. This is illustrated in Fig. 2.33. As the spacing of the dislocations decreased,

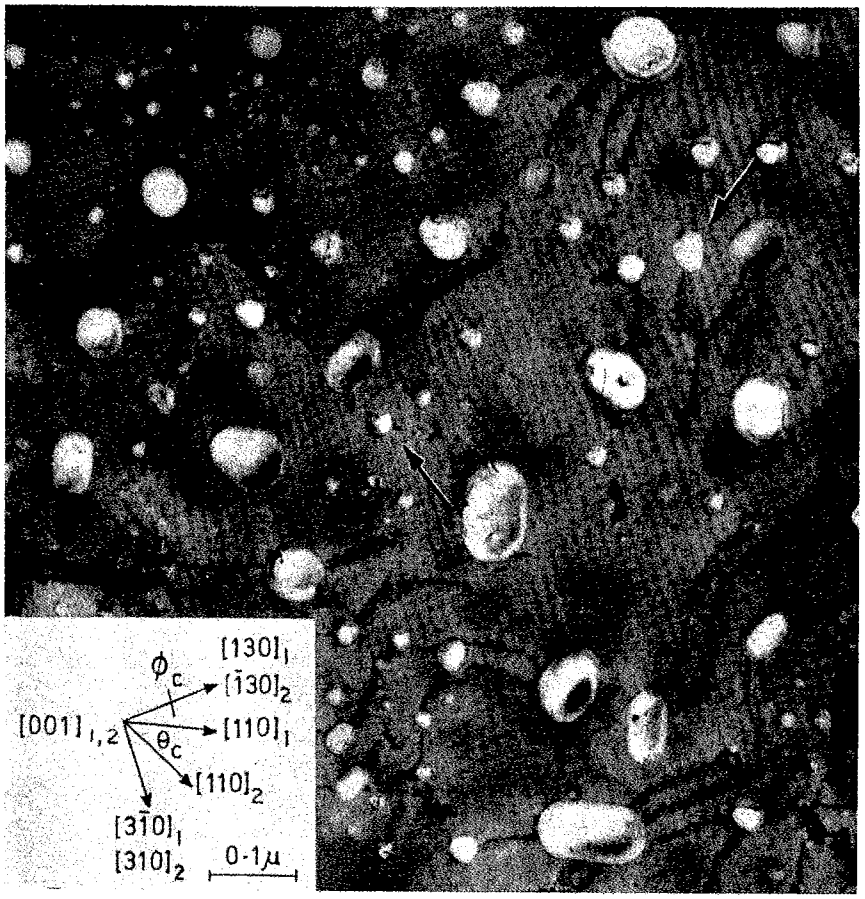

Fig. 2.32 Electron micrograph of a manufactured (001) twist grain boundary in gold with a misorientation vicinal to $\Sigma = 5$, showing a square array of $a/10\langle 310\rangle$ DSC screw dislocations. (From Schober and Balluffi (1970).)

and as the magnitude of the Burgers vectors decreased, the line contrast faded and the dislocations became increasingly difficult to detect. Thus, in Fig. 2.33 it is seen (black dots only) that the arrays of screw dislocations were detectable only within 9° of the $\theta = 0°$ orientation, 2° of the $\Sigma = 5$ orientation, and about 0.6° of the $\Sigma = 13$ and $\Sigma = 17$ orientations. However, no dislocations were seen in the vicinity of the $\Sigma = 25$ orientation. This raised the questions of whether the dislocations were present near the $\Sigma \geq 25$ orientations and at greater deviations from the exact coincidence orientations, or whether they were simply indetectable. From the viewpoint of Frank–Bilby theory the dislocations are always present for purely geometrical reasons. Physically, the question concerns the localization of the Burgers vector density into discrete dislocations and whether forces to bring about this localization exist in the boundary plane. It was also not clear from these experiments whether the line contrast was indeed due to dislocations or Moiré fringes. As discussed by Babcock and Balluffi (1987), if Moiré fringes were present they could have the same directions and spacings as the reported dislocation networks.

Babcock and Balluffi (1987) clarified these questions by repeating the experiments for manufactured (001) twist boundaries in gold and silver. In addition to repeating the earlier

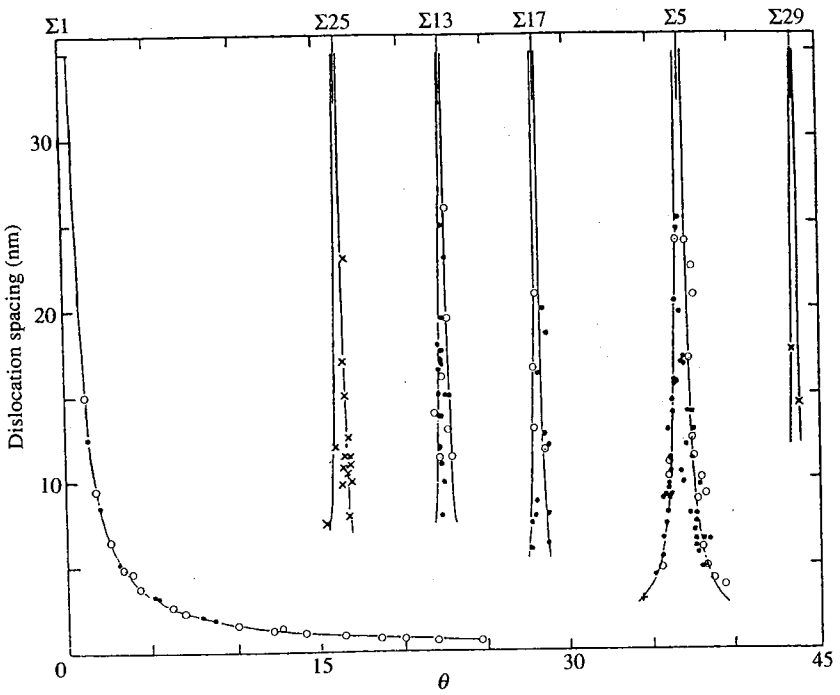

Fig. 2.33 Observed dislocation spacings in manufactured (001) twist grain boundaries in gold as a function of the twist angle. The lines show the spacings expected by Frank's formula, eqn (2.193), for DSC dislocations of the Σ1, 5, 13, 17, 25, and 29 orientations. (From Babcock and Balluffi (1987).)

observations of arrays of line contrast near $\Sigma = 1$, 5, 13, and 17, they also observed arrays of line contrast near $\Sigma = 25$ and $\Sigma = 29$ (see Fig. 2.33). They showed, by a series of tests, that in each case the line contrast was indeed due to dislocations and not Moiré fringes. The fact that dislocations were found in boundaries vicinal to $\Sigma \geq 25$ reflects the increased resolution of the more modern instruments and the improvements in specimen preparation.

Similar observations of arrays of screw dislocations in twist boundaries in NiO and MgO have been made by Liou and Peterson (1981) and Sun and Balluffi (1982). One of the interesting features about these observations is that there is some evidence that the Burgers vectors of the dislocations are not always primitive DSC vectors. Obviously it is not a requirement of the Frank–Bilby theory that the Burgers vectors of discrete dislocations, which make up the Burgers vector content of the boundary, are primitive DSC vectors.

The contrast from dislocation arrays depends on the Burgers vectors of the dislocations, the spacing of the dislocations, the foil thickness, and the angle at which the array is viewed. It also depends on the resolution of the microscope and the magnification at which it is operated. Under certain conditions arrays of coarsely spaced dislocations are detected. But if the imaging conditions are changed, for the same specimen, additional, finer spaced networks of dislocations may be detected. This was first demonstrated by Cosandey and Bauer (1981) and it was studied systematically by Kvam and Balluffi (1987) who examined a large number of manufactured symmetric [001] tilt boundaries in gold. Dislocation-like strain contrast was detected effectively throughout the 90° misorientation

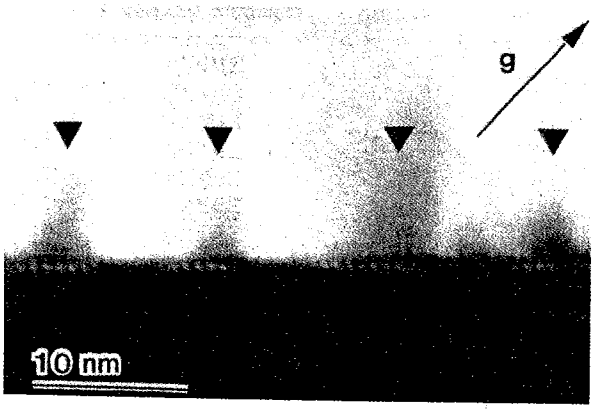

Fig. 2.34 Electron micrograph of a boundary vicinal to a $\Sigma = 13$ (320) symmetric [001] tilt boundary in gold seen almost edge on, showing two patterns of strain contrast. The fine scale contrast is due to $\frac{1}{2}$ [110] crystal lattice dislocations, while the coarser scale contrast (arrowed) is due to $\frac{1}{13}$ [320] DSC dislocations. (From Kvam and Balluffi (1987).)

range. This indicates that at all misorientations there are forces acting in the boundary plane tending to localize the Burgers vector density of the Frank–Bilby equation into discrete dislocations.

In Fig. 2.34 we show a boundary with a misorientation of 21.7°, which is less than 1° from that of the $\Sigma = 13$ (320) symmetric tilt boundary. The boundary is viewed at a highly oblique angle and therefore it appears very narrow. The strain contrast associated with it appears on two length scales. The fine contrast is due to $\frac{1}{2}$[110] edge dislocations and their measured spacing is 0.77 nm, as compared with the predicted spacing from Frank's formula of 0.75 nm. The strain contrast of this array decays very rapidly into the adjoining crystals, as expected from the elastic field analysis of Section 2.10. The coarser scale contrast, arrowed in Fig. 2.34, is associated with an array of $\frac{1}{13}$[320] dislocations, which are DSC dislocations of the $\Sigma = 13$ coincidence site lattice. Their measured spacing is 7 nm, as compared with the predicted spacing of 7.1 nm. In Fig. 2.35 we show a plot of the observed dislocation spacings in symmetric [001] tilt boundaries as a function of the tilt angle. Taken together with Fig. 2.34 this provides strong experimental confirmation of the Frank–Bilby analysis of the Burgers vector content of interfaces and of the localization of the Burgers vector density into discrete dislocations. The localization is a result of relaxation processes within the interface, whose origin is beyond the scope of the Frank–Bilby theory.

For grain boundaries between h.c.p. crystals the selection of a suitable reference structure is even more complex. In general, CSLs are very rare in h.c.p. crystal lattices where $(c/a)^2$ is not a rational fraction. In that case the near CSL model is applied in which the actual value of $(c/a)^2$ is approximated by a rational approximant (Chen and King 1988, Antonopoulos *et al.* 1990, Shin and King 1991). Thus the selection of a reference structure entails first the choice of a rational approximant to $(c/a)^2$ to produce a 'constrained' CSL. Secondly with a chosen rational approximant to $(c/a)^2$ there is an infinity of possible constrained CSLs to choose from, just as there is for cubic crystals. Stress annihilator dislocations are required to accommodate the deviation of the actual value of $(c/a)^2$ from the chosen rational approximant as well as the misorientation of the boundary from the orientation relation for the constrained CSL. The selection of the

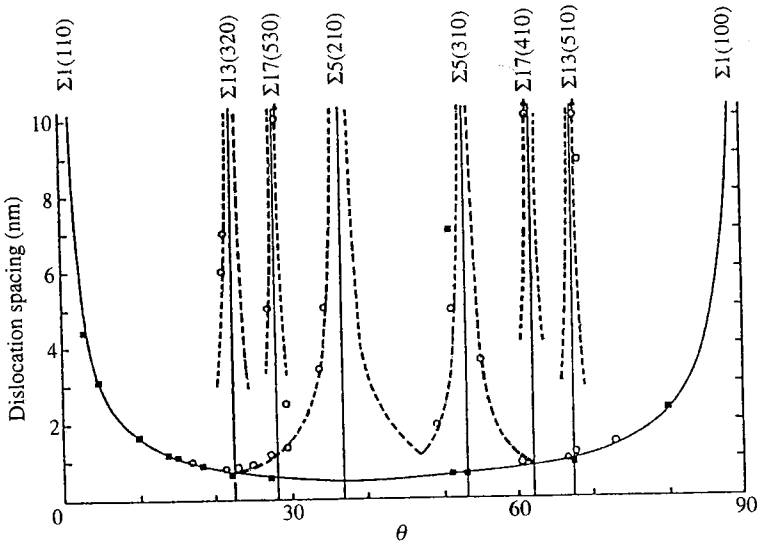

Fig. 2.35 A plot of the observed dislocation spacings (shown as points) in [001] symmetric tilt boundaries in gold as a function of tilt angle, θ. The solid line shows the spacings expected by Frank's formula for crystal lattice dislocations, and the dashed lines show the expected spacings of DSC dislocations. (From Kvam and Balluffi (1987).)

rational approximant to $(c/a)^2$ and the constrained CSL for that rational approximant is again made (Shin and King 1991) on the grounds that the predicted secondary dislocation configuration is consistent with the strain contrast in the electron microscope, at the operating level of spatial resolution.

An interesting example of this approach was presented by Shin and King (1991) who analysed the linear strain contrast features in grain boundaries in zinc at temperatures between 140 and 300 K. In zinc the (c/a) ratio varies markedly with temperature. Therefore the most appropriate choice of reference structure may change from one rational approximant to another as $(c/a)^2$ changes with temperature. Correspondingly the predicted secondary dislocation configuration may change discontinuously. Since this would involve a discontinuous change in the reference periodic boundary structure and the Burgers vectors of the secondary dislocations it amounts to a first-order phase transformation of the boundary structure. Possible indications of a reversible transformation of this kind at grain boundaries in zinc were presented by Shin and King and are shown in Fig. 2.36. In Fig. 2.36(a) we see a room-temperature observation of a grain boundary in which the misorientation is 86.2° [2.0, −0.983, −1.017, 0.0] and the observed dislocation configuration is consistent with that predicted by choosing a $\Sigma = 15$ reference structure. Figure 2.36(b) shows the same boundary after cooling to 77 K. The dislocation configuration is heavily disrupted, which Shin and King interpret as evidence that the dislocation structure is transforming to that of another reference structure. But because the temperature is so low the transformation cannot be completed in the time available in the experiment. Estimates of the elastic strain field energy of the boundary indicate that the lower energy dislocation configuration does indeed change to that of a $\Sigma = 32$ reference structure at the lower temperature. The disruption to the dislocation array of Fig. 2.36(b) is reversed upon returning to room temperature, and the structure shown in Fig. 2.36(a) is again obtained. This example illustrates once again the difficulty in

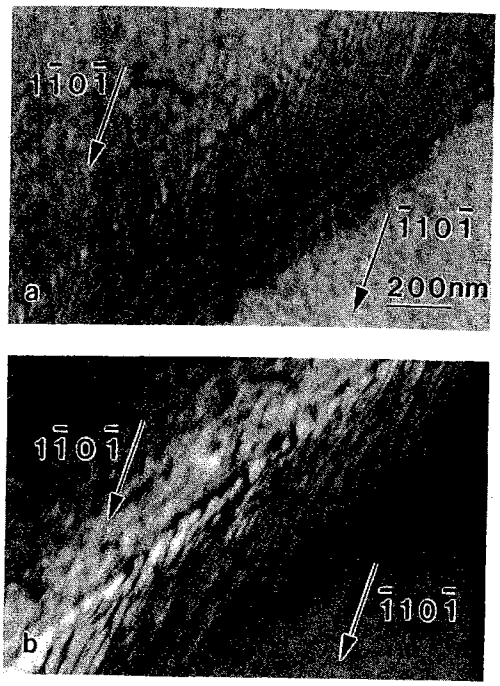

Fig. 2.36 Electron micrographs of a grain boundary in zinc with a misorientation of 86.2° [2.0, −0.983, −1.017, 0.0] imaged (a) at room temperature and (b) at 77 K. Note the disruption of the dislocation configuration in (b). (From Shin and King (1991).)

selecting a suitable reference structure to account for observed contrast features in the electron microscope at interfaces.

Positive identification of Burgers vectors of dislocations detected in boundaries vicinal to $\Sigma = 3,9,27$ and 81 coincidence site lattices has been made by Clarebrough and Forwood (1980*a*,*b*), and Forwood and Clarebrough (1985, 1986) using the image matching technique of Head *et al.* (1973). Transmission electron microscope images of a dislocation were compared with calculated images computed for different Burgers vectors. Boundaries within 0.1° of the exact coincidence orientations were selected from a Cu + 6 at % Si alloy. In all cases the Burgers vectors of the dislocations were identified as DSC vectors, and in most cases, though not all, the vectors were the smallest possible DSC vectors in their respective lattices.

It is not always the case that the Burgers vectors of dislocations accommodating a misorientation from a coincidence boundary are DSC vectors. It is sometimes possible for a DSC dislocation to dissociate into partial dislocations separating regions of a boundary with different structures. If the regions are related by symmetry then they are energetically degenerate (see Section 1.7.2.3). Periodic arrays of such partial dislocations have been identified in a boundary vicinal to $\Sigma = 5$ in germanium (Bacmann *et al.* 1981 and in boundaries vicinal to $\Sigma = 9$ and $\Sigma = 27$ boundaries in a copper silicon alloy by Forwood and Clarebrough (1982, 1983). Forwood and Clarebrough (1986) showed that the partial dislocations could also separate grain boundary structures that are not related by symmetry. Two of the three independent arrays of dislocations, in a $\Sigma = 3$ $(2\bar{4}1)/(\bar{5}\ 10\ 8)$ $\cos^{-1}(-2/3)/[210]$ asymmetric tilt boundary facet, were dissociated into partial DSC dislocations that separated non-equivalent regions of the boundary plane. They estimated that the difference in energy of the two regions was 2.5 mJ m^{-2}.

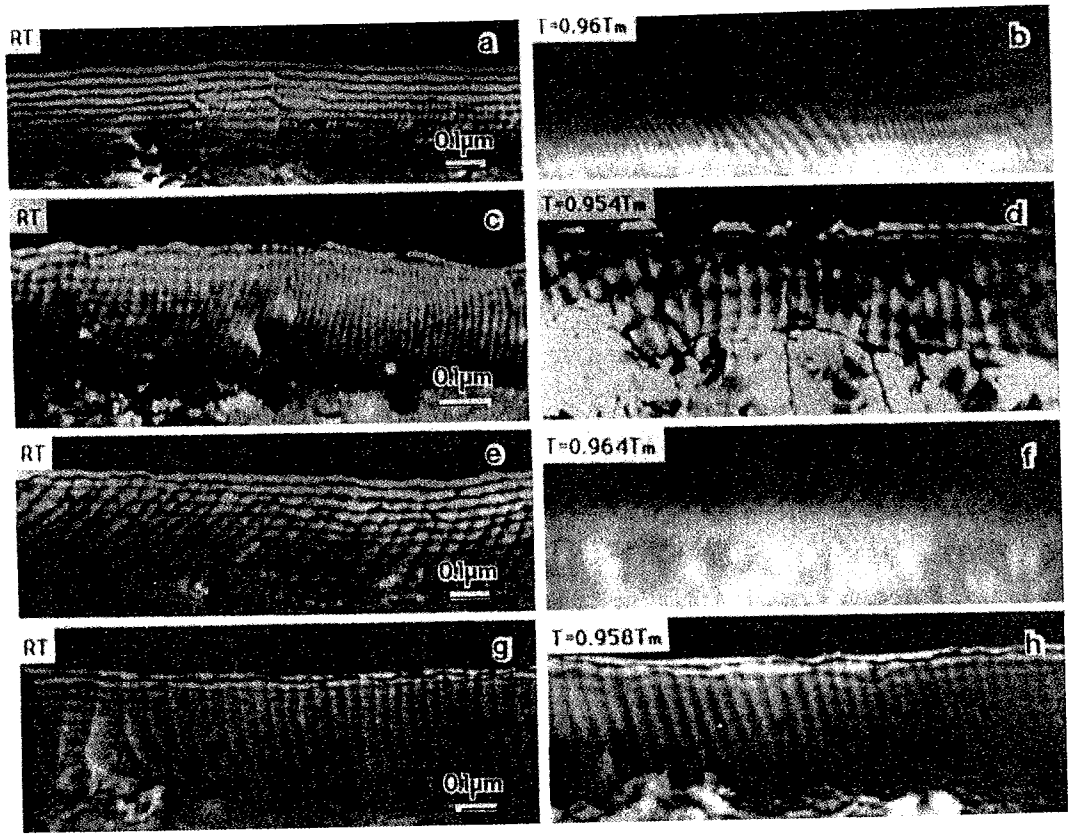

Fig. 2.37 Dark-field electron micrographs of localized grain boundary dislocation arrays in various boundaries in aluminium at room temperature (left) and at the highest temperature of observation (right). (a) and (b) $\Sigma = 13$ (510) symmetric tilt boundary showing grain boundary DSC edge dislocations with $\boldsymbol{b} = \frac{1}{26}\langle 510\rangle$. (c) and (d) $\Sigma = 17$ (410) symmetric tilt boundary showing grain boundary DSC edge dislocations with $\boldsymbol{b} = \frac{1}{17}\langle 410\rangle$. (e) and (f) incommensurate (100) twist boundary with $\theta = 45°$ showing dislocations with $\boldsymbol{b} = \frac{1}{2}\langle 001\rangle$. (g) and (h) incommensurate symmetric [001] tilt boundary with $\theta = 45°$ showing dislocations with $\boldsymbol{b} = \frac{1}{2}\langle 100\rangle$. (From Hsieh and Balluffi (1989).)

2.12.2 High-temperature observations

Experiments designed to reveal any extensive delocalization of the cores of primitive secondary interfacial dislocations at elevated temperatures have been performed by Hsieh and Balluffi (1989). The experiments consist of following the change in the strain contrast of dislocation arrays as the specimen is heated in the electron microscope. The results for aluminium indicate that sufficient localization of the dislocation strain field to give line contrast features in the electron microscope exists up to 96 per cent of the melting point of the material. These authors manufactured bicrystals close to (310), (410), and (510) symmetric tilt orientations and also a $\theta = 45°$ $\langle 100\rangle$ tilt boundary and a $\{100\}$ twist boundary with $\theta = 45°$. The first three boundaries vicinal to misorientations at which there is two-dimensional periodicity in the boundary plane. There is no periodicity in the boundary plane of the 45° twist boundary. The 45° $\langle 100\rangle$ tilt boundary is periodic only along the tilt axis. In all cases dislocation arrays were seen in these boundaries at

temperatures up to 0.96 of the melting point. This must mean that the cores remained localized to a sufficient extent that the elastic strain field associated with them produced the contrast in the microscope. This is shown in Fig. 2.37.

REFERENCES

Amelinckx, S. (1979). In *Dislocations in solids*, Vol. 2 (ed. F. R. N. Nabarro), p. 67. North-Holland, Amsterdam.

Amelinckx, S. and Dekeyser, W. (1959). *Solid State Physics*, **8**, 325.

Antonopoulos, J. G., Delavignette, P., Karakostas, Th., Komninou, Ph., Laurent-Pinson, E., Lay, S., Nouet, G., and Vincens, J. (1990). *J. Phys.* (Paris), **51**, C1-61.

Babcock, S. E. and Balluffi, R. W. (1987). *Phil. Mag. A*, **55**, 643.

Bacmann, J. J., Silvestre, G., Petit, M., and Bollmann, W. (1981). *Phil. Mag. A*, **43**, 189.

Balluffi, R. W. and Olson, G. B. (1985). *Met. Trans. A*, **16**, 529.

Balluffi, R. W., Brokman, A., and King, A. H. (1982). *Acta Metall.*, **30**, 1453.

Barnett, D. M. and Lothe, J. (1974). *J. Phys. F: Metal Phys.*, **4**, 1618.

Bilby, B. A. (1955). *Report on the conference on defects in crystalline solids*, p. 123. The Physical Society, London.

Bilby, B. A., Bullough, R., and Smith, E. (1955). *Proc. Roy. Soc.*, **231A**, 263.

Bollmann, W. (1970). *Crystal defects and crystalline interfaces*. Springer-Verlag, Berlin.

Bollmann, W., Michaut, B., and Sainfort, G. (1972). *Phys. Stat. Sol.* (*a*), **13**, 637.

Bonnet, R. (1981*a*). *Acta Metall.*, **29**, 437.

Bonnet, R. (1981*b*). *Phil. Mag. A*, **43**, 1165.

Bonnet, R. (1981*c*). *Phil. Mag. A*, **44**, 625.

Bonnet, R. (1982). *J. Physique*, **43**, C6-215.

Bonnet, R. (1985). *Phil. Mag. A*, **51**, 51.

Bonnet, R. (1988). *Mat. Res. Soc. Symp. Proc.*, **122**, 281.

Bonnet, R., Marcon, G., and Ati, A. (1985). *Phil. Mag. A*, **51**, 429.

Bristowe, P. D. (1986). In *Grain boundary structure and related phenomena*, p. 89. Japan Institute of Metals, Sendai (Suppl. to *Trans. Jap. Inst. Mets.* **27**.)

Bullough, R. (1955). PhD thesis, University of Sheffield.

Bullough, R. and Bilby, B. A. (1956). *Proc. Phys. Soc. B*, **69**, 1276.

Bullough, R. and Tewary, V. K. (1979). In *Dislocations in solids*, Vol. 2. (ed. F. R. N. Nabarro), p. 1. North-Holland, Amsterdam.

Burgers, J. M. (1939). *Proc. Kon. Ned. Akad. V. Wet. Amsterdam*, **42**, 293.

Burgers, J. M. (1940). *Proc. Phys. Soc.*, **52**, 23.

Burgers, W. G. (1947). *Proc. Kon. Ned. Akad. V. Wet. Amsterdam*, **50**, 595.

Chen, F.-R. and King, A. H. (1988). *Phil. Mag. A*, **57** 431.

Chou, Y. T. and Lin, L. S. (1975). *Mat. Sci. Eng.*, **20**, 19.

Christian, J. W. (1981). *The theory of transformations in metals and alloys*, Part I. Pergamon, Oxford.

Clarebrough, L. M. and Forwood, C. T. (1980*a*). *Phys. Stat. Sol.* (*a*), **58**, 597.

Clarebrough, L. M. and Forwood, C. T. (1980*b*). *Phys. Stat. Sol.* (*a*), **59**, 263.

Clark, W. A. T. and Smith, D. A. (1978). *Phil. Mag. A*, **38**, 367.

Cosandey, F. and Bauer, C. L. (1981). *Phil. Mag. A*, **44**, 391.

Dahmen, U. and Westmacott, K. H. (1988). *Scr. Metall.*, **22**, 1673.

Dundurs, J. and Sendeckyj, G. P. (1965). *J. Appl. Phys.*, **36**, 3353.

Dundurs, J. (1969). *Mathematical theory of dislocations*, p. 70. American Society of Mechanical Engineers, New York.

Dupeux, M. (1987). *Phil. Mag. Letts.*, **55**, 7.

Eshelby, J. D. (1957). *Proc. Roy. Soc., A*, **241**, 376.

Forwood, C. T. and Clarebrough, L. M. (1982). *Acta Metall.*, **30**, 1443.

Forwood, C. T. and Clarebrough, L. M. (1983). *Phil. Mag.*, **47**, L35.
Forwood, C. T. and Clarebrough, L. M. (1985). *Aust. J. Phys.*, **38**, 449.
Forwood, C. T. and Clarebrough, L. M. (1986). *Phil. Mag. A*, **53**, 863.
Frank, F. C. (1950). *Symposium on the plastic deformation of crystalline solids*, p. 150. Office of Naval Research, Pittsburgh, Pennsylvania.
Frank, F. C. and van der Merwe, J. H. (1949). *Proc. R. Soc. A*, **198**, 205.
Goodhew, P. J., Darby, T. P., and Balluffi, R. W. (1976). *Scr. Metall.*, **10**, 495.
Head, A. K., Humble, P., Clarebrough, L. M., Morton, A. J., and Forwood, C. T. (1973). *Computed electron micrographs and defect identification*. North Holland, Amsterdam.
Hirsch, P. B. (1991). *Polycrystalline semiconductors II*, Springer Proc. Phys. Vol. 54, (eds. J. H. Werner and H. P. Strunk), p. 54. Springer-Verlag, Berlin.
Hirth, J. P. and Balluffi, R. W. (1973). *Acta Metall.*, **21**, 973.
Hirth, J. P. and Lothe, J. (1982). *Theory of dislocations*. Wiley, New York.
Hirth, J. P., Barnett, D. M., and Lothe, J. (1979). *Phil. Mag. A*, **40**, 39.
Hsieh, T. E. and Balluffi, R. W. (1989). *Acta Metall.*, **37**, 1637.
Jain, S. C., Gosling, T. J., Willis, J. R., Totterdell, D. H. J., and Bullough, R. (1992). *Phil. Mag. A*, **65**, 1151.
Jesser, W. A. and Kuhlmann-Wilsdorf, D. (1967). *Phys. Stat. Sol.* **19**, 95.
Knowles, K. M. (1982). *Phil. Mag. A*, **46**, 951.
Knowles, K. M. and Goodhew, P. J. (1983*a*). *Phil. Mag. A*, **48**, 527.
Knowles, K. M. and Goodhew, P. J. (1983*b*). *Phil. Mag. A*, **48**, 555.
Kvam, E. P. and Balluffi, R. W. (1987). *Phil. Mag. A*, **56**, 137.
Liou, K.-Y., and Peterson, N. L. (1981). In *Surfaces and interfaces in ceramics and ceramic—metal systems* (eds. J. A. Pask and A. G. Evans). Plenum, New York.
Matthews, J. W. and Blakeslee, A. E. (1974). *J. Cryst. Growth*, **27**, 118.
Nabarro, F. R. N. (1947). *Proc. Phys. Soc.*, **59**, 256.
Nakahara, S., Wu, J. B. C., and Li, J. C. M. (1972). *Mat. Sci. Eng.*, **10**, 291.
Olson, G. B., and Cohen, M. (1979). *Acta Metall.*, **27**, 1907.
Peierls, R. E. (1940). *Proc. Phys. Soc.*, **52**, 23.
Pond, R. C. (1977). *Proc. Roy. Soc.*, **A357**, 471.
Pond, R. C. and Vlachavas, D. S. (1983). *Proc. Roy. Soc. Lond., A*, **386**, 95.
Read, W. T. (1953). *Dislocations in crystals*. McGraw-Hill, New York.
Read, W. T. and Shockley, W. (1950). *Phys. Rev.*, **78**, 275.
Rosenhain, W. and Humphrey, J. C. W. (1913). *J. Iron and Steel Inst.*, **87**, 219.
Sargent, C. M. and Purdy, G. R. (1975). *Phil. Mag.*, **32**, 27.
Schober, T. and Balluffi, R. W. (1970). *Phil. Mag.*, **21**, 109.
Shieu, F.-S., and Sass, S. L. (1990). *Acta Metall. Mater.*, **38**, 1653.
Shin, K. and King, A. H. (1991). *Phil. Mag. A*, **63**, 1023.
Sun, C. P. and Balluffi, R. W. (1982). *Phil. Mag. A*, **46**, 49.
Sutton, A. P. and Balluffi, R. W. (1987). *Acta Metall.*, **35**, 2177.
Tan, T. Y., Sass, S. L., and Balluffi, R. W. (1975). *Phil. Mag.*, **31**, 575.
Taylor, G. I. (1934). *Proc. Roy. Soc.*, **145A**, 388.
van der Merwe, J. H. (1950). *Proc. Phys. Soc.*, **A63**, 616.
Vitek, V. (1968). *Phil. Mag.*, **18**, 773.
Willis, J. R., Jain, S. C., and Bullough, R. (1990). *Phil. Mag. A*, **62**, 115.
Wolf, D. (1989). *Scr. Metall.*, **23**, 1713.